PRESENTATION SESSION NO. 1

- RESISTANCE AND FLOW

- POWERING PERFORMANCE

Chairman: Prof. T. Inui

PS-1.1

K. MORI and Y. DOI
Hiroshima University, Japan

VISCOUS EFFECTS ON THE STERN WAVES

When the viscous effects on the stern waves are discussed, the boundary layer development or separation is taken into account for the wave calculation. Mori [1] entrained the viscous double model flow onto his wave calculation by the Rankine source method. Stern et al. [2] considered the boundary layer effects in terms of its displacement thickness. In these calculations it is assumed that the viscous flows are less affected by the free-surface.

Our recent study casts a doubt on this assumption.

Fig. 1 shows the wave patterns of S-103, an Inuid model, at four different Froude numbers. Although the difference in the Froude numbers is not so large, the stern wave patterns are drastically different; stern wave is not so much generated at Froude number 0.27, while those at 0.26 or 0.28 are obvious. Even an intensive breaking wave is observed at 0.30.

Fig. 2 shows the calculated wave contours by the N-S solver code. The calculations are carried out at the three Froude numbers but their Reynolds numbers are the same, 10^6. As have been seen in Fig. 1, less developed stern wave is seen at Froude number 0.27 compared with the other two speeds.

Fig. 3 shows the calculated and the measured limiting streamlines around the stern at the two Froude numbers. The measurements are carried out by the

twin tufts method; solid lines are on the surface and the broken 10mm vertically off. It can be mentioned that the separation region is wider at 0.27 than at 0.30 both in the calculated and the measured (the tufts close to the free-surface are much affected by the free-surface wave breaking).

Because the calculations are carried out at the same Reynolds number, the difference in the calculated stern viscous flows has come from the free-surface flow effects. The bow wave phase may play an important role for the development of the boundary layer and separation. The significant separation of the viscous

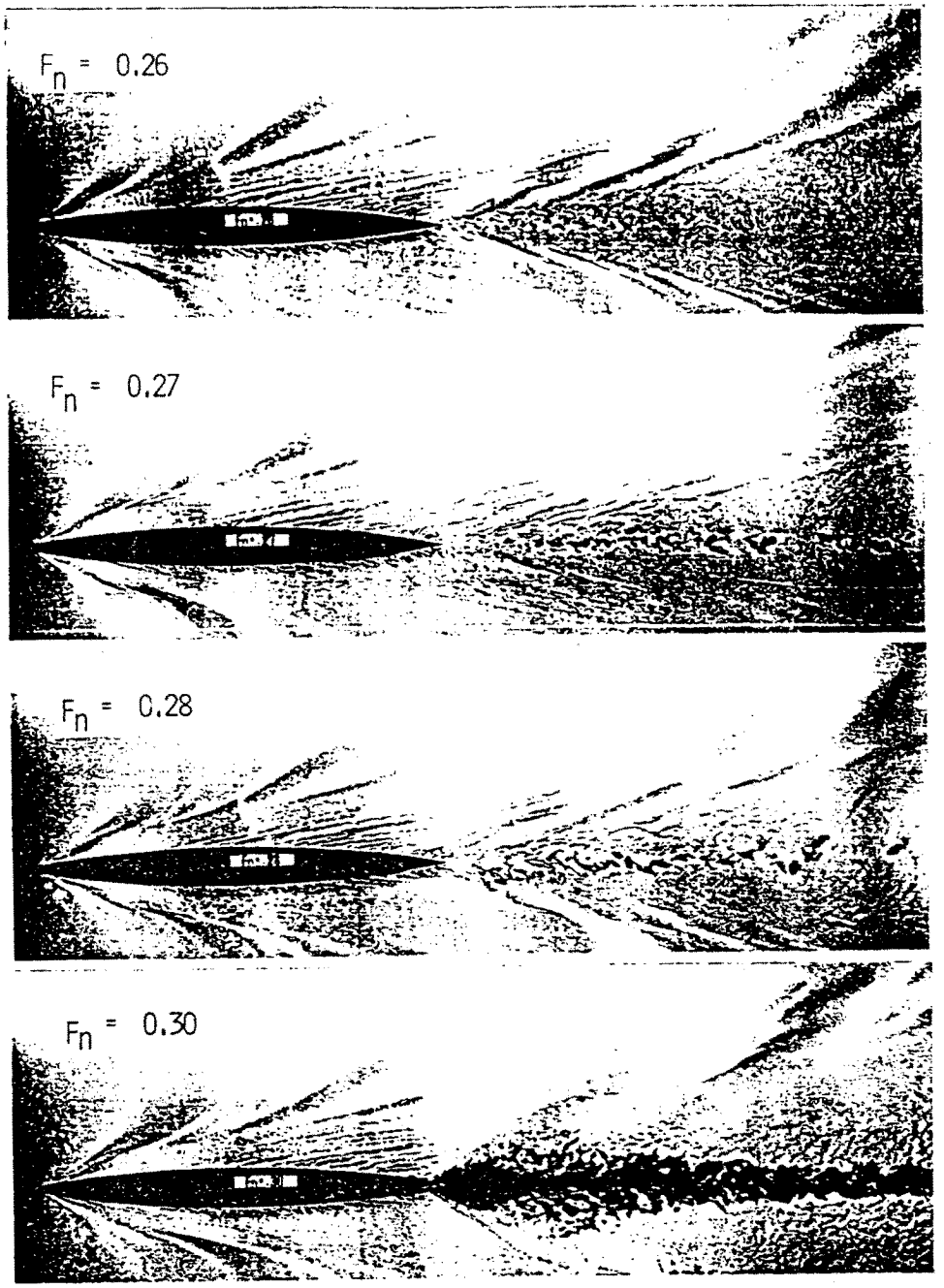

Fig. 1. Wave patterns of S-103 at four different Froude numbers

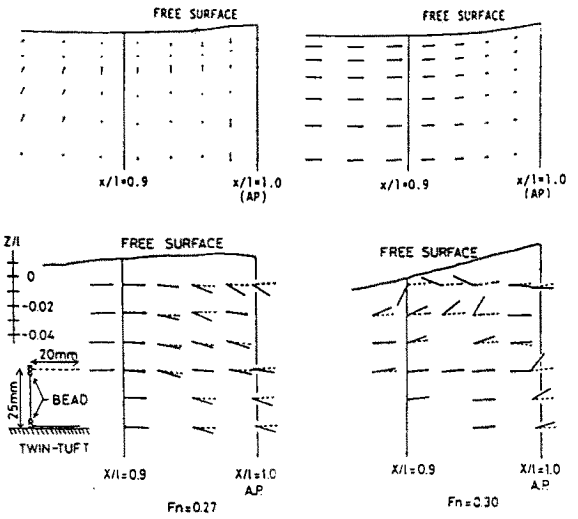

Fig. 2. Stern wave patterns of S-103 at $Rn=10^6$
(a) Fn=0.27
(b) Fn=0.28
(c) Fn=0.30
(Contour interval is $0.02x2g\zeta/U_o^2$ and dotted lines show negative values)

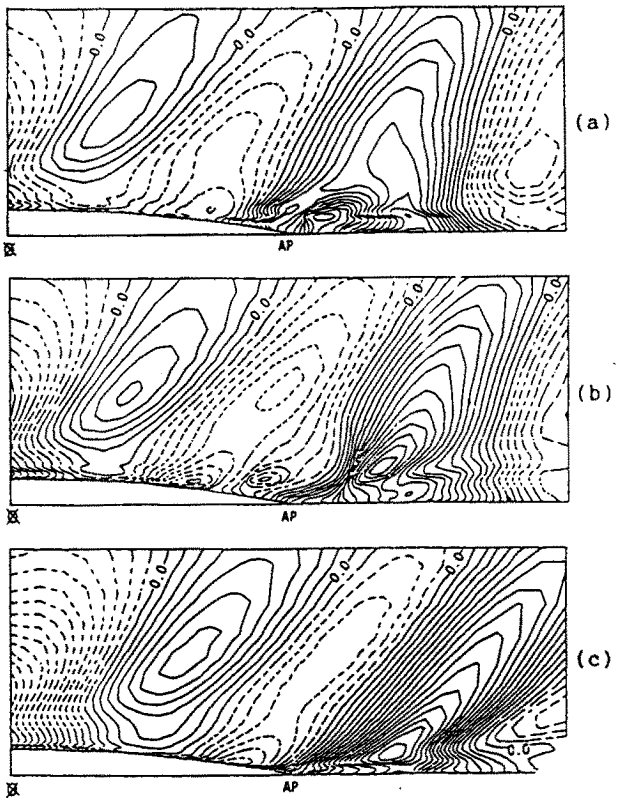

Fig. 3. Calculated (above) and observed (below) at Fn=0.27 and 0.30
limiting streamlines

flow at Froude number 0.27 moderates the stern wave generation. On the other hand, the scarcely separated flow at 0.30 generates an intensive stern wave enough to break.

We can conclude that the free-surface flow affects much on the viscous flows to change the stern wave phenomena eventually. It should be remembered that the methods used in [1] or [2] do not include the free-surface flow effects on the viscous flows.

References

[1] Mori, K.: "Prediction of Viscous Effects on Wave Resistance of Ship in Framework of Low Speed Wave Resistance Theory". Mem. of the Fac. of Eng. Hiroshima Univ., Vol. 7, No. 1, (1979), pp. 9-19.

[2] Tahara, Y., Stern, F., Rosen, B.: "An Interactive Approach for Calculating Ship Boundary Layers and Wakes for Nonzero Froude Number". 18th Symposium of Naval Hydrodynamics.

PS-1.2

L. CONG and C.C. HSIUNG
Centre for Marine Vessel Design and Research
Department of Mechanical Engineering
Technical University of Nova Scotia, Halifax, Nova Scotia, Canada

A SIMPLE METHOD OF COMPUTING WAVE RESISTANCE, WAVE PROFILE, AND SINKAGE AND TRIM OF TRANSOM STERN SHIPS

In evaluating the sinkage and trim of ships, Yeung [1] has already obtained good results by using the thin-ship theory, but these calculations were limited to ships without transom sterns. In Yim's work [2], the influence of the transom stern was investigated, but no sinkage and trim were considered. It is intended to predict the wave resistance, wave profile as well as sinkage and trim for surface ships with transom sterns by using a simple numerical method in this paper. The hull without the transom stern is approximated by a source system distributed on the center-plane as the thin-ship theory, while the transom stern is approximated by a sink line along the bottom edge of the transom stern based on Yim's work [2]. The third singularity system is distributed on the bottom of the overhang aftbody which is approximated by the flat-ship theory locally.

In the coordinate system as shown in Fig. 1 the perturbation potential of a ship can be written as

$$\phi(x,y,z)=\iint_S \sigma(x_0,y_0,z_0,)G(x,y,z;x_0,y_0,z_0)ds \quad (1)$$

where the Green function is defined in Newman's work [3].

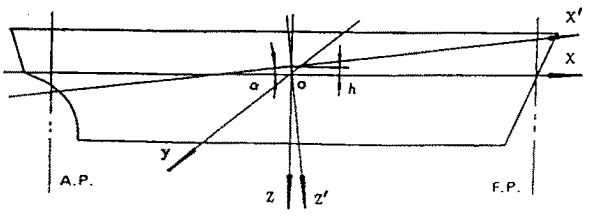

Fig. 1. Coordinate systems

By the thin-ship theory, strength of source distributed on the center-plane of a ship is

$$\sigma_M(x,z)=-\frac{C}{2\pi}f_x(x,z) \quad (2)$$

where C is constant ship speed, f(x,z) defines the local half-beam of the hull surface and can be expressed by the tent function as given by Ref. [4]. For a ship with a transom stern the derivative of the hull with respect to the ox-axis $f_x(x,z)$, is usually undefined on the bottom around the overhang aftbody near the stern, thus the thin-ship approximation fails at this local area. The so-called flat ship theory could be introduced to handle this case. Through a similar perturbation technique as in thin-ship theory, the sink strength on the bottom of the overhang aftbody can be determined as

$$\sigma_F=-\frac{C}{4\pi}d_x(x,y) \quad (3)$$

where $d_x(x,y)$ is the derivative of local draft d(x,y) with respect to the ox-axis.

To replace the transom stern itself, a sink line is distributed on the bottom edge of the stern. In terms of Yim's work [2], the strength of this sink line is:

$$\sigma_T=-\frac{C}{4\pi}Z_T \quad (4)$$

where Z_T is the transom stern draft.

Thus, the whole ship can be expressed in terms of three singularity systems: (1) a source system distributed on the center-plane which is discretized into a set of quadrilaterals, associated with a few triangular elements to improve the numerical accuracy, as shown in Fig. 2; (2) a sink plane on the bottom of the overhang aftbody; and (3) a sink line distributed along the bottom edge of the stern. Then the wave resistance can be found by

$$R=16\pi\rho k_0^2\int_0^{\infty}[P^2+Q^2]/\sqrt{1+u^2}\,du \qquad (5)$$

where $k_0 = g/C^2$, and the Kochin functions P and Q can be expressed as the sum of three terms for the ship center-plane panel sink distribution, bottom sink plane and transom sink line:

$$\begin{pmatrix} P \\ Q \end{pmatrix} = \sum_{i=1}^{M}\sum_{j=1}^{N}\begin{pmatrix} P_{ij} \\ Q_{ij} \end{pmatrix} + \begin{pmatrix} P_F \\ Q_F \end{pmatrix} + \begin{pmatrix} P_T \\ Q_T \end{pmatrix} \qquad (6)$$

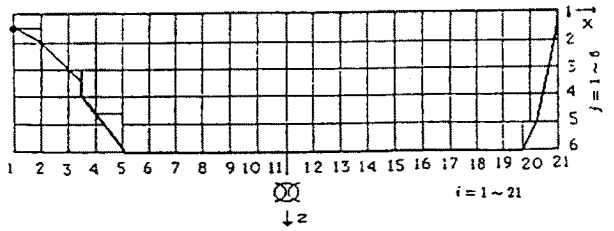

Fig. 2. Discretization of Center-Plane of DREA Model 316

Likewise, the total wave system can also be expressed by a summation of the contributions from center-plane panel elements, the bottom sink plane and the transom sink line:

$$\zeta=\sum_{i=1}^{M}\sum_{j=1}^{N}\zeta_{ij}+\zeta_F+\zeta_T \qquad (7)$$

Detailed analysis for wave resistance and wave profile computations is given in Ref. [5].

Based on the wave calculated above, the sinkage h and trim angle α can be obtained according to the static equilibrium principle as:

$$\begin{pmatrix} h+x_w\alpha \\ x_w h+\frac{\nabla}{A_w}H_p\alpha \end{pmatrix} = \frac{2}{A_w}\int_{-\frac{L}{2}}^{\frac{L}{2}}\begin{pmatrix} \zeta(x)f(x,0 \\ x\zeta(x)f(x,0) \end{pmatrix} dx \qquad (8)$$

where x_w is th x-coordinate of the center of flotation, A_w is the water-plane area, ∇ is the displacement volume and H_p is the longitudinal $\overline{GM}$ of the ship.

The effect of sinkage and trim on the wave resistance and wave profile should not be ignored, especially in the case that Froude number F_n is higher than 0.3. An iterative procedure has been used to deal with this problem. The offsets of the ship with fixed sinkage and trim have been used to determine the initial wave profile. Then, the sinkage h_1 and trim α_1 of the first iteration can be solved from equations (8) in terms of the wave system ζ_1. Thus, the new stern draft Z_{T1} can be found as:

$$Z_{T1}=Z_{T0}-[h_1+(\frac{L}{2}+x_w)\alpha_1] \qquad (9)$$

where the subscript "0" is for the parameters under the original condition, namely, the input data, and the subscript "1" denotes the parameters obtained from the first iteration. Then a new sink line with the strength, $-Z_{T1}C/4\pi$, will be used to calculate an additional wave system ζ_{T1}. By superpositioning ζ_1 and ζ_{T1}, the wave in the second iteration $\zeta_2 = (\zeta_1 - \zeta_{T0}) + \zeta_{T1}$ will be introduced into (8) again to obtain the sinkage h_2 and trim α_2. Moreover, the wave resistance coefficient c_{w2} can also be computed by including the effect of h_2 and α_2. This procedure can be continued until convergent

results for h_k and α_k are obtained. In practical calculation, two iterations already satisfy engineering requirements, thus h_2 and α_2 may be taken as the final results.

A computer program based on the aforementioned method has been developed to predict the wave resistance, wave profile, and sinkage and trim for ships with transom sterns. DREA Model 316 [6] and ATHENA Model [7] have been chosen for calculation. Computed wave resistance coefficients under the conditions of fixed and free to sinkage and trim are shown in Fig. 3 and Fig. 4. The wave profile of ATHENA Model is shown in Fig. 5, while the sinkage and trim of DREA Model 316 are shown in Fig. 6. The computational results have shown a good agreement with the experimental results.

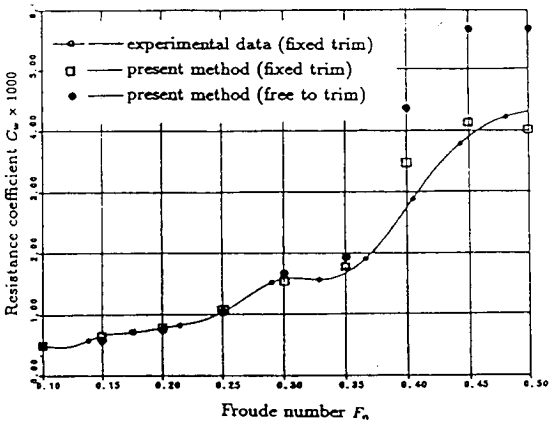

Fig. 3. Wave Resistance Coefficient of DREA Model 316

The mathematical model with three singularity systems represents a ship with transom stern to provide reasonable numerical results in predicting wave resistance, wave profile, sinkage and trim. The calculation based on this model can be carried out by a computer with a relatively little cpu time, for example: the total cpu time for computing the wave resistance, wave profile, sinkage and trim of DREA Model 316 with 100 panels in the center-plane for 9 Froude numbers (F_n = 0.1~0.5) is about 6.7 minutes on a VAX 785 computer. However, attention should be paid to the fact that the computed results are quite sensitive to the discretization of panels, particularly near the stern area of the bottom sink plane.

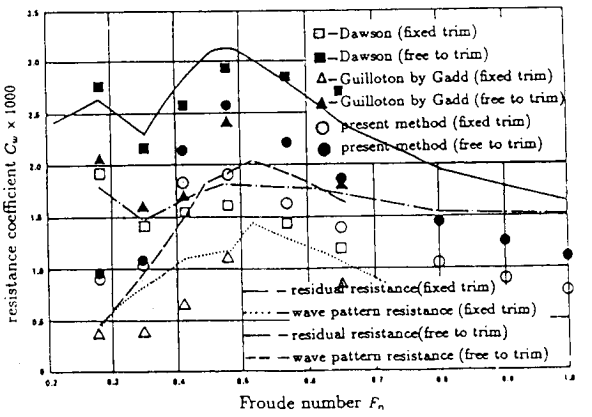

Fig. 4. Wave Resistance Coefficient of ATHENA Model

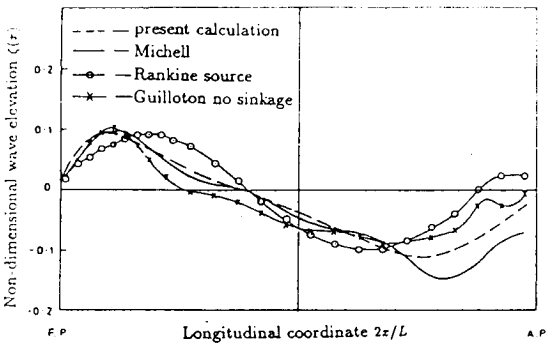

Fig. 5. Wave Profile for ATHENA Model (F_n = 0.48)

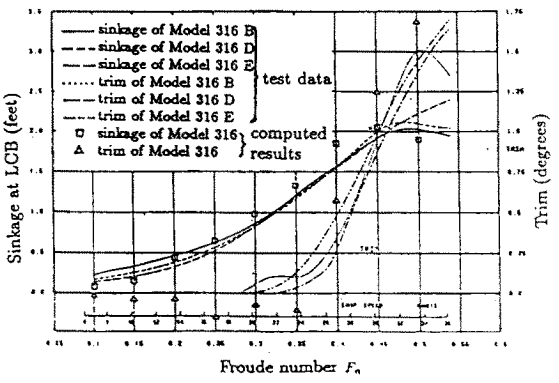

Fig. 6. Sinkage and Trim of DREA Model 316

ACKNOWLEDGEMENTS

The authors wish to thank the Natural Sciences and Engineering Research Council of Canada and the Defence Research Establishment Atlantic for the research support.

References

[1] Yeung, R.W., "Sinkage and Trim in First Order Thin Ship Theory", Journal of Ship Research, Vol.16, No. 1, March 1972.

[2] Yim, B., "Analyses of Waves and the Wave Resistance due to Transom-Stern Ships", Journal of Ship Research, Vol. 13, No. 2, June 1969.

[3] Newman, J.N., "Evaluation of the Wave-Resistance of the Green function: Part 1-the Double Integral" Journal of Ship Research, Vol. 31, No. 2, June 1987.

[4] Hsiung C.C., "Optimal Ship Forms for Minimum Wave Resistance", Journal of Ship Research, Vol. 25, No. 2, July 1981.

[5] Cong, L.Z. and Hsiung, C.C., "Computing Wave Resistance, Wave Profile, and Sinkage and Trim of Transom Stern Ships", Proceedings of The Third International Conference on Computer Aided Design, Manufacture and Operation in the Marine and Offshore Industry, in press, Florida, USA, January 1991.

[6] Murdey, D.C., "Resistance, Propulsion, and Seakeeping Experiments with Model 316, and Propellers 53L and 53R", NCR Report LTR-SH-265, February 1980, Limited Distribution.

[7] Proceedings of the Workshop on Ship Wave-Resistance Computations, Washington D.C., November 1979.

PS-1.3

YU XUEWEN*, LI SHIMO** and WU XIUHENG**

*Marine Design & Research Institute of China, Shanghai, P.R. China

**Wuhan University of Water Transportation Engineering, Wuhan, P.R. China

NUMERICAL ANALYSIS OF NONLINEAR SHIP WAVE RESISTANCE

Based on the new decomposition and order assumption for ship wavemaking potential, the nonlinear free surface conditions of ship wavemaking are analysed and simplified. A numerical calculation of nonlinear ship wave resistance is carried out for different ships by the coupled element method. An emphasis is laid on the discussion of relations between terms of free surface conditions and shipforms.

1. Introduction

As well known, the low speed ship theory, developed by Baba[1] ,Dawson[2] , Eggers[3] , gets great achievements in the recent decade. Especially Dawson's method is one of the most successful numerical methods in the nonlinear ship wave calculation. But there are two shortcomings in the method. One is that sources are distributed on finite free surface and the cutting-off effects are ignored. The cutting-off method lacks theoretical basis. Another one is that the free surface condition can not be calculated on plan z=0 but $z=\zeta_r$.

Recently we have done a theoretical and numerical test in order to overcome the two shortcomings. We assume that $\Phi = x + \varphi_r + \varphi_v$, where φ_r is double model disturbing potential and has order $\varphi_r = O(F_r^k)$, $K>1$, based on this assumption, the free surface conditions can be simplified and calculated on plan z=0. In order to overcome the cutting-off effects of distributing sources on finite free surface, we use the coupled element method to treat nonlinear ship wavemaking problem. First, we cut up the flow domain into two parts: internal part aroud body and external one far from body, then assume that the effects of free surface nonlinearity is important in the internal part, but negligible in the external one. We use finite element methhod to treat the nonlinear boundary value problems in the internal part, and boundary integral method for linear problem in the external one. Kelvin wave source function is used as the Green function of boundary integral method so that the difficulty of numerical treatment of radiation condition can be overcome. In the paper we carry out the calculations of ship wavemaking resistance for ship model Series 60(S60) and its modified models MS60, NS60 and get many useful results.

2. Analysis and Simplification of Free Surface Condition

§2.1 the representation of boundary value problem for wavemaking potential

The coordinate system is shown in Fig.1. By means of coming flow speed U, ship lenghth L, we can nondimensionalized the coordinates and relative variables. Froude number is $F_r = U/\sqrt{gL}$.

We write the total velocity potential Φ as a sum of uniformed coming flow

potential x and disturbing potential φ :

$$\Phi = x + \varphi(x,y,z) \tag{1}$$

thus, φ must satisfy following conditions:

$$\nabla^2\varphi = 0 \qquad \text{in D} \tag{2}$$

$$\eta + F_r^2\left(\frac{\partial\varphi}{\partial x} + \frac{1}{2}\nabla\varphi\cdot\nabla\varphi\right) = 0 \qquad z = \eta(x,y) \tag{3}$$

$$\frac{\partial\eta}{\partial x} + \frac{\partial\varphi}{\partial x}\cdot\frac{\partial\eta}{\partial x} + \frac{\partial\varphi}{\partial y}\cdot\frac{\partial\eta}{\partial y} - \frac{\partial\varphi}{\partial z} = 0 \qquad z = \eta(x,y) \tag{4}$$

$$\frac{\partial\varphi}{\partial n} = -n_x \qquad \text{on } S_B \tag{5}$$

$$\varphi = \begin{cases} O\left(1/\sqrt{x^2+y^2}\right) & x<0 \\ & \text{for } x^2+y^2 \to \infty \\ O(1) & x>0 \end{cases} \tag{6}$$

§2.2 the simplification of free surface conditions

We substitute (3) into (4) and neglect the terms of order higher than the square of derivative of φ:

$$\frac{\partial\varphi}{\partial z} + F_r^2\frac{\partial^2\varphi}{\partial x^2} + 2F_r^2\nabla\varphi_x\cdot\nabla\varphi = 0 \qquad z = \eta(x,y) \tag{7}$$

If we neglect the nonlinear terms in (7) and the free surface condition is satisfied on z=0:

$$\frac{\partial\varphi}{\partial z} + F_r^2\frac{\partial^2\varphi}{\partial x^2} = 0 \qquad z=0 \tag{8}$$

formula (8) is linear free surface condition.
In formula (7) we use Taylor expansion and neglect the square terms:

$$\frac{\partial\varphi}{\partial z} - F_r^2\frac{\partial\varphi}{\partial x}\cdot\frac{\partial^2\varphi}{\partial z^2} + F_r^2\cdot\frac{\partial^2\varphi}{\partial x^2} - F_r^4\frac{\partial\varphi}{\partial x}\cdot\frac{\partial^3\varphi}{\partial x^2\partial z} + 2F_r^2\nabla\varphi_x\cdot\nabla\varphi = 0 \qquad z=0 \tag{9}$$

We let:

$$\varphi = \varphi_r + \varphi_w \tag{10}$$

Where φ_r is double model disturbing potential, φ_w is wave disturbing potential.
we assume:

$$(1)\quad \left|\frac{\partial\varphi_r}{\partial x_i}\right| = O(F_r^k), \quad \frac{\partial}{\partial x_i} = O(1) \qquad \text{for } \varphi_r,\ i=1,2,3$$

$$(2)\quad \varphi_w = O(F_r^n), \quad \frac{\partial}{\partial x_i} = O(F_r^{-2}) \qquad \text{for } \varphi_w,\ i=1,2,3$$

substituting (10) into (9), we discuss the orders of terms under the condition of low speed ship, so that we can neglect the terms with higher

order F_r^{n+k} and F_r^{2n-4} . Taking the symbol v away from φ_v , finally we get the free surface condition:

$$\frac{\partial\varphi}{\partial z} + F_r^2\frac{\partial^2\varphi}{\partial x^2} + 3F_r^2\frac{\partial\varphi_r}{\partial x}\cdot\frac{\partial^2\varphi}{\partial x^2} + 2F_r^2\frac{\partial\varphi_r}{\partial y}\cdot\frac{\partial^2\varphi}{\partial x\,\partial y} + F_r^2\frac{\partial\varphi_r}{\partial x}\cdot\frac{\partial^2\varphi}{\partial y^2}$$

$$- F_r^4\frac{\partial\varphi_r}{\partial x}\cdot\frac{\partial^3\varphi}{\partial x^2\partial z} + F_r^2\frac{\partial^2\varphi_r}{\partial x^2} + 3F_r^2\frac{\partial\varphi_r}{\partial x}\cdot\frac{\partial^2\varphi_r}{\partial x^2}$$

$$+ 2F_r^2\frac{\partial\varphi_r}{\partial y}\cdot\frac{\partial^2\varphi_r}{\partial x\partial y} + F_r^2\frac{\partial\varphi_r}{\partial x}\cdot\frac{\partial^2\varphi_r}{\partial y^2} = 0 \quad , \qquad z = 0 \qquad (11)$$

In (11) there are three terms that do not appear in the other slow ship free surface conditions:

$$- F_r^4\frac{\partial\varphi_r}{\partial x}\cdot\frac{\partial^3\varphi}{\partial x^2\partial z} + F_r^2\frac{\partial\varphi_r}{\partial x}\cdot\frac{\partial^2\varphi}{\partial y^2} + F_r^2\frac{\partial\varphi_r}{\partial x}\cdot\frac{\partial^2\varphi_r}{\partial y^2}$$

These three terms come free the expansion of the potential φ on plan z=0, so we give an emphasis about the relations between them and shipforms in the numerical calculations.

3. the Coupled Element Method for Nonlinear Ship Wavemaking Problem

First we cut up the flow domain into internal part around body and external one far from body. We assume that nonlinearity of free surface is important in the internal region but negligible in the external one. The finite element method is used to treat nonlinear problem, and boundary integral is used to represent the velocity potential in the external region.

The cutting of flow domain is shown in Fig.1. D_1 is internal region, its boundary is $S_1 = S_B + S_{F1} + S_j$. D_2 is external region, its boundary is $S_2 = S_j + S_{F2} + S_\omega$.

The velocity potential φ_1 in D_1 must satisfy the formula (2), (5), (11). The velocity potential φ_2 in D_2 must satisfy the formula (2), (6), (8). On S_j φ_1 and φ_2 must satisfy the following matching conditions:

$$\varphi_1 = \varphi_2 \qquad \text{on } S_j \qquad (12)$$

$$\frac{\partial\varphi_1}{\partial n} = -\frac{\partial\varphi_2}{\partial n} \qquad \text{on } S_j \qquad (13)$$

§3.1 the boundary integral for φ_2

In D_2 the boundary intergral is used for velocity potential φ_2:

$$\varphi_2(P) = \iint_{S_2}\left(\frac{\partial G}{\partial n}\varphi_2 - \frac{\partial\varphi_2}{\partial n}G\right)ds$$

$$= \iint_{S_j+S_{F2}+S_\omega}\left(\frac{\partial G}{\partial n}\varphi_2 - \frac{\partial\varphi_2}{\partial n}G\right)ds \qquad P \in D_2 \qquad (14)$$

By means of the characters of G and φ_2 and matching conditions, (14) can be written as:

$$\frac{\alpha\,\varphi_1(p)}{4\pi} + \iint_{S_j} \frac{\partial G}{\partial n}\,\varphi_1\,ds - F_r^2 \int_{L_1+L_2} \frac{\partial G}{\partial n}\,\varphi_1\,dy$$

$$= \iint_{S_j} G\,\frac{\partial \varphi_1}{\partial n}\,ds - F_r^2 \int_{L_1+L_2} G\,\frac{\partial \varphi_1}{\partial n}\,dy \qquad P \in S_j \qquad (15)$$

Where α is a solid angle at P. In the finite element method φ_1 and $\frac{\partial \varphi_1}{\partial n}$ are represented as:

$$\varphi_1 = \sum_{i=1} \varphi_{1i}\,N_i \quad , \quad \frac{\partial \varphi_1}{\partial n} = \sum_{i=1} \left(\frac{\partial \varphi_1}{\partial n}\right)_i \cdot N_i$$

Substituting the above representations into (14), we can establish equation at every node. Because Kelvin source function has no definition when $z+z_0=0$, we encounter the difficulty of line integral on the free surface. Based on the characteristics of line integral road, free surface condition and continuity condition, the additional equations are obtained to close the equation group.
Thus (15) can be written as:

$$[A][\varphi_1] = [B]\left[\frac{\partial \varphi_1}{\partial n}\right] \qquad (16)$$

Where $\left[\frac{\partial \varphi_1}{\partial n}\right] = [C][\varphi_1] \qquad [C] = [B]^{-1}[A]$

§3.2 the treatment of nonlinear problem in D_1

The free surface condition and body surface condition can be written as:

$$\frac{\partial \varphi}{\partial z} = \frac{\partial \varphi}{\partial n} = f_1(x,y) \qquad z=0 \qquad (17)$$

$$\frac{\partial \varphi}{\partial n} = f_2(x,y,z) \qquad \text{on } S_B \qquad (18)$$

For the linear ship wave problem: $f_1 = -F_r^2 \frac{\partial^2 \varphi}{\partial x^2}$, $f_2 = -n_x$; for the nonlinear ship wave problem f_1 can be obtained from (11) and $f_2=0$.
According to Galerkin method, for all N_i, φ_1 must satisfy the following formula:

$$\iiint_{D_1} \nabla^2 \varphi_1\,N_i\,dv = 0 \qquad (19)$$

Based on the Green theorem (19) can be written as:

$$\iiint_{D_1} \nabla\varphi_1 \cdot \nabla N_i\,dv - \iint_{S_j} \frac{\partial \varphi_1}{\partial n}\,N_i\,ds - \iint_{S_B} f_2(x,y,z)\,N_i\,ds$$

$$- \iint_{S_{F1}} \frac{\partial \varphi_1}{\partial z}\,N_i\,dxdy = 0 \qquad (20)$$

For the nonlinear problem: $f_2 = 0$, $f_1 = g_1(x,y) + g_2(x,y)$

$$g_1(x,y) = -F_r^2 \left[\frac{\partial^2 \varphi_r}{\partial x^2} + 3 \frac{\partial \varphi_r}{\partial x} \frac{\partial^2 \varphi_1}{\partial x^2} + 2 \frac{\partial \varphi_r}{\partial y} \frac{\partial^2 \varphi_1}{\partial x \partial y} + \frac{\partial \varphi_r}{\partial y} \frac{\partial^2 \varphi_1}{\partial y^2} - F_r^2 \frac{\partial \varphi_r}{\partial x} \frac{\partial^3 \varphi_1}{\partial x^2 \partial z} \right] \quad (21)$$

$$g_2(x,y) = -F_r^2 \left[\frac{\partial^2 \varphi_r}{\partial x^2} + 3 \frac{\partial \varphi_r}{\partial x} \frac{\partial^2 \varphi_r}{\partial x^2} + 2 \frac{\partial \varphi_r}{\partial y} \frac{\partial^2 \varphi_r}{\partial x \partial y} + \frac{\partial \varphi_r}{\partial y} \frac{\partial^2 \varphi_r}{\partial y^2} \right] \quad (22)$$

Thus (22) becomes:

$$\iiint_{D_1} \nabla\varphi_1 \cdot \nabla N_i \, dv - \iint_{S_j} \frac{\partial \varphi_1}{\partial n} N_i \, ds - \iint_{SF_1} g_1(x,y) N_i \, dxdy = \iint_{SF_1} g_2(x,y) N_i \, dxdy \quad (23)$$

According to the matching conditions, on S_j we has:

$$\frac{\partial \varphi_1}{\partial n} = \sum_{j=1} \sum_{k=1} C_{jk} \varphi_{1k} N_j \quad (24)$$

Finally (23) can be written as:

$$[A_1 + B_1][\varphi_1] = [P_1] \quad (25)$$

Where the elements a_{1ij} of matrix A_1 are:

$$a_{1ij} = \iiint_{D_1} \nabla N_i \cdot \nabla N_j \, dv + F_r^2 \iint_{SF_1} \left[-\frac{\partial N_i}{\partial x} \frac{\partial N_j}{\partial y} - 3 \frac{\partial N_j}{\partial x} \left(\frac{\partial^2 \varphi_r}{\partial x^2} N_i + \frac{\partial \varphi_r}{\partial x} \frac{\partial N_i}{\partial x} \right) - 2 \frac{\partial N_j}{\partial y} \left(\frac{\partial^2 \varphi_r}{\partial x \partial y} N_i + \frac{\partial \varphi_r}{\partial y} \frac{\partial N_i}{\partial x} \right) - \frac{\partial N_j}{\partial y} \left(\frac{\partial^2 \varphi_r}{\partial x \partial y} N_i + \frac{\partial \varphi_r}{\partial x} \frac{\partial N_i}{\partial y} \right) + F_r^2 \frac{\partial^2 N_j}{\partial x \partial z} \left(\frac{\partial^2 \varphi_r}{\partial x^2} N_i + \frac{\partial \varphi_r}{\partial x} \frac{\partial N_i}{\partial x} \right) \right] dxdy + F_r^2 \int_{LB} \left[\frac{\partial N_j}{\partial x} N_i + 3 \frac{\partial \varphi_r}{\partial x} \frac{\partial N_j}{\partial x} N_i + 2 \frac{\partial \varphi_r}{\partial y} \frac{\partial N_j}{\partial y} N_i - F_r^2 \frac{\partial \varphi_r}{\partial x} \frac{\partial^2 N_j}{\partial x \partial z} N_i \right] dy + F_r^2 \int_{LB} \frac{\partial \varphi_r}{\partial x} \frac{\partial N_j}{\partial y} N_i \, dx + F_r^2 \int_{L_2} \left[2 \frac{\partial \varphi_r}{\partial y} \frac{\partial N_j}{\partial y} N_i - F_r^2 \frac{\partial \varphi_r}{\partial x} \frac{\partial^2 N_j}{\partial x \partial z} N_i \right] dy + F_r^2 \int_{L_1} \left[-2 \frac{\partial \varphi_r}{\partial y} \frac{\partial N_j}{\partial y} N_i + F_r^2 \frac{\partial \varphi_r}{\partial x} \frac{\partial^2 N_j}{\partial x \partial z} N_i \right] dy \quad (26)$$

The matrix B_1 represents the matching conditions, its elements b_{1ij} are:

$$b_{1ij} = -\iint_{S_j} N_i \sum_{k=1} N_k C_{kj} \, ds + F_r^2 \int_{L_1+L_2} N_i \sum_{k=1} N_k C_{kj} \, dy + 3F_r^2 \int_{L_1+L_2} \frac{\partial \varphi_r}{\partial x}$$

$$N_i \sum_{k=1} N_k C_{kj}\, dy + F_r^2 \int_{L3} \frac{\partial \varphi_r}{\partial y} N_i \sum_{k=1} N_k C_{kj}\, dx \qquad (27)$$

The elements p_{i1} of the known vector P_i are:

$$p_{i1} = -F_r^2 \iint_{SF1} \left(\frac{\partial^2 \varphi_r}{\partial x^2} + 3 \frac{\partial \varphi_r}{\partial x} \frac{\partial^2 \varphi_r}{\partial x^2} + 2 \frac{\partial \varphi_r}{\partial y} \frac{\partial^2 \varphi_r}{\partial x \partial y} + \frac{\partial \varphi_r}{\partial y} \frac{\partial^2 \varphi_r}{\partial y^2} \right) N_i\, dxdy \qquad (28)$$

φ_{i1} on every node in D_i can be obtained by solving equation (25).

4. the Analysis and Discussion of Numerical Results

In the paper, the calculations of nonlinear wave resistance are carried out for Model Series 60(C_b=0.60) and its modified model MS60(C_b=0.625), NS60(C_b=0.614). In order to investigate the relations between the terms of the free surface condition and shipforms, we use 4 programs for the numerical calculations. The free surface condition of program 1 is the complete formula (11). The free surface condition of program 2 excludes $\frac{\partial \varphi_r}{\partial x} \frac{\partial^3 \varphi}{\partial x^2 \partial z}$ in (11). The program 3 excludes $\frac{\partial \varphi_r}{\partial y} \frac{\partial^2 \varphi}{\partial y^2}$, the program 4 excludes $\frac{\partial \varphi_r}{\partial x} \frac{\partial^3 \varphi}{\partial x^2 \partial z}$ and $\frac{\partial \varphi_r}{\partial y} \frac{\partial^2 \varphi}{\partial y^2}$

The wave resistance is calculated by the method of surface pressure integral.

The model S60, MS60, NS60 are shouwn in Fig.2. The comparision between numerical results of differert programs and test results is shown in Fig.3. Fig.4 and Fig.5 give numerical results respectively for MS60 and NS60. Fig.6, 7, 8, 9 represent the differences of numerical results of four programs because of the changes of forebodies. According to these comparisions, we can conclude:

a, For model S60, the numerical results of program 1 is closer to test results than ones of other programs. It indicates that the nonlinear free surface condition with complete formula (11) can better simulate nonlinear ship wavemaking of models such as S60.

b, There are comparitive differences among the results of different programs. For the model MS60, NS60 with fuller forebodies the difference are more obvious.

REFERENCES

[1] Baba E. & Takekama K., A Study on Free-Surface Flow Around Bow of Slowly Moving Full Forms, JSNAJ, Vol,.137, 1975

[2] Dawson C. W., A Practical Computer Method for Solving Ship-Wave Problem, 2nd ICNSH, 1977

[3] Eggers K., Non-Kelvin Dispersive Waves Around Non-Slender Ships, Schiffstenchnik, 1981

[4] Shen H. T. & Farell C., Numerical Calculation of Wave Integrals in the Linearized Theory of Water Waves, JSR, Vol.21, 1977

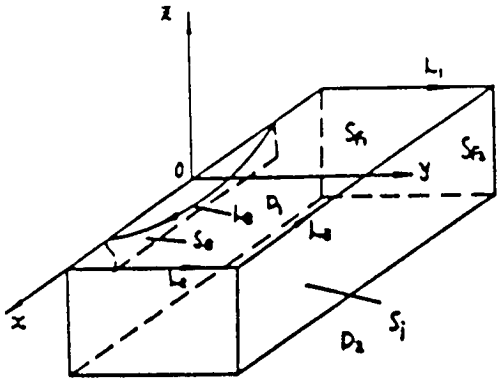

Fig.1 Coordinate System and Flow Domain Cutting

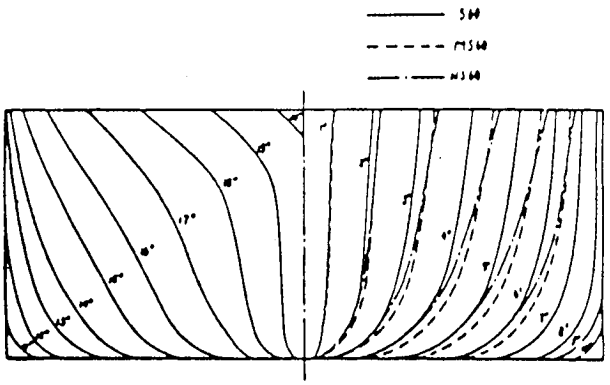

Fig.2 Ship Model S60, MS60, NS60

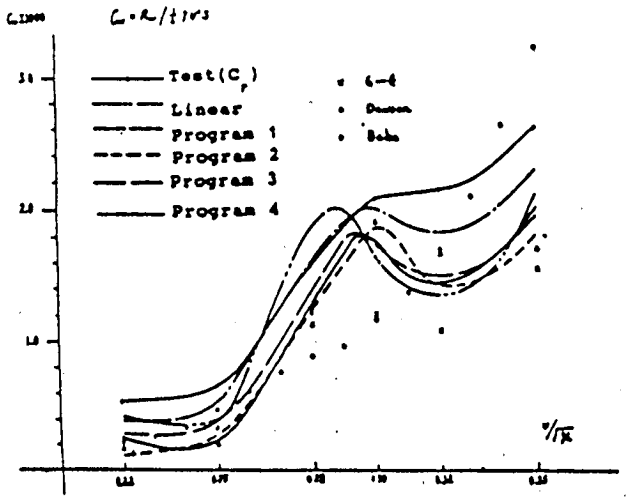

Fig.3 Numerical Results for Model S60

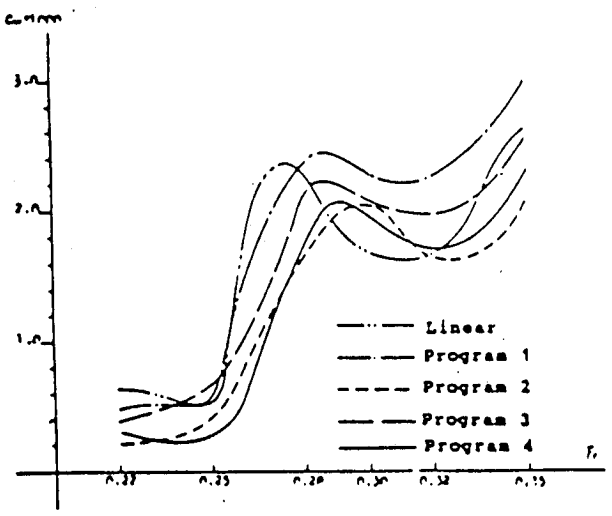

Fig.4 Numerical Results for Model MS60

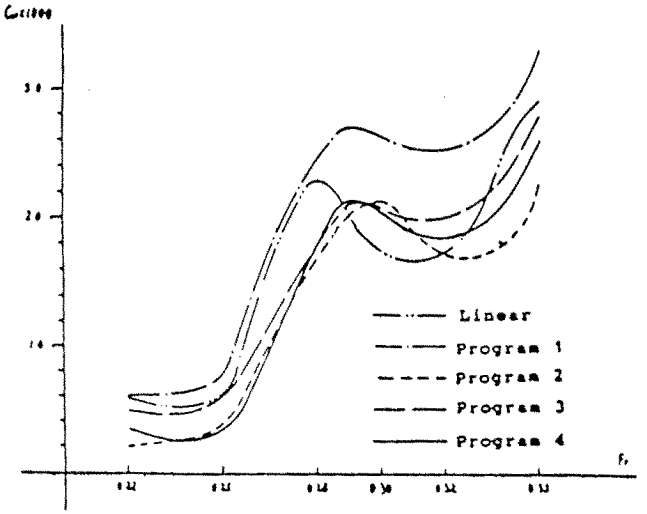

Fig.5 Numerical Results for Model NS60

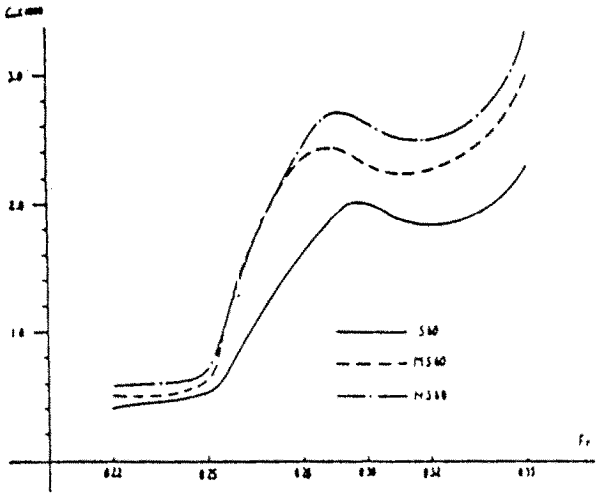

Fig.6 Results for Different Models(Program 1)

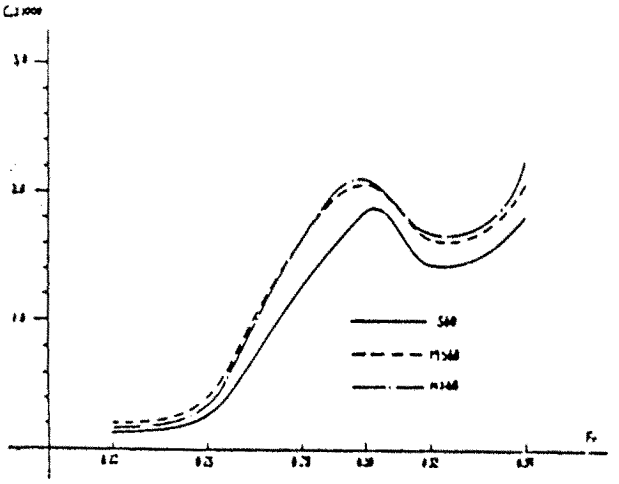

Fig.7 Results for Different Models(Program 2)

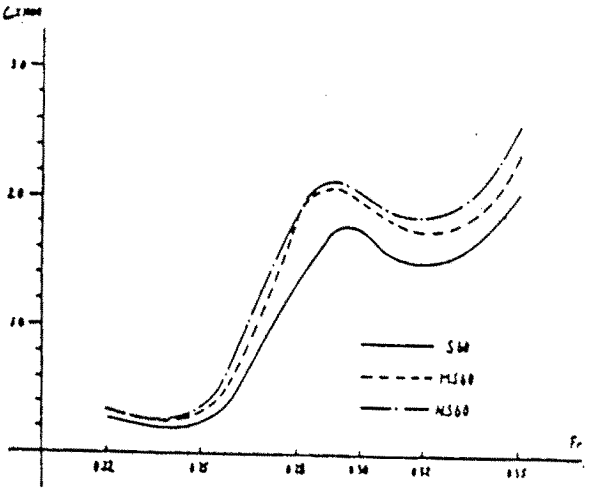

Fig.8 Results for Different Models(Program 3)

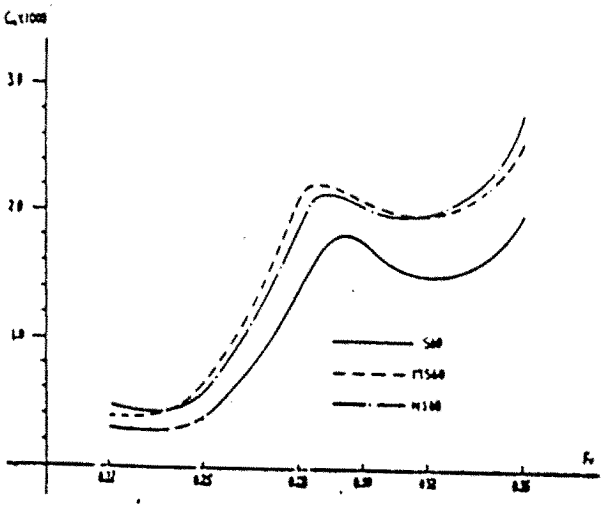

Fig.9 Results for Different Models(Program 4)

PS-1.4

G.M. BAILO*
G. CAPRINO**

*Italian Navy, C.E.I.M.M.
**CETENA

DETERMINATION OF THE VISCOUS WAKE OF A SUBMERGED BODY WITH COMPUTATIONAL FLUID DYNAMIC CALCULATIONS AND EXPERIMENTAL MEASUREMENTS

ABSTRACT

In this memory a viscous flow calculation of a submerged body is presented, determined through computational fluid dynamics (CFD) and compared also with experimental trials conducted at the Rome Towing Tank.

Good quality results have been obtained in the comparison between potential, viscous and experimental data.

1. INTRODUCTION

The Italian Navy (C.E.I.M.M.), in collaboration with INSEAN (Rome Towing Tank) and CETENA, Genova, has conducted a comparation study of the induced pressures on the hull of a submerged body, estimated with computational fluid dynamic (CFD) calculations by CETENA and measured with experimental trials by INSEAN.

2. EXPERIMENTAL TESTS

The model of the submerged body, in LAMBDA = 12.5 scale, made in P.V.C. and 5.77 mt. long, has been fitted with 82 measuring points, placed in order to measure the pressure in the most significant locations and also with a certain grade of graduality.

The towing runs at deep depth have been conducted in a range of Rn from 3.88 * 10^6 to 20.41 * 10^6 (Fn = 0.08/0.16/0.40).

The pressure on the submerged body is measured through differential pressure transducers, with a static referring pressure installed inside the hull.

The measured pressures have been converted in pressure coefficient

$$C_p = \frac{\Delta P}{0.5 \varrho V^2}$$

The good quality of the measurements has been supported by the ripetivity of the measures in different days and runs and also by the coincidence of the Cp values for all three Fn, as the pressure is proportional with the square of the velocity.

3. MATHEMATICAL MODEL

The mathematical model that describes the flow around a hull cannot be general and univocal, but the flow calculations must be modified as we move from the bow to the stern, with different simplifications of the Navier-Stokes equations.

Referring to a viscous fluid, the flow field around a body can be summarized as in Fig. 1, where we can

notice three different areas:

a. non viscous zone, with potential flow
b. thin boundary layer zone
c. thick boundary layer zone and wake

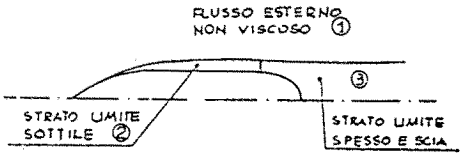

Fig. 1.

In the first area, the calculation procedures do not consider the real viscous fluid and the flow far away from the hull can be determined, as there the viscous phenomena can be negliged.

In the second area, the so called "thin boundary layer zone", calculations have been conducted along with the 3-D Cebeci procedures. This simplification consists mainly of the fact that the Navier-Stokes equations are solved considering the fluid inside the boundary layer as bidimensional: this assumption reduces considerably the computational ti ne, but is not adequate in the stern region.

In the third and final area, there are large calculation difficulties as we are regarding a thick boundary layer, so that some of the previous assumptions are no longer valid. Therefore the Spalding elliptic algorithm, inside the PHOENICS code, has been adopted in order to solve the equations, in the integral form, all over the computation domain.

The CFD calculations have been conducted through the following steps:

a. Grid of the submerged body

Just half of the hull has been described with different types of grid depending on the ubication, but all sections with constant x (Fig. 2)

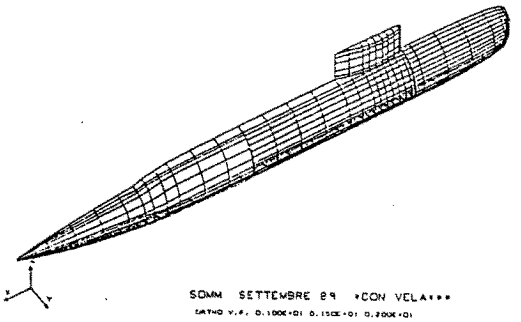

Fig. 2.

b. Boundary condition determination, using potential flow theory.

The computational method that has been used is the traditional Hess-Smith system, with approximative solutions of the integral equation along the body surface; the discretization consist mainly in substituting the punctiform sources with superficial constant intensity sources. The computational code is the so-called FLUPOT, elaborated by CETENA for non viscous fluid.

As a result of this work, the three local velocity components and the local pressure coefficient Cp have been obtained (Figs. 3 and 4).

With appropriate interpolation, the previous data have been calculated in the experimental measuring points, in order to achieve a comparison capability.

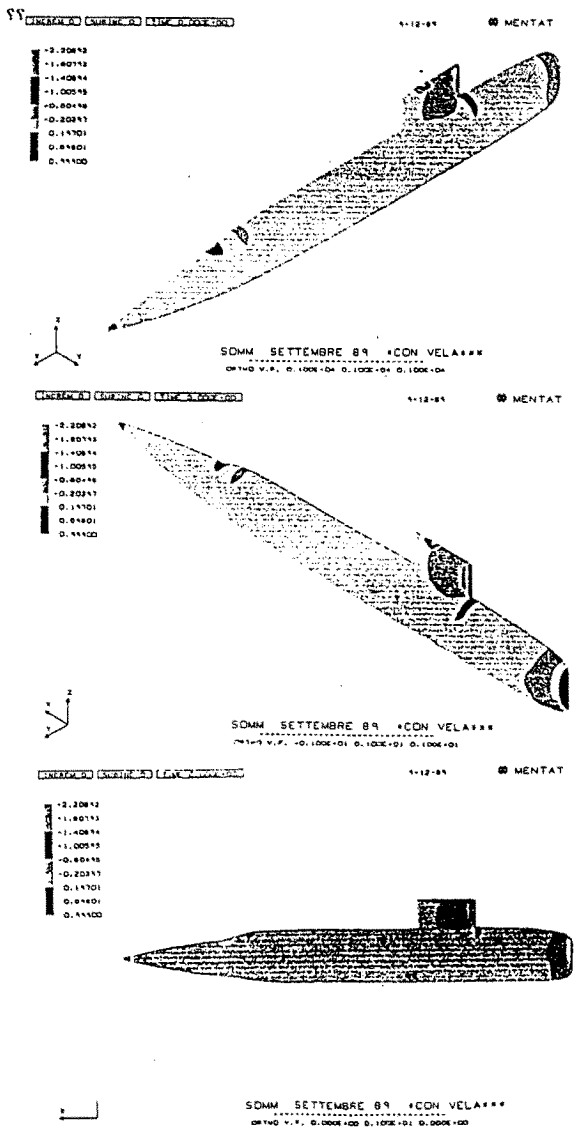

Fig. 3.

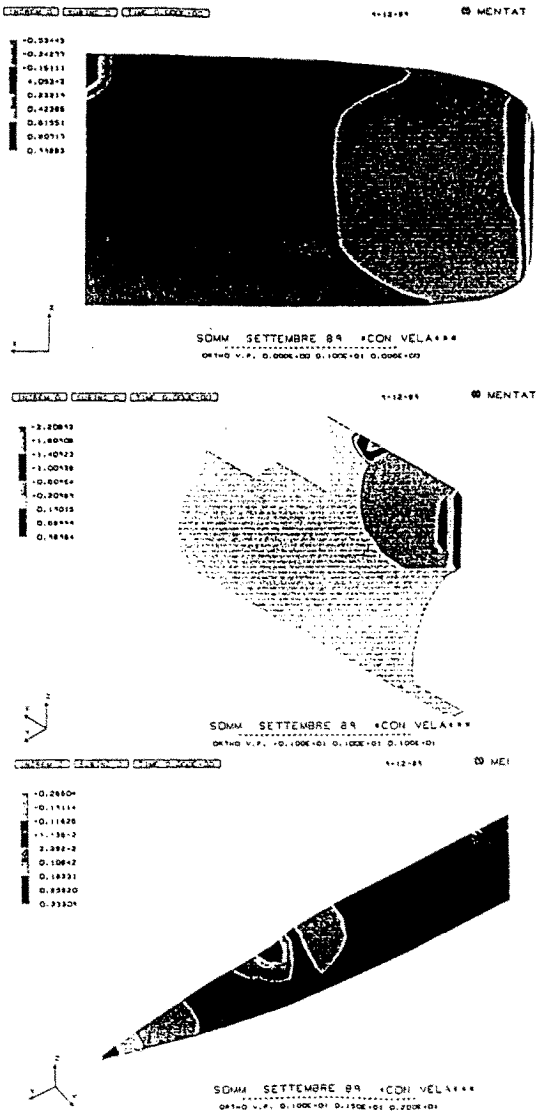

Fig. 4.

c. Experimental data vs. potential flow data.

Along with the previous step, it has been possible to make a comparison, in terms of Cp, between the experimental data and the potential flow computational results. In Figs. 5, 6 and 7, for a specific transverse section, Cp values vs. girth are displayed while in Figs. 8.9 and 10 the same data are presented longitudinally, for constant girth.

The remarks that come along with the previous graphs are univocal and:

- there is a good quality correlation, section by section, between theory and experiments.
- the experimental values are, generally, higher than the potential flow calculation, of a constant DELTA Cp value.

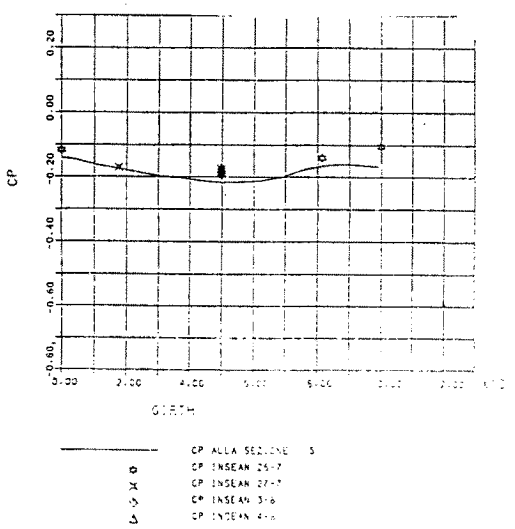

Fig. 5.

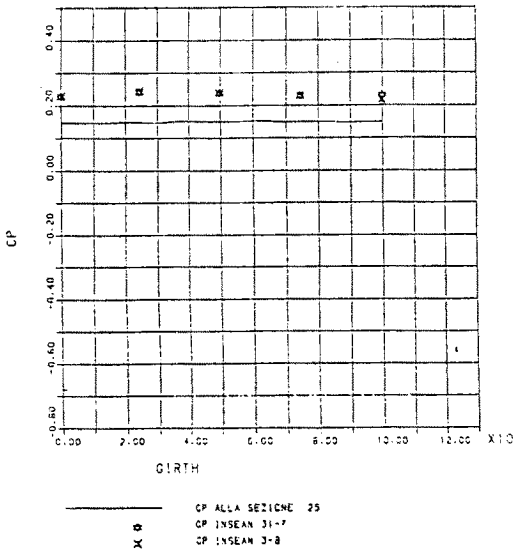

Fig. 6.

d. Thin boundary layer calculations

A differential method has been used, in order to solve the Navier–Stokes equations (partially simplified) through finite difference (FD) methods. The Cebeci proposed solution has been adopted along with the so–called Bound P0 and Bound P3 codes, elaborated by CETENA.

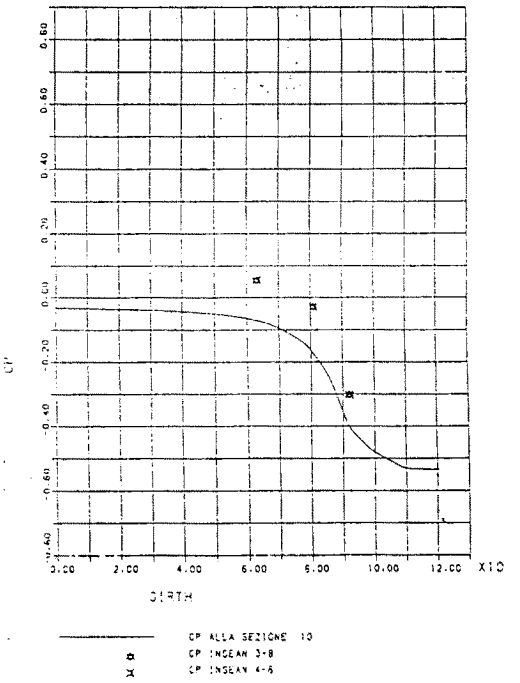

Fig. 7.

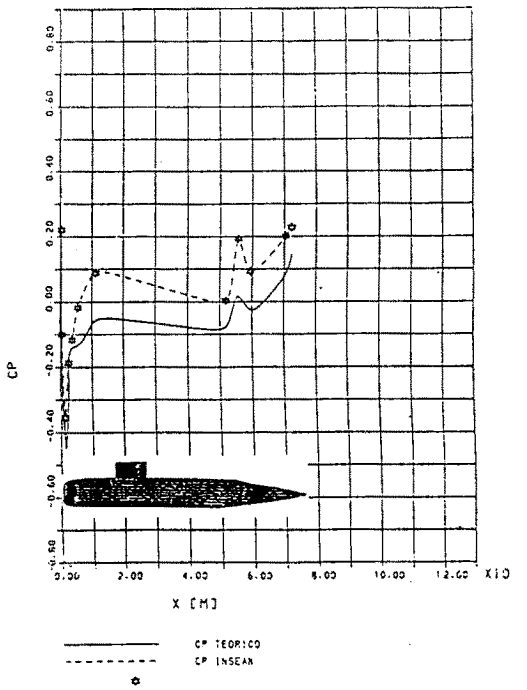

Fig. 8.

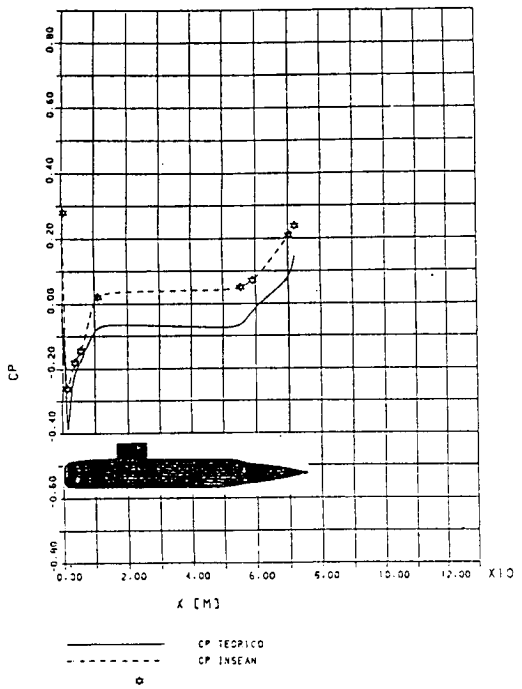

Fig. 9.

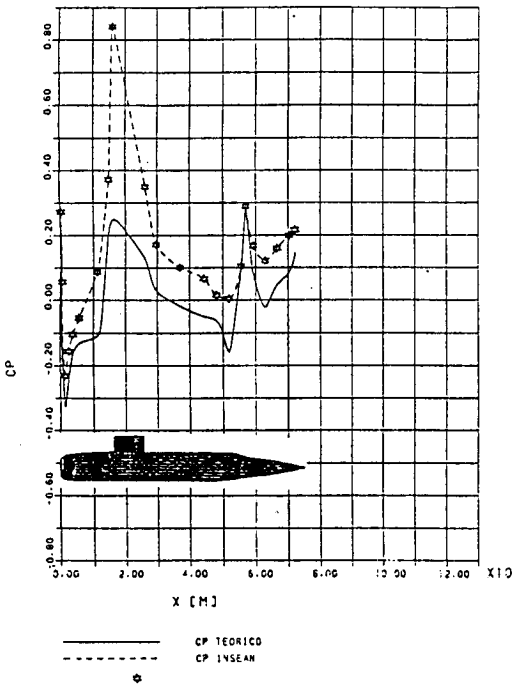

Fig. 10.

The first code, Bound P0, creates a dense grid on the hull, calculating hl, h2, k12, k21, k1 and k2 in the nodes and also the local velocity components. It is essential, in this stage, to adopt a narrow interpolation step, in order to obtain a number of sections above one hundred.

The second code, Bound P3, using the output data of Bound P0, calculates, along with Cebeci assumptions, all the thin boundary layer parameters as:

Cfs	viscous resistance coefficient
H11	form factor
beta	cross–flow angle
Us	velocity components, inside the thin boundary layer.

Some of the previous parameters are graphically displayed for certain steamlines as n.1 (upper part of the hull), n.3 (influence of the sail), n.13 (lower part of the hull): in Fig. 11 we can see the viscous resistance coefficient versus x, longitudinal length.

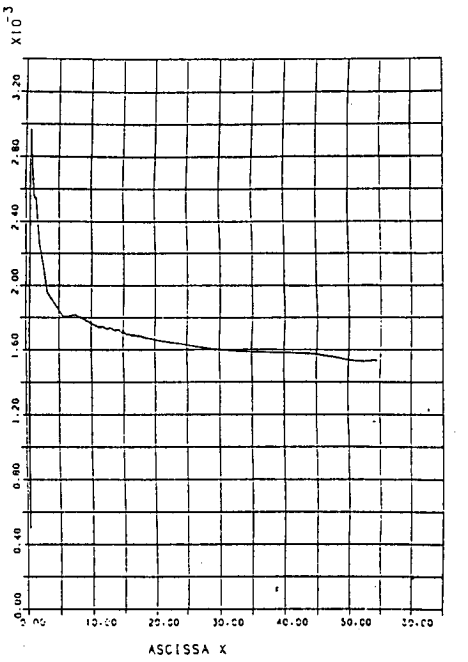

Fig. 11.

e. Hydrodynamic noise, in turbulent flow

Noise in water is very important either for surface ships, either for submerged vessels, as it can make the hull easily identifiable and can obscure the self-detection capability. The noise power level in water is rather low but this does not mean that it is without consequences; as a matter of fact, high acoustic pressures are associated with low power levels and, as the detection systems respond to pressure, the pressure is the parameter that must be calculated.

The noise we are dealing with, is the noise that is confined inside the boundary layer and is called turbulent flow noise.

The used method takes cue from the measurements made by Blake, where the wall pressure spectrum density function $\phi(w)$ is presented. CETENA has elaborated a noise code, the so-called RUMORE code, for determining the cut-off frequency w and the noise level.

The input data are the pressure coefficient Cp (already available through potential calculations) and the displacement thickness (available from the thin boundary layer computations). In output we obtain, among other data:

w cut-off frequency
L noise level

In Fig. 12, we can see the noise level for streamline n.13 while in Fig. 13 the cut-off frequency for the same streamline is displayed.

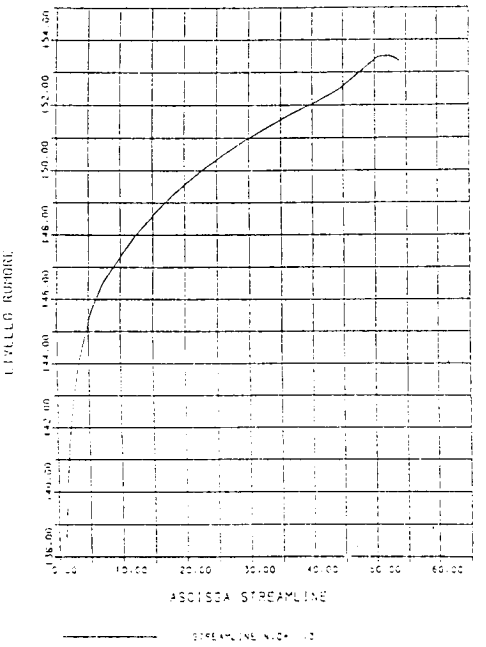

Fig. 12.

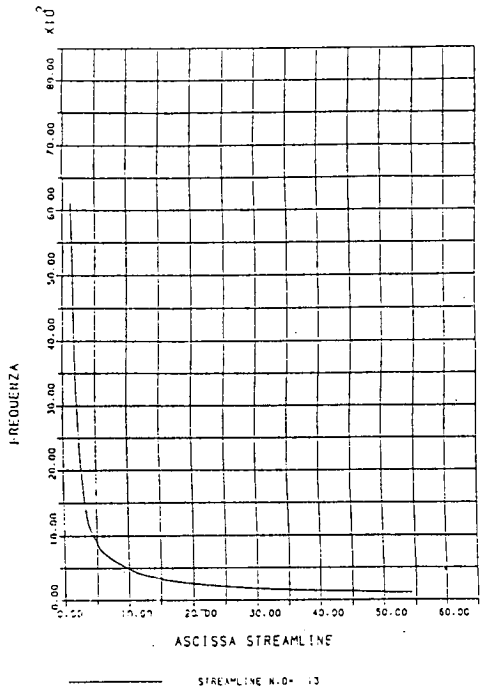

Fig. 13.

f. Thick boundary layer calculations

The flow in the third area of Fig. 1 is definitively more complicated and the equations that apply can not be of the parabolic type but must be elliptic, as the

conditions in a specific point are affected from variations upstream and downstream.

It is possible to describe the Reynolds equation, the energy conservation equation and the continuity equation in a general form:

$$\frac{\partial}{\partial t}(\varrho\phi) + Div(\varrho u\phi - \delta_\phi GRAD\phi) = S\phi$$

where, changing the values of ϕ(w), we can obtain all three preceeding equations.

A possible algorithm for the solution of these equations is the PHOENICS code by CHAM (Parabolic Hyperbolic Or Elliptic Numerical Integration Code Series). For the viscous calculation, just the stern part of the hull has been considered (42.8 mt. real length) and it has been inserted in a cilinder of 80 mt. radius and ending 200 m. astern the hull (Fig. 14).

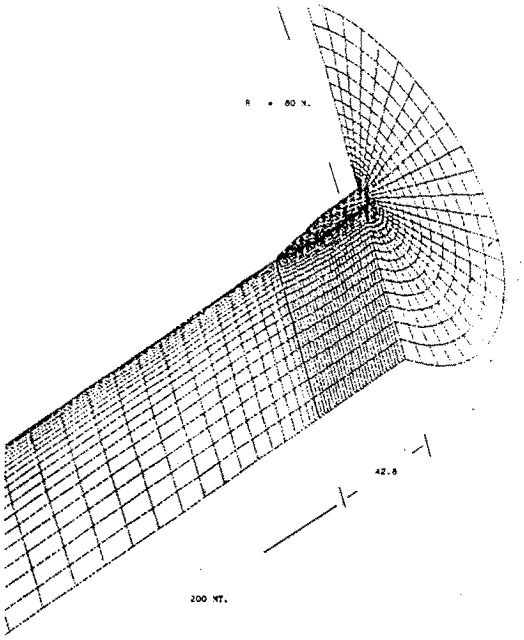

Fig. 14.

Such a large grid helps in determining the boundary conditions but a larger grid would make the computation excessively time-consuming.

Input data for the PHOENICS code are most of the values obtained through the previous steps; in output, for the center of each cell of the grid, are obtained:

- the three velocity components
- the pressure values
- the turbulence factor

As before, these data are interpolated in order to obtain them in the experimental measuring points. We can therefore present:

- isopressure curves, on the surface, 3D
- wake, in the propeller transverse section
- velocity vectors, seen from astern (Figure 15)
- velocity vectors, 3D (Fig. 16)

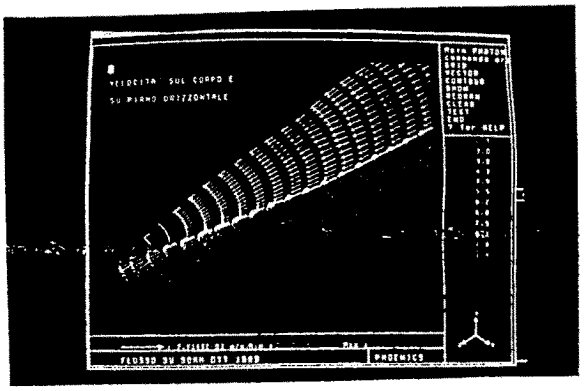

Fig. 15.

4. FINAL CONCLUSIONS

In Figs. 17 and 18, for two transverse sections, a comparison between experimental measurements, potential data and viscous flow calculation is shown.

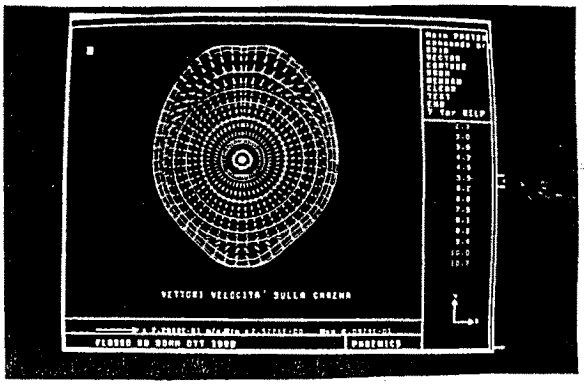

Fig. 16.

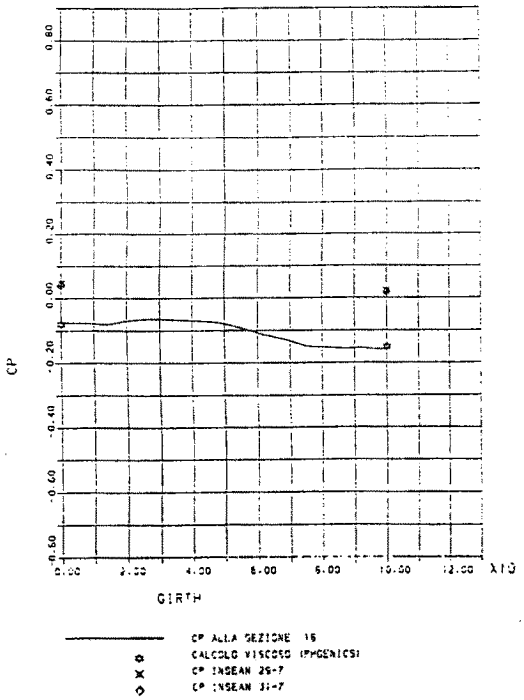

Fig. 17.

It can be seen that in these stern regions, the viscous flow calculations are close to the potential data and that both values differ from the experimental points. However, it is important to notice that all calculations have been made without the presence of the sail, due to grid capability.

In the future, it is likely that new measurements will be made using not any more differential pressure transducers but membrane devices.

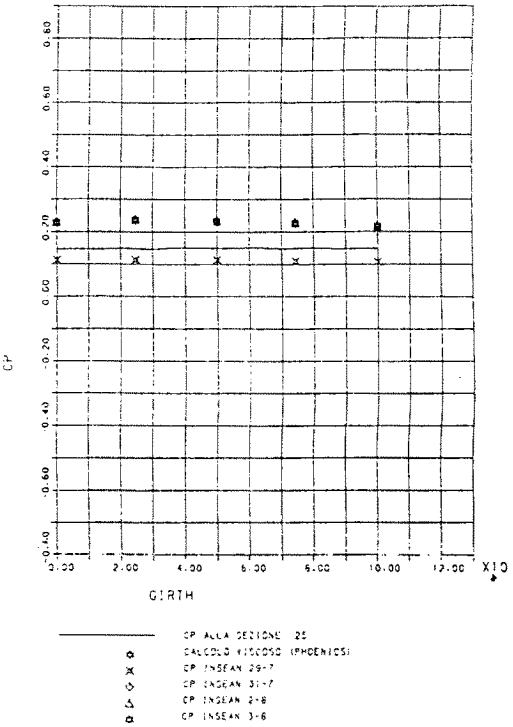

Fig. 18.

References

[1] Hess, Smith: "Calculation of Non Lifting Potential Flow Around Arbitrary Three Dimensional Bodies".

[2] Bruzzone, Caprino: "Applicazione di una Procedura Numerica per il Calcolo dello Strato Limite Sottile". CETENA Q 67, in Italian

[3] Cebeci, Chang, Kaups: "A General Method for Calculating Three Dimensional Boundary Layers on Ship Hulls". D.A.C. Report No. MDCJ&((*

[4] Spalding, Abdelmeguid, Markatos: "A Method of Predicting Three Dimensional Turbulent Flow around Ship Hulls".

[5] Di Ció: INSEAN Report No. 14/c/2024/III.

[6] Sansalone, Caprino: "Utilizzo del Programma PHOENICS per la Determinazione del Flusso Viscoso su Forma Poppiera di Sommergibile". CETENA R 3017.

[7] Markatos: "The Computation of Thick Axisymmetric Boundary Layers and Wakes around a Body of Revolution". Proceedings Inst. Mech. Engrs. Vol 198c.

[8] Janson, Larsson: "Ship Flow Calculation with Phoenics" 2d Resistance Symposium, 1985.

PS-1.5

O.P. ORLOV
Krylov Shipbuilding Research Institute,
Leningrad, U.S.S.R.

MODELLING OF TURBULENT BOUNDARY LAYER AND VISCOUS RESISTANCE OF SHIP'S HULL

INTRODUCTION

It is a widespread opinion that the similarity of parameters of the boundary layer and viscous resistance in turbulent flows as well as in laminar flows is characterized by Reynolds number only. Discrepancy between Reynolds numbers for the full-scale ship and geosim model in laboratory conditions accounts for impossibility to model viscous effects in full in model experiments. It is valid when under conditions of model and full-scale tests the physical characteristics of the medium (typically, of ordinary water) are similar, and the hull surface is hydraulically smooth or in any case the influence of roughness is small.

At the same time it is well known that in case of the roughness increase due to the hull fouling the nondimensional hydromechanical characteristics of resistance and boundary layer start to grow and approach the values typical of laboratory conditions. It is also known that introduction of the polymer mixture into the fluid will lead to reduction of nondimensional resistance coefficients and boundary layer thickness decrease, i.e. shift of viscous parameters characteristic for R_n number increase.

If in any case mentioned above the relative changes in the characteristics of boundary layer and viscous resistance are governed by one and the same law, the modelling of the boundary layer and resistance characteristics becomes possible.

The present paper deals with verification of possibility to model the viscous flow for full-scale ships by changing the friction on the surface of geosim models in the towing tank.

GENERAL LOGICAL CONSIDERATIONS

For explicit representation of the interrelation between the viscous resistance coefficient

$$C_v = \frac{R_v}{0.5 \varrho U_0^2 \Omega} \qquad (1)$$

and Reynolds number,

$$R_n = \frac{UoL}{\nu}$$

the relationship (1) shall be written in the following form:

$$C_v = 2\frac{\left(\sqrt{\frac{R_v}{\rho\Omega}}\frac{L}{\nu}\right)^2}{\left(\frac{U_0 L}{\nu}\right)^2} = 2\frac{R_n^{*2}}{R_n^2} \qquad (2)$$

The following symbols have been used in formulae (1) and (2)

R_v = viscous resistance;

U_o = inflow velocity;

L = body length

Ω = wetted surface

ρ = fluid density

ν = kinematic viscosity coefficient;

$\frac{Rv}{\Omega}$ = average viscous resistance per unit wetted surface.

When parameter

$$U_\tau^* = \sqrt{\frac{Rv}{\rho\Omega}}$$

is introduced as some analog of the dynamic velocity, the relationship $R_n^* = U_\tau^* L/\nu$ will characterize the losses (for friction, in the main) in the form of the conventional Reynolds number.

Relationship (2) offers vivid representation of the possibility to vary the value of the viscous resistance coefficient with the fixed conventional Reynolds number Rn.

With this aim in view, in laboratory conditions it is sufficient that parameter Rn* should be purposefully changed. The increase in the degree of roughness for the model hull surface will obviously lead to Rn* rise and application of polymer admixtures, to Rn* drop.

Naturally, the question is raised, whether the changes in the characteristics of the boundary layer and resistance are adequate, in case of Rn* parameter control, to their natural development depending on Rn number. In order to elucidate this question in principle, two velocity profiles: u/U (y) are considered for the simplest case of the turbulent boundary layer on the flat plate:

- on the hydrodynamically-smooth surface at a certain arbitrary Reynolds number

$$Rn_o = \frac{U_0 x}{\nu}$$

and

- on rough surface at a different Reynolds number

$$Rn_1 = \frac{Ux_1}{\nu} \neq Rn_o$$

but on condition that the friction resistance coefficients C_F and C_{F1} are equal in both cases.

As $C_F = 2\theta$, the momentum thicknesses will be also equal in both cases, i.e.

$$\bar{\theta}_o \approx \bar{\theta}_1 \qquad (3)$$

where

$$\bar{\theta} = \frac{\theta}{x} = \frac{1}{x_o}\int^{y}\frac{u}{U}\left(1-\frac{u}{U}\right)dy$$

It is known that for the smooth and rough surfaces of the flat plate the velocity defect law

$$\frac{U-u}{u_\tau} = f(y/\delta)$$

is observed, therefore such parameters as

are universal constants in this case.

$$C_1 = \int_0^1 \left(\frac{U-u}{u_\tau}\right) d\left(\frac{y}{\delta}\right)$$
$$C_2 = \int_0^1 \left(\frac{U-u}{u_\tau}\right)^2 d\left(\frac{y}{\delta}\right) \qquad (4)$$
$$y = \frac{C_2}{C_1}$$

The characteristics of the boundary layer are interrelated by the following relationships:

$$\bar{\theta} = \bar{\delta}^* \left(1 - y\sqrt{\frac{C_f}{2}}\right)$$
$$\bar{\delta}^* = \bar{\delta} C_1 \sqrt{\frac{C_f}{2}} \qquad (5)$$

whence it follows that the fulfilment of condition (5) with regard to (4) is feasible only when

$$\bar{\delta}^*(R_{no}) = \bar{\delta}^*(R_{n1})$$
$$\bar{\delta}(R_{no}) = \bar{\delta}(R_{n1}) \qquad (6)$$

and

$$C_f(R_{no}) = C_f(R_{n1})$$

In formulae (6)

$$\bar{\delta} = \frac{\delta}{X}$$

is thicknes of boundary layer, and

$$\bar{\delta}^* = \frac{\delta^x}{X} = \frac{1}{X_0}\int_0^y \left(1 - \frac{u}{U}\right) dy$$

In such an event, it is inferred from the velocity defect law that in the boundary layer the velocity profiles are equal.

Similar arguments may be adduced for the case of reducing the resistance through supply of the weak polymer solution to the turbulent boundary layer of the flat plate.

Thus during experiments it turned out to be possible to reproduce the same relative (nondimensional) characteristics of the boundary layer either by "natural way", i.e. by variation of Rn number, or by control of the friction resistance for the model hull surface.

Then for modelling the viscous flow under regular conditions in the towing tank with Reynolds numbers less than

$$R_n = \frac{U_o L}{\nu}$$

it is necessary to increase the degree of surface roughness, and for modelling the flow with Reynolds number more than

$$R_n = \frac{U_o L}{\nu}$$

the tests shall be performed in polymer solution.

For experimental verification of the above logical conclusions, the comparative experimental studies were undertaken based on the results of full-scale measurements for determination of the velocity profiles in the boundary layer and the wake of the full-scale ships and also on the results of measurements of similar characteristics obtained during special experiments on geosim models in the fully polymerized towing tank. In the laboratory experiment polyox of WSR-301 type with 6 ppm concentration was used.

RESULTS OF COMPARATIVE MEASUREMENT OF VELOCITY PROFILES IN BOUNDARY LAYER OF THE SHIP AND ITS MODEL IN THE TOWING TANK WITH POLYMER SOLUTION

Recently the research staff of the Krylov Shipbuilding Research Institute have obtained data on the mean velocity profile for the after end of the "Krym" type tanker and data on the value of the wake of the "Pobeda" type tanker suitable for the planned comparative analysis. It accounts for the choice of models of the above ships for laboratory studies.

The full-scale data on the velocity profiles for the "Krym" type tanker were obtained by F.I. Kanevsky and V.M. Stumpf at the point on the hull with relative coordinates

$$\bar{X}=\frac{X}{L} = 0{,}865$$

and

$$\bar{Z} = \frac{Z}{T} = 0{,}5$$

The ship's lines of this tanker are presented in Fig. 1. The model constructed to scale 1:35 was used for experiments in the test tank.

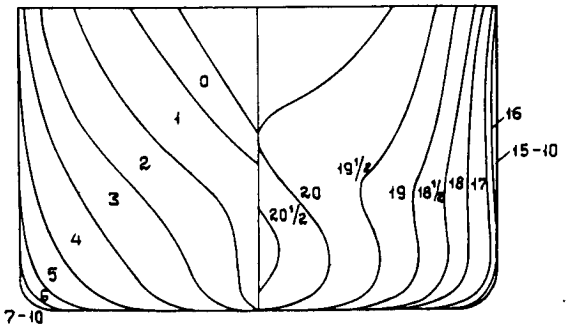

Fig. 1. Lines of the "Krym" type tanker

The results of measurements under model and full-scale conditions are given in Fig. 2. With the polymer concentration taken for the model experiment, the value of the resistance coefficient of the full-scale ship has not been reached. The difference between the resistance coefficient value of the model in polyox solution and full-scale ship is approximately equal to $0{,}3 \cdot 10^{-3}$. The discrepancy between the velocity profiles in the boundary layer lies within the limits of measurement accuracy, though there is a tendency for a shift of the points u/Uδ (y/x) obtained on the model to the left of the middle curve. This correlates with the data on resistance. Approximate estimates obtained with the use of the quantity of momentum theorem permit one to assume that an error in the viscous resistance equal to 10 % can lead to an error in the local velocity (u/Uδ) in the profile midheight portion equal to about 1.5 %.

With regard to the comments made one may assume that the presented results of the measurement of velocity profiles in the boundary layer confirm the possibility to model the flow in the boundary layer of a ship by testing the ship's model in a towing tank filled with a weak polymer solution.

RESULTS OF COMPARATIVE MEASUREMENT OF THE WAKE OF THE SHIP AND ITS MODEL IN A TOWING TANK WITH POLYMER SOLUTION

The study of the wake was performed on a "Pobeda" type tanker and its model. During full-scale tests the torque was determined. Basing on the results of the torque measurement the value of the wake coefficient was determined. The torque was determined on two

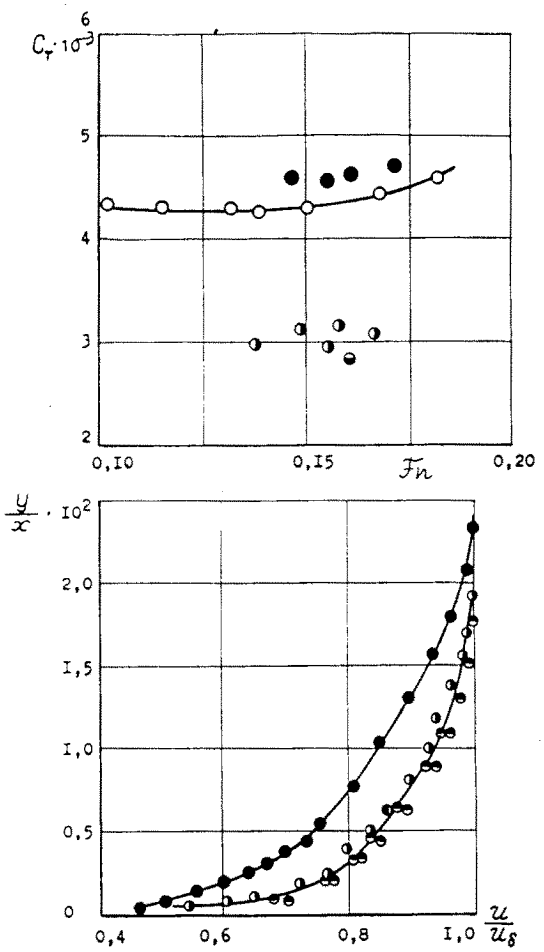

Fig.2. Results of comparative tests confirm the identity of viscous flow around the hull in case of the viscous resistance coefficients equality under model and full-scale tests

- ● $R_n = 5{,}3 \cdot 10^6$;
- ○ - model $R_n = 8{,}8 \cdot 10^6$
- ◑ - model, $R_n = 8{,}8 \cdot 10^6$, solution WSR-301, C_o 6 ppm;
- ⊖ - full-scale, $R_n = 1{,}3 \cdot 10^9$

different ships with newly painted hulls during delivery trials. The full-scale measurements of the torque were performed under the guidance of V.G. Mishkevich and O.I. Bezzubik, S.N. Kruglova and V.M. Stumpf processed the results of the torque measurements with the aim to determine the value of the wake with regard to the actual propeller roughness In both cases practically the same value of the wake W_{qs} = 0.34 were obtained.

Model studies included the measurement of the nominal velocity field as well as the towing and self-propelled tests of the model in ordinary water and in a weak polymer solution. Propeller model tests in open water necessary for the self-propelled tests were also conducted both in ordinary water and in polymer solution. They were a bit different from each other, therefore during self-propelled tests in water propeller performance curves for water were assumed, and in polymer solution – for polymer.

The form of the hull of the "Pobeda" type tanker model and the results of the towing tests are shown in Fig. 3 and Fig. 4. The results of the self-propelled tests are given in Fig. 5.

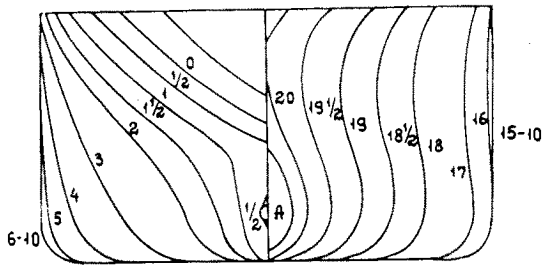

Fig. 3. Lines of the "Pobeda" type tanker

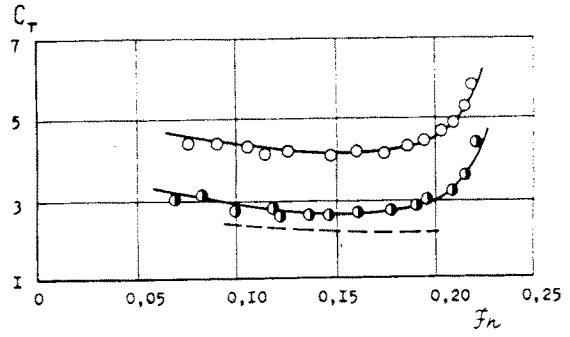

Fig.4. Resistance coefficient of the "Pobeda" type tanker

- ○ - water
- ◑ - polymer solution
- – – – viscous resistance coefficient of the ship (scaled by conventional method)

As in the previous case the value of the resistance coefficient in the polymer solution proved to be slightly larger than the value of the full-scale ship resistance coefficient. Reasoning from the estimates made during the tests we had little hope on the

required reduction of resistance by increasing the concentration of the polyox (WSR-301 type) used. Consequently it was kept at the given level 6 ppm. The use of a more effective polymer will permit one to elucidate the problem in question.

For the speed value Fn = 0.15 in full load the following mean (over the propeller disc) values of the wake coefficients were obtained:

- in the nominal velocity field in water $\bar{\Psi}\alpha m$ = 0.55
- during self-propelled test in water Wtm = 0.44
- in the nominal velocity field in a weak polymer solution $\bar{\Psi}\alpha m$ = 0.40
- during self-propelled tests in a weak polymer solution Wtm = 0.35.

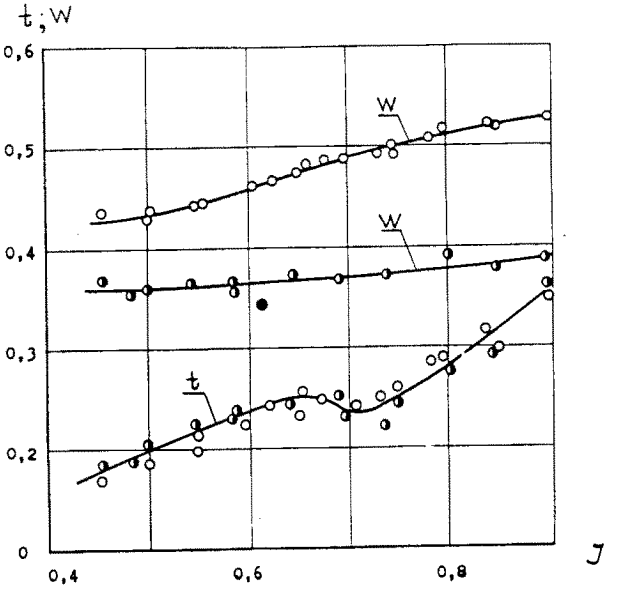

Fig.5. Scale effect of the coefficient of "Pobeda" tanker propeller/hull interaction

○ - conventional self-propelled tests
◑ - self-propelled tests in polyox solution of WSR-301 type, 6 ppm
● - full-scale measurement results

The good agreement between the wake coefficients of the model in the polymer solution and under full-scale test conditions shown in Fig. 5 is yet another confirmation of the validity of the basic assumption of the possibility to physically model viscous flow around the ship hull. The data considered above clearly indicate the possible application of the results of the present study – they can be used for a more reliable estimation of the scale effect of resistance, boundary layer and propeller/hull interaction characteristics. The data shown in Fig. 5 give a vivid idea of the scale effect values of the wake and suction coefficients (the suction scale effect is practically nonexistent) and permit one to verify on the basis of facts the logic of the existing conventional methods of predicting the characteristics in question.

CONCLUSIONS

1. In the present paper we considered and confirmed by the results of comparative full-scale and model tests the possibility in principle of modeling viscous flow and full-scale ship resistance by performing tests on geometrically similar models in towing tanks filled with weak polymer solutions.

2. We consider it promising to develop and use a method of physical modeling like the one discussed above for obtaining data on scale effects resulting from viscosity in solving applied problems of ship hydromechanics and allied branches of technology.

3. Conducting experiments in a fully polymerized towing tank provides the easiest work and high reliability of measurement.
Since it is easier to polymerize and perform studies like that in comparatively medium and small-size towing tanks, the author believes that the proposed method of testing in weak polymer solutions offers new possibilities primarily for medium and small-size towing tanks.

PS-1.6

P. CHIKOLOV

Bulgarian Ship Hydrodynamics Center, Varna, Bulgaria

NON-LINEAR SOLITARY WAVE AFTER SHIP STERN IN VERY SHALLOW WATER

The 19th R & F Committee Report treats the problem of solitons generation in front of a ship model at near critical speeds. In addition to this, our numerical investigation have shown [Chikolov (1990)] the possibility of generation of nonlinear solitary wave behind the ship model in very shallow water conditions. The numerical experiments are performed by the method proposed by Soh (1984) and further on expanded for shallow water conditions [Chikolov (1988)]. The realized numerical procedure satisfied exactly the nonlinear condition on the free surface. In our calculations the motion of a cylinder (radius r=1 and submergence f=1) with critical speed (Fh=1 at g=1) at water depth h=1.2, 1.5, 2.0 in time interval 0<t<400, is considered. The numerical results are shown on Figs. 1, 2, 3 in the form of wave profiles at t=350 for each water depth respectively. It can be

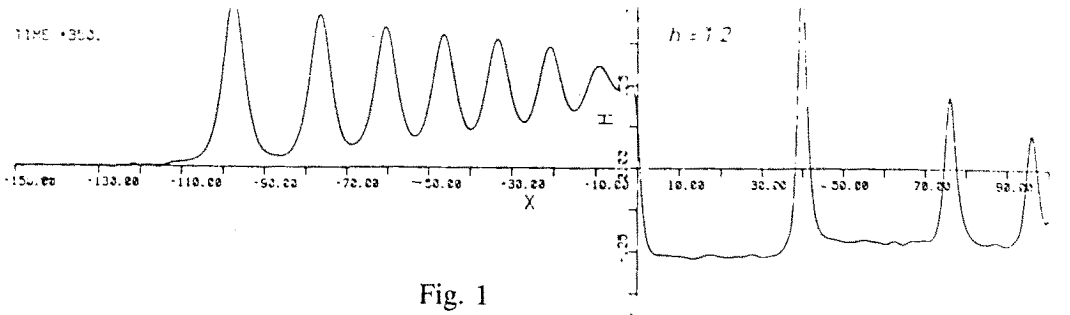

Fig. 1

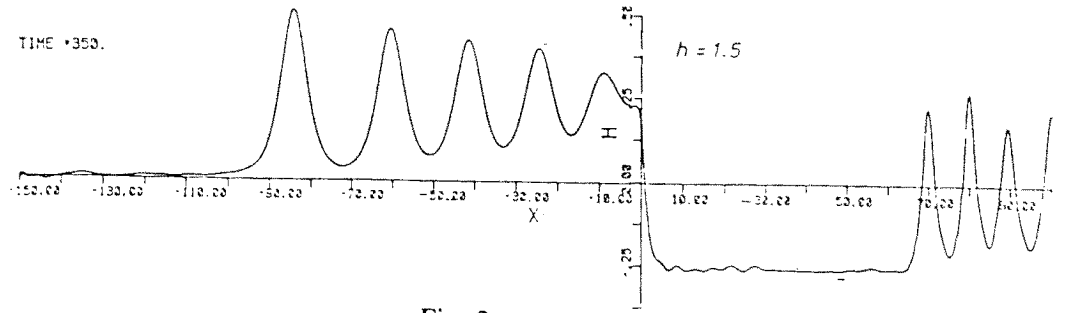

Fig. 2

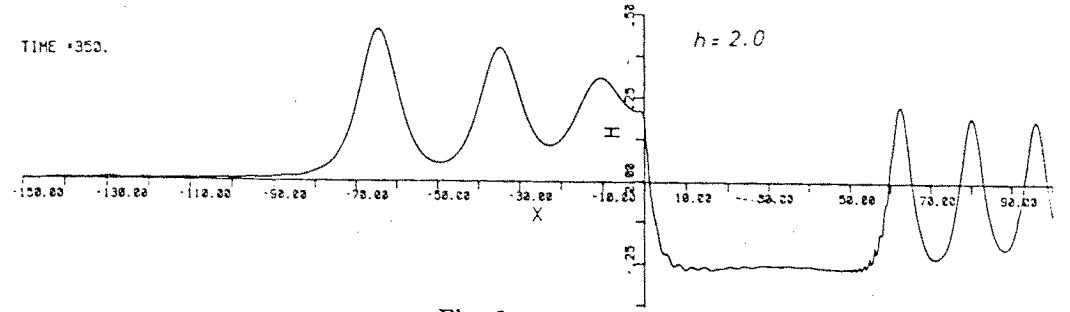

Fig. 3

seen from Figs. 2 and 3 that the results obtained are very similar to those reported by other authors [Wu (1981)]. But for the case of very shallow water conditions (h=1.2, Fig. 1) the wave group is substantially changed, so that the leading stern wave seems to be formed as a solitary wave. The analysis of this process (see fig. 4) shows that three periods can be distinguished:

- in the first (initial) period 0<t<120 the velocity "c" of the wave profile corresponds to that determined by the linear theory, so that the wave height constantly increases;
- in the second (transitional) period 120<t<300 the velocity. and the height of the leading wave strongly increases, approaching to the critical one;
- in the third (stationary) period the velocity and the amplitude keep their values constant. In this period the wave has the character of nonlinear solitary wave having velocity greater than the critical one for the local water depth.

We think that from the numerical results reported by Ertekin (1989), for the case of 3-D formulation may also be distinguished generation of a solitary nonlinear wave after stern.

Usually in real conditions (model tests) the solitary wave in the stern of the model loses stability and breaks down as observed and discussed by Kostov et al. (1986). But this phenomena cannot be predicted by the used numerical procedure.

We think that the R & F Committee have to pay attention to this problem and recommend its investigation in the cooperative experimental program on shallow water.

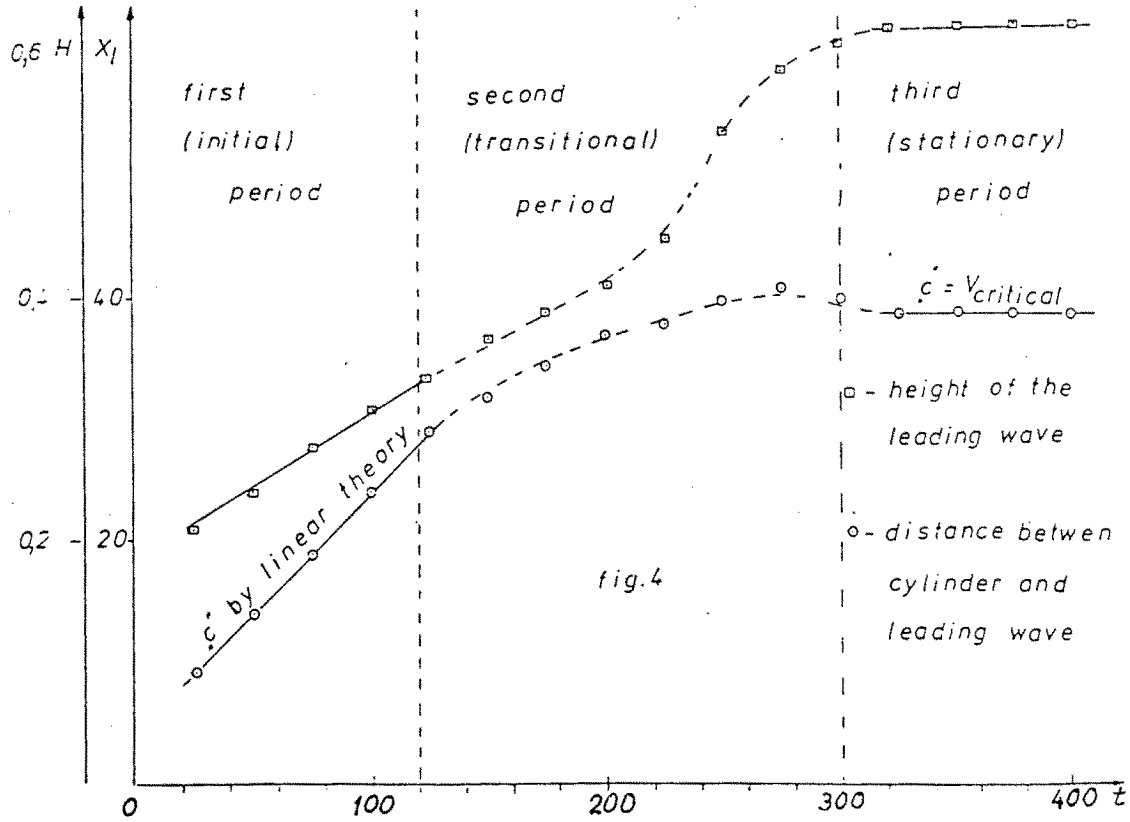

fig.4

References

[1] Chikolov, Ṕ., "Non-linear solitary wave back the stern in very shallow water", (to be published)

2] Chikolov P., "Numerical solution of non-linear wave problem at critical speed in shallow water". 17th Session of SMSSH 1988, Varna

[3] Ertekin R.C., Z. -M. Qian, "Numerical grid generation and upstream waves for ships moving in restricted waters". The Proceedings of Fifth International Conference on Numerical Ship Hydrodynamics, 24-28 September 1989, Hiroshima, Japan

[4] Kostov D., Chikolov P., Lazarov G., "Resistance tests and wave-pattern measurements of Wigley parabolic hull in shallow water". Written contribution to the 17th ITTC Resistance Committee report, 1986

[5] Soh W.K., "A numerical method for non-linear water waves". Journal Computers & Fluids, 1984, vol. 12, nº 2

[6] Wu T.Y., "Long waves in ocean and coastal waters". Journal of Eng. Mech. Div., ASCE, Vol. 107, June 1981

T. BUGALSKI and S. JAWORSKI*

A. MINCHEV**

***Ship Propeller Department, Institute of Fluid Flow Machinery, Polish Academy of Sciences, Poland.**

****Bulgarian Ship Hydrodynamics Center, Bulgarian Academy of Science, Bulgaria**

PRELIMINARY PREDICTION OF EFFECTIVE WAKE FIELD FOR SHIP MODELS

INTRODUCTION

Computer method for calculation of effective wake-field of ship model is presented. The method is based on an idea of equivalent body of revolution and empirical corrections obtained from experimental tests.

The method can be described as follows:

1. The form of ship defined as distribution of frame areas, is transformed into the axisymmetric body with surface of sections equal to ship model frame areas.

2. For such an axisymmetric body, the nominal velocity field is calculated, and transformed into the effective field in the first approximation with help of empirical correction for the influence of the propeller and real ship geometry.

3. For this velocity field, propeller is designed and new effective velocity field is calculated.

4. New effective velocity field is used for design of the next propeller and for calculating the next effective velocity field.

Iterative process is repeated until the required convergence of pressure distribution on the axisymmetric body surface and, of course, the required of propeller thrust are obtained. Usually, the convergence is obtained after 4 to 5 iterations. In the last iteration there are calculated the project (effective) velocity field and hydrodynamics characteristics of the propeller working in it.

The above described method is the basis of the computer program "EFWAKE-3".

THE COMPUTER PROGRAM "EFWAKE-3"

The computer program "EFWAKE-3" is based on the "VISINT" program subroutines, described in the paper [1]. With comparison to "VISINT", "EFWAKE-3" is completed with three subroutines needed for propeller design. These subroutines (SUBDAN, SUBSUR, SUBDES) are adopted from J. Szantyr's program, described in the paper [2]. In the current form the program works as follows:

- it opens input and output files and reads input data.

  The data set is formed by: model name, length between perpendiculars, breadth on waterline, draft, block coefficient, slope of tangent to hull section at station 2 at WL_0 and frame-areas - this part of data is connected with model; for the propeller: number of blades, thrust, number of revolutions, diameter, hub diameter and development area ratio. In this subroutine the operations of geometry change from ship model to the equivalent axisymmetric body (EBOR) are performed.
- in next subroutine are obtained the parameters of flow around EBOR without propeller, and, among others, the nominal velocity field in the propeller plane.
- The corrections EVC(r/R) for the model's designed velocity field are calculated.
- the characteristics non-dependent on the velocity field are calculated, for instance profile thickness distribution, blade length and others.
- it starts the iteration process of calculation of the flow around EBOR with propeller. This propeller is designed in every iteration step.

The design of propeller is based on the lifting line theory, supplemented by lifting surface corrections [2]. It is assumed that propeller blade has no skewback and no rake. The blade outline and the radial blade thickness distribution are taken from the Wageningen Standard B series. The propeller has fixed pitch (type of blade sections - NACA16, thickness form with NACA a=0.8). The design calculation is based on the Lerbs optimum condition for wake-adapted propellers. The program "EFWAKE-3" was written in MS FORTRAN 4.1 for the PC AT/386.

EFFECTIVE VELOCITY CORRECTION (EVC)

Effective velocity field of equivalent body of revolution evaluated analytically differs from the effective velocity field of the ship model obtained from model tests. In order to obtain compatibility between experimental and analytical results an EVC

correction is applied. The method of evaluation of the EVC correction is presented in paper [3]. In the former version, because of small quantity of accessible data, the EVC correction was the function of block coefficient C_B only. In current version the EVC correction is evaluated with use of regression analysis. It becomes a function of six ship's parameters: L/B, B/T, C_B, τ_2, L/D, K_T.

The EVC correction is evaluated as follows:

$$EVC(r/R)=a_o+\sum_{i=1}^{3} a_i \cdot (r/R)^i$$

where

$a_i = b_{i1} \bullet L/B + b_{i2} \bullet B/T + b_{i3} \bullet C_B + b_{i4} \bullet \tau_2 + b_{i5} \bullet L/D + b_{i6} \bullet K_T$

i=0, 1,2,3,4,

τ_2 –slope of tangent to hull section at station 2 at WL_0,

b_{ij} –regression coefficients

C_B –block coefficient

K_T –thrust coefficient

r/R –relative radius of propeller

B –breadth on waterline

D –propeller diameter

L –length between perpendiculars

T –draft

Applied values of the hull parameters are presented in table 1, and the parameters range is given below:

L/B = 4.725 - 7.316

C_B = 0.588 - 0.828

L/D = 19.17 - 38.22

B/T = 2.375 - 3.586

τ_2 = -0.133 - 1.231

K_T = 0.127 - 0.269

TABLE 1

Main parameters of ship models
(used in evaluation of EVC correction)

Mod.no.	L[m]	B[m]	T[m]	C_b	D[m]	τ_2	V[m/s]	RPS	W_T	K_T
m0098	6.000	0.857	0.347	0.700	0.240	0.143	1.547	7.50	0.280	0.216
m0080	6.250	0.983	0.388	0.694	0.231	0.322	1.890	9.48	0.370	0.224
298	6.167	0.843	0.355	0.818	0.230	0.560	1.362	7.84	0.383	0.158
295	5.030	0.954	0.266	0.618	0.222	-.133	1.637	8.46	0.286	0.155
211	7.193	1.289	0.386	0.662	0.250	-.026	1.885	9.96	0.219	0.194
248	7.500	1.085	0.347	0.602	0.250	0.022	2.168	9.06	0.340	0.210
258	5.288	1.000	0.344	0.595	0.250	-.068	1.874	10.23	0.264	0.127
275	4.792	1.014	0.365	0.588	0.250	-.116	2.046	9.68	0.273	0.226
M1	6.000	1.250	0.357	0.663	0.229	1.231	1.800	9.00	0.280	0.229
M2	6.000	1.091	0.312	0.669	0.200	1.166	1.800	11.00	0.315	0.256
M3	6.000	0.968	0.277	0.664	0.177	1.160	1.800	14.00	0.282	0.269
M4	6.000	0.857	0.245	0.667	0.157	1.200	1.800	16.00	0.264	0.200
m285A	7.187	1.258	0.421	0.782	0.219	0.265	1.535	13.65	0.506	0.141

To make the method efficient, a lot of ship models must be investigated. In the program a correction is used for the difference between theoretical and empirical effective velocity fields. This correction is a function of six parameters. To get this correction one needs the results of measurements of the whole velocity fields before the working propeller.

The analysis shows that different versions of program should be developed for different ship types with similar form of the aft part. It is necessary to conduct systematical research of velocity field before the working propeller on the ship models and to collect the data base.

References

[1] Bugalski T.J., "Analytical Prediction of Pressure Distribution on Surface of Axisymmetric Body due to Propeller Action". IFFM Report. No. 118/87, 1987, (Ph.D. thesis in Polish).

[2] Szantyr J.A., "An Interactive Program for Design of Ship Propellers". The Naval Architect, October 1987.

[3] Bugalski T., Jaworski S., Minczew A., "Analysis of Wake-field Calculation Based on Equivalent Body of Revolution Possibility". VII Symposium on Ship Hydrodynamics, Gdansk. November 11-13. 1987, (in Polish).

[4] Reports of Ship Design and Research Center. Gdansk (in Polish) №: RH-87/Z-060, RH-87/Z-115. RH-87/Z-116, RH-87/Z-117, RH-87/Z-156, RH-88/Z-147.

[5] Report of Bulgarian Ship Hydrodynamics Center, Varna:
"Results of Measuring the Nominal and Total Velocities Distribution at the Propeller Plane of Four Container Ship Models". BSHC Technical Report, № PD-88-226.
Report BSHC № 4-3-2, 1983.

[6] Information about BSHC experiments:
ship model m0080 with propeller p0311
ship model m285A-III with propeller p0525

[7] Bugalski T., Jaworski S., "Preliminary Calculations of Effective Wake Field for Ship Models". PRAD'89 - Fourth International Symposium on Practical Design of Ships and Mobile Units - Varna 1989.

PS-1.8

LI SHIMO and CHEN KEQIANG*
K. YOSSIFOV and D. KISHEVA**
***Wuhan University of Water Transportation Engineering, Wuhan, China**
****Bulgarian Ship Hydrodynamics Centre, Varna, Bulgaria**

ON SOME ASPECTS OF BARGE TRAIN RESISTANCE PREDICTIONS BY MODEL TESTS

1. INTRODUCTION

The existing methods for prediction of push-train resistance still do not ensure sufficiently accurate

results, due to peculiarities of flow around barges, their interaction and some other influences. When processing push-train model test results, these peculiarities should be properly accounted for.

Some evaluations in this respect were elaborated in the joint work of WUWTE-China and BSHC-Bulgaria [1], [2].

This paper summarizes the main results of the systematic towing tests of push-trains and composing barges in deep calm water, carried out in the two Institutes. The purpose of these tests was to determine the resistance distribution between barges in the push-train configuration and its sensitivity to barge draught changes.

As a main result of reported investigations, new approach for model tests based resistance prediction is suggested.

2. NOMENCLATURE

B	- Breadth moulded of ship	L
C_B	- Block coefficient	--
C_F	- Specific frictional resistance coefficient	--
ΔC_f	- Roughness allowance	--
C_{fo}	- Frictional resistance coefficient in two dimensional flow	--
C_R	-Specific residuary resistance coefficient	--
C_T	-Specific total resistance coefficient	--
Fn	-Froude number	--
L_{OA}	-Length, overall	L
L_{PP}	-Length between perpendiculars	L
L_{WL}	-Length of waterline	L
Rn	-Reynolds number	--
R	-Total resistance	L^2M/T
S	-Wetted surface	L^2
T	-Draught moulded	L
W	-Weight displacement	$L.M/T^2$
∇	-Volume displacement	L^3
ρ	-Mass density	M/L
ν	-Coefficient of kinematic viscosity	L^2/T

3. EXPERIMENTAL PROGRAMME

3.1. Model description

The single barge models at the disposal of the two Institutes are quite different - the WUWTE model has a streamlined stern form, while in BSHC the semi-integrated type barges were modelled. For obtaining the desirable similarity of form and the character of flow around it, consequently, it was decided to carry out the WUWTE experiments with two single barges in line ahead, and two barge units in a row to be tested in BSHC. By barge unit, a composition of two barges rigidly joined by their stern transoms is denoted. In this way, streamlined bow and stern of compound body is ensured.

The main particulars of the models tested are given in Table 3.1.

3.2 Experimental conditions

The train compositions tested at the two Institutes are shown in Table 3.2

The single barge (or the barge unit, respectively), in which the measuring equipment is situated, i.e., on which the resistance forces are measured, is otherwise

Table 3.1

Main particulars of single barge models			
No.	I t e m	WUWTE	BSHC
1	Length between perpendiculars Lpp (m)	3.0	4.0
2	Breadth B (m)	0.692	1.004
3	Draught T (m)	0.0635	0.252
4	Volume displacement (m³)	0.112	0.947
5	Wetted surface S (m²)	2.200	5.699
6	Block coefficient C_B	0.852	0.936

Table 3.2

	№	Investigated models	Temperature of the water	
WUWTE	1	1 + 1	6°	26°
	2	1_{free} + 1_{fixed}	6°	26°
	3	1_{fixed} + 1_{free}	6°	26°
	4	Single barge	6°	26°
BSHC	5	1 + 1 + 1 + 1	14°	20.4°
	6	$(1 + 1)_{free}$ + $(1 + 1)_{fixed}$	14°	20.6°
	7	$(1 + 1)_{fixed}$ + $(1 + 1)_{free}$	14°	20.6°
	8	1 + 1	14°	20.6°

free to move in a longitudinal vertical plane, while the second barge (barge unit) is fixed to the towing carriage, i.e., it participates in the forming of flow just by its presence. The distance between fixed and free towed barges is 0.03m.

The model speed range was determined on the basis of the practically expected service speeds. The tests under No. 1.4, carried out in WUWTE, were repeated again at two water temperatures for another draught amounting to 0.08.

3.3 Presentation of resistance tests results

The original data from resistance model tests are presented in Figs. № 1–6, without any fairing. At that, the corresponding total resistance coefficients are drawn in Figs. № 1, 2, 4 and 5 versus Froude number and the residuary resistance coefficients versus Froude number – in Figs № 3 and 6.

4. ANALYSIS OF THE RESULTS

4.1. Interaction between barges composing the train

The resistance of the first barge (unit) is less than that of the second barge (unit) as well as that of the single barge, the total resistance coefficient being even less

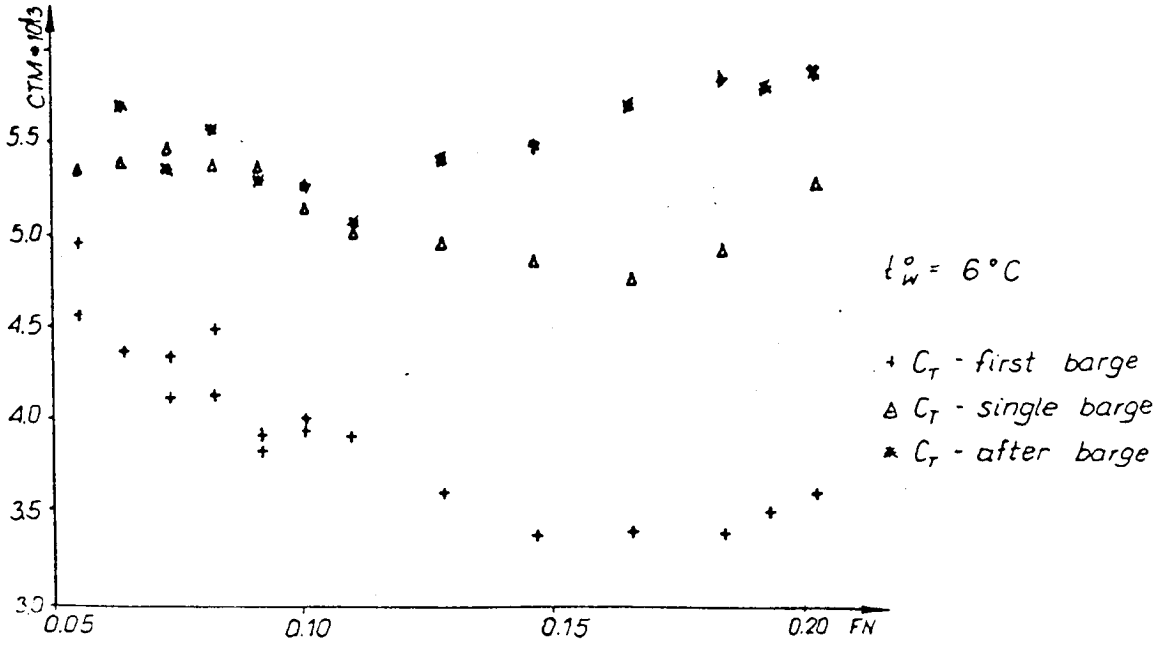

Fig. 1

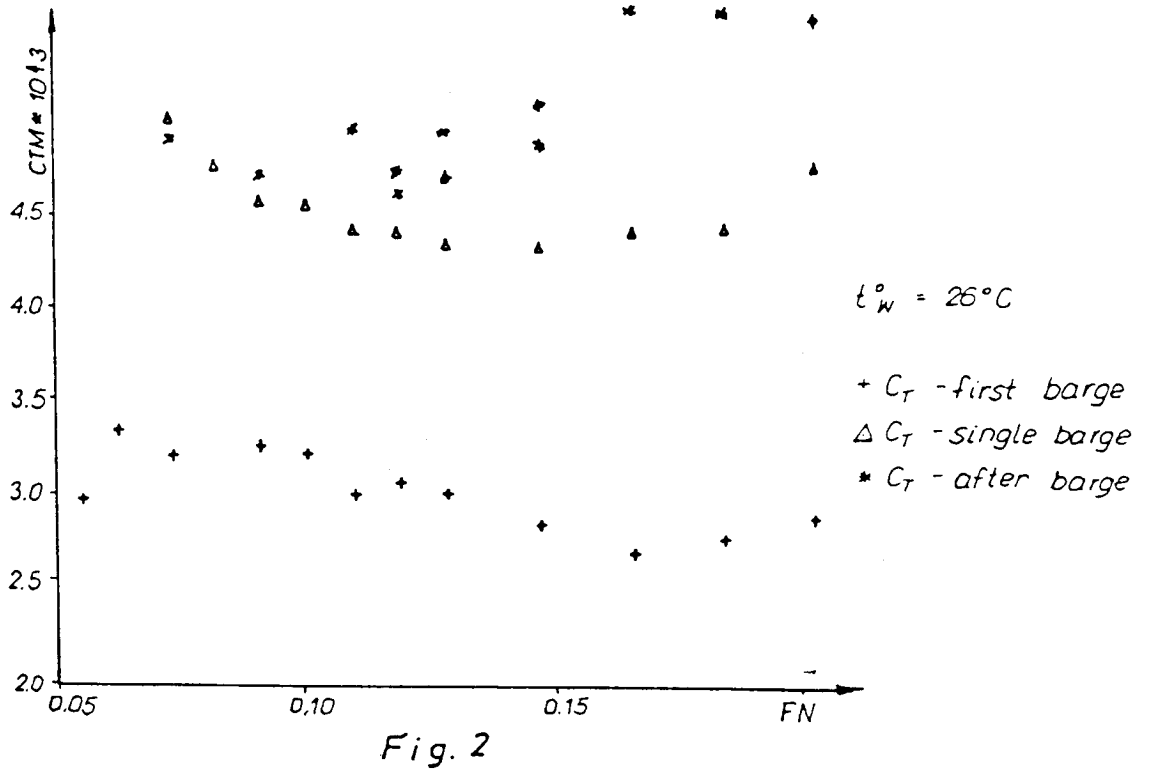

Fig. 2

than C_{fo} calculated by ITTC – 1957 correlation line (see Fig. 3 and Fig. 6).

The phenomenon could be explained by the fact of flow separation around blunt barge forms; in which case the interaction between the train elements is much stronger.

During the tests, it was visually observed that the region of separation shifts along the length behind the stern of the second barge, i.e., the pressure at the rear part of the front barge increases, and that at the front

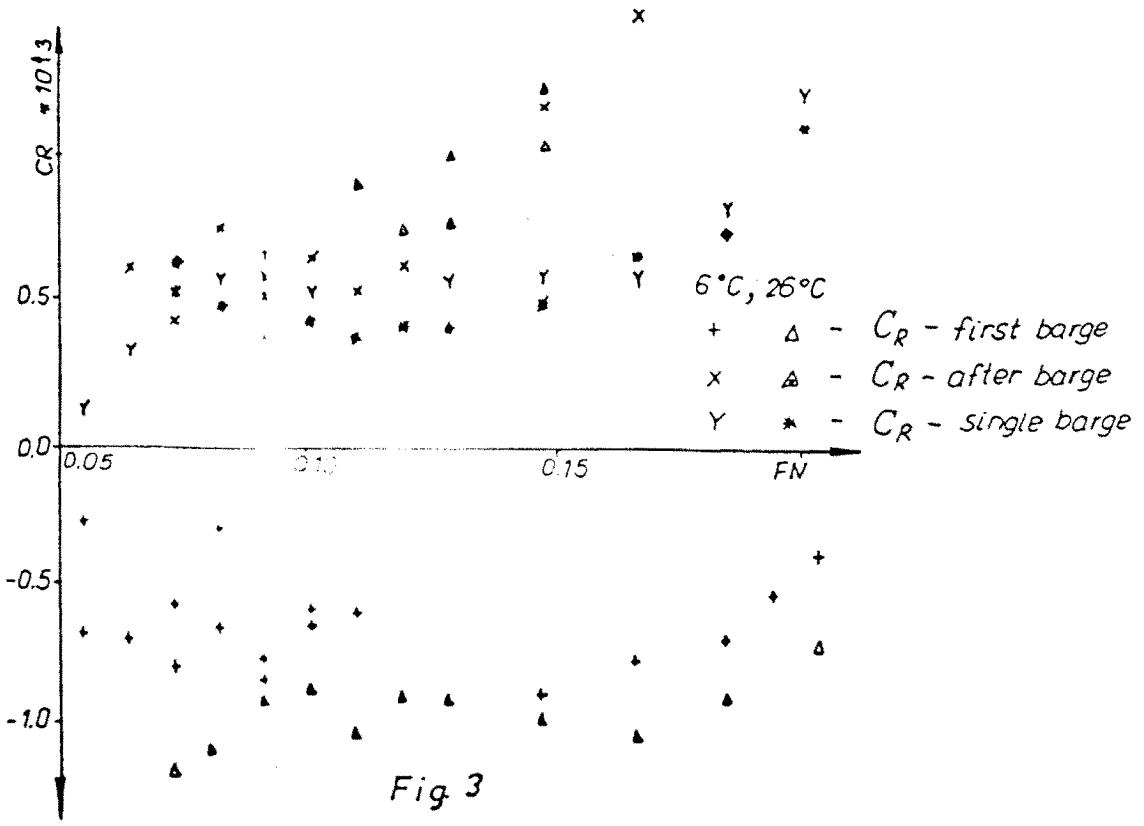

Fig. 3

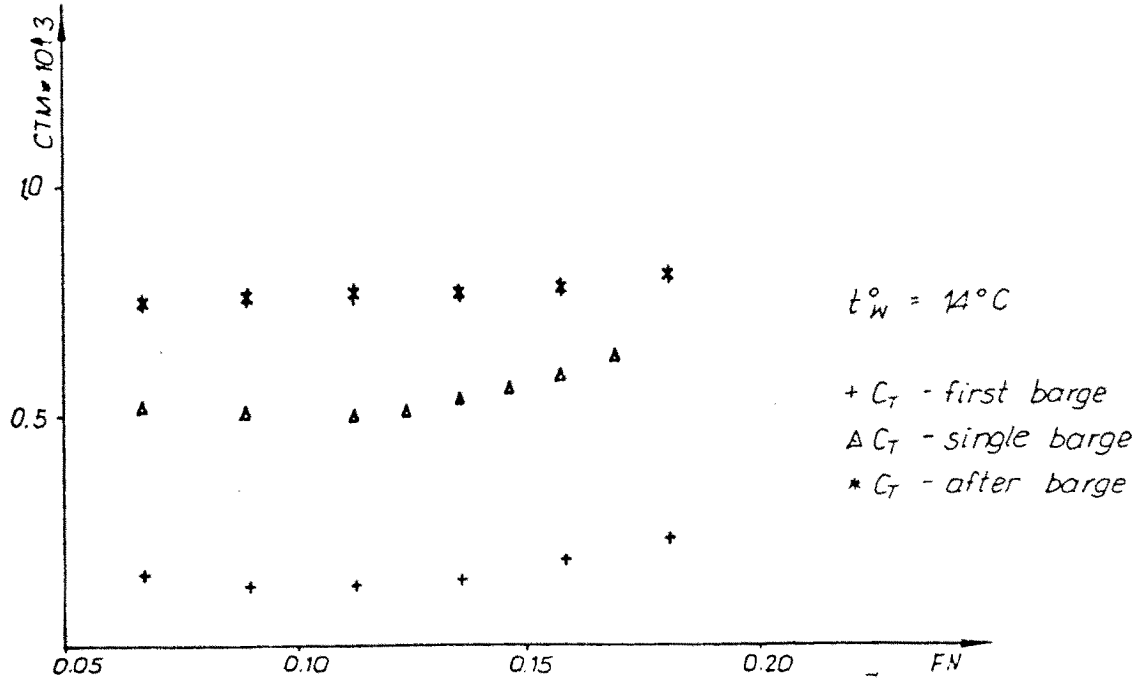

Fig. 4

part of the rear barge consequently decreases. Respectively decreases the form resistance of the front barge, and that of the rear barge increases.

Besides, repulsive force commonly exists between two barges composing the train. Even if it is an internal force, which does not influence the total resistance, its action reduces the resistance of the front barge and consequently increases the resistance of the rear barge.

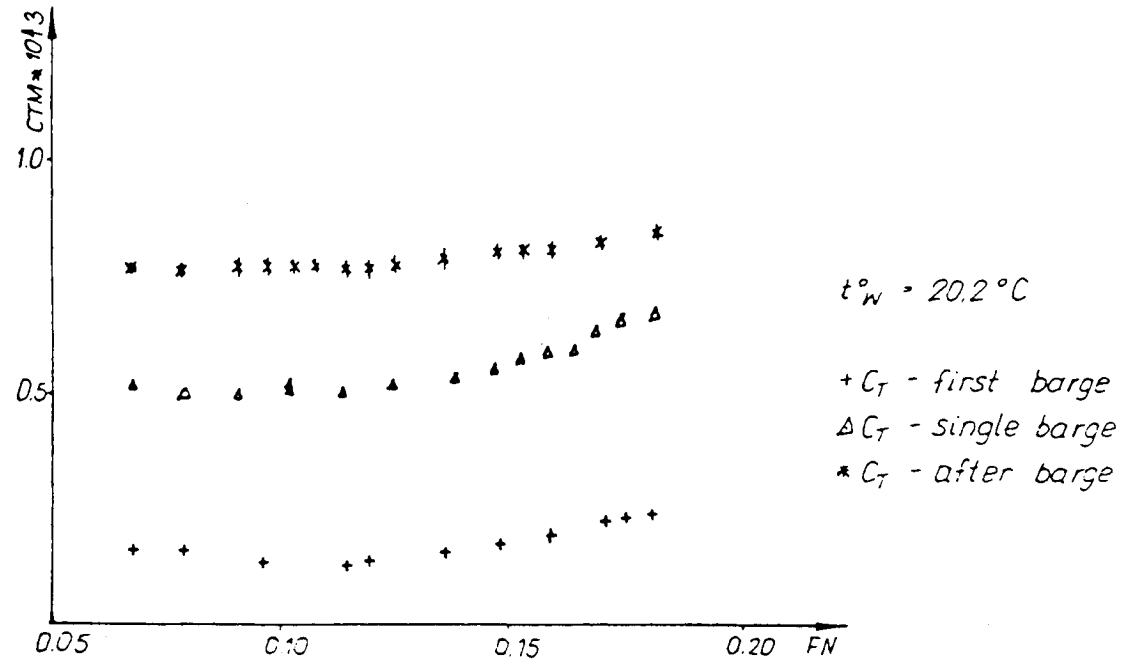

Fig. 5

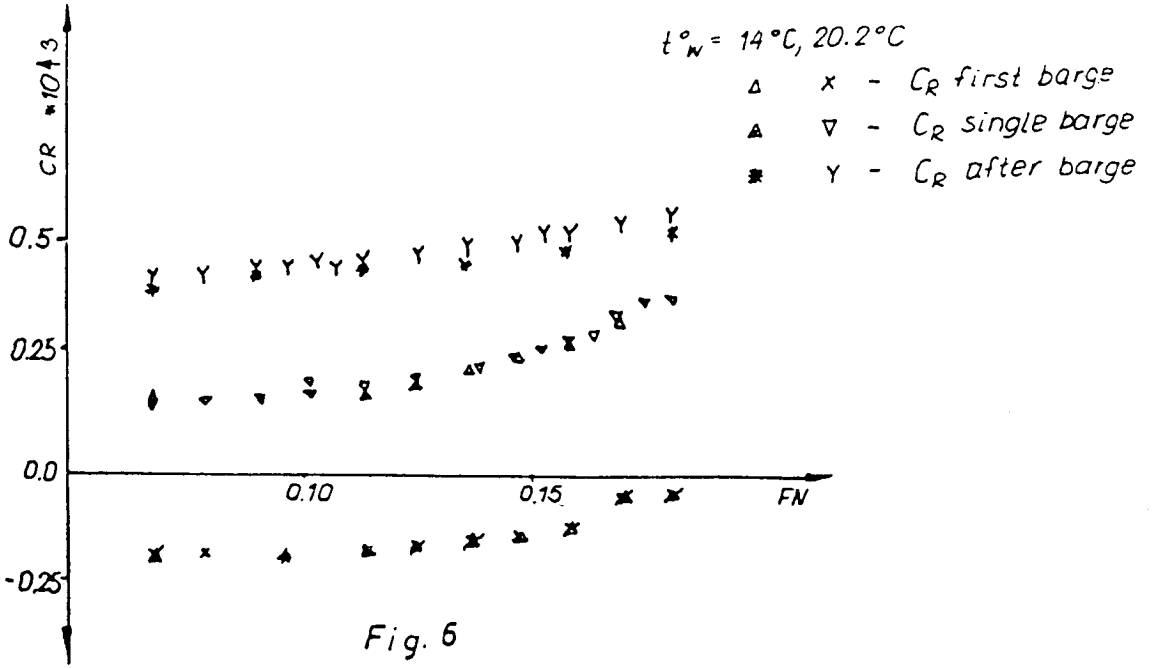

Fig. 6

It should be noted that the measured resistance of the front barge is in good agreement with similar data published in [3], but the recommendations given in [3] about practical equality of the rear barge resistance with that of a single barge prove to be incorrect, as the measured resistance of the second barge in the train is considerably greater.

4.2. Influence of the draught changes

The influence of draught changes on the measured model resistance was evaluated during the model tests as well. The experimental results obtained show that 25 % in draught leads to 3.5 times greater difference in resistance fractions of the first and the second

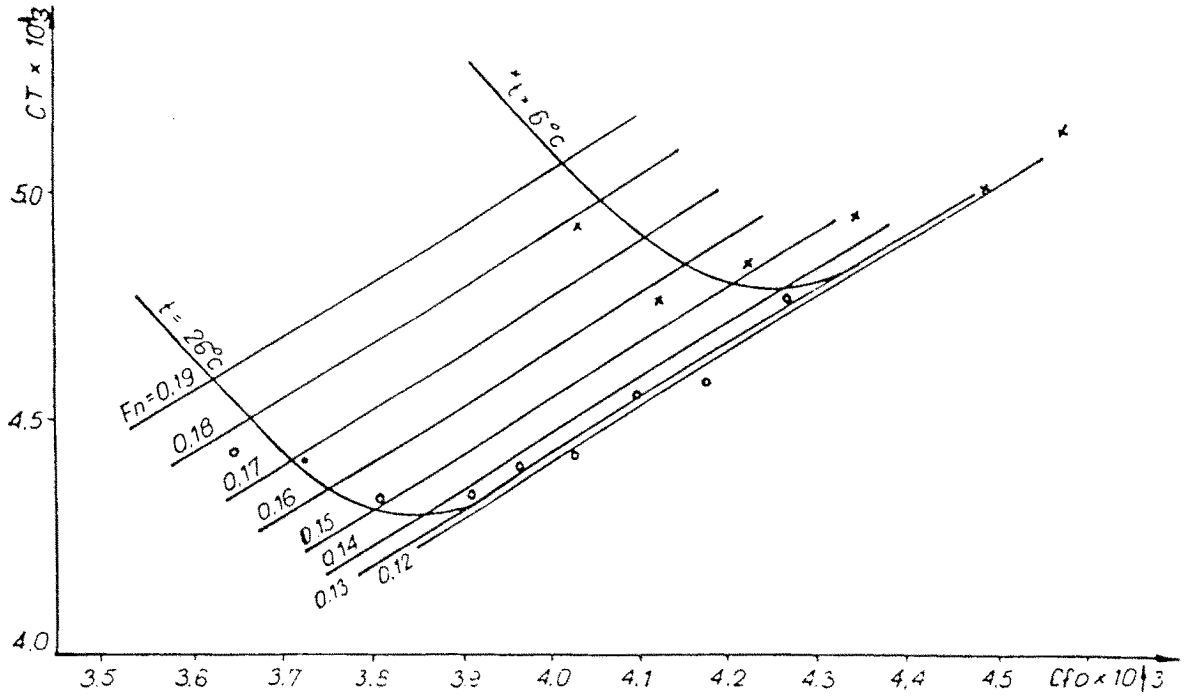

Fig. 7

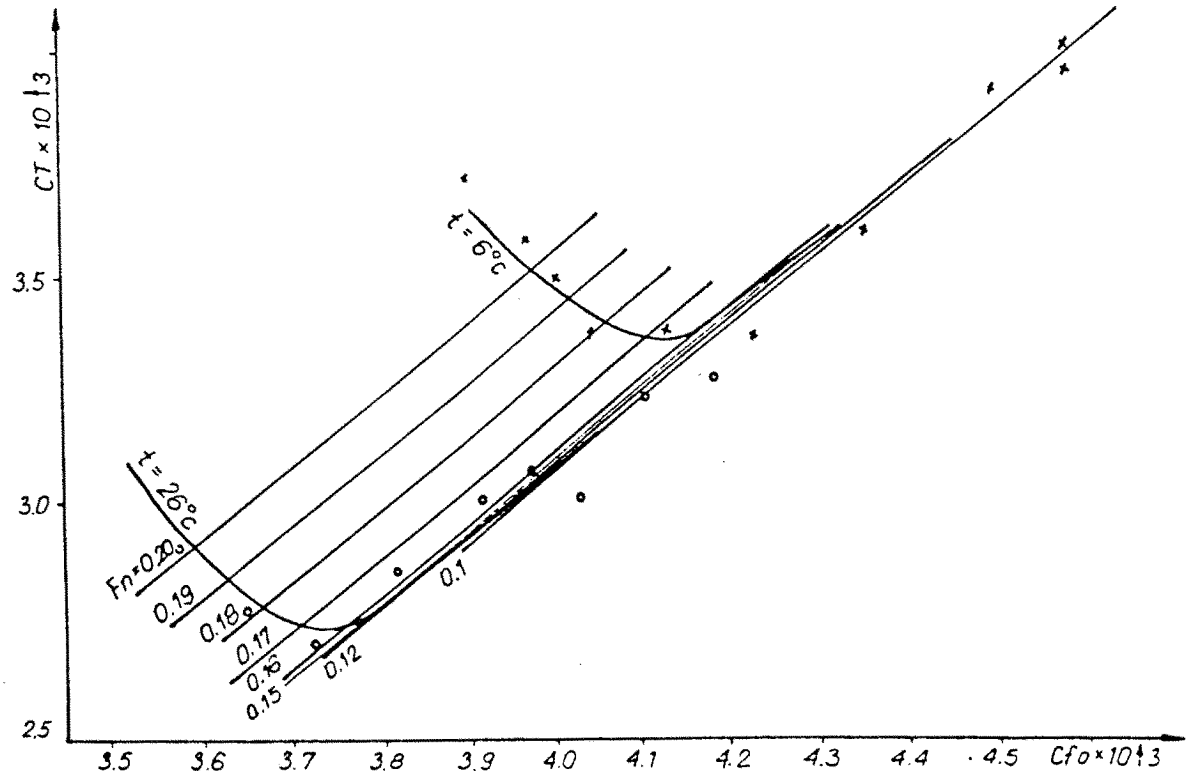

Fig. 8

barge, in direction of reducing R_T of the front barge and consequently increasing R_T of the rear one. At that, the resistance of the single barge changes insignificantly.

4.3. Form factor evaluation

In order to investigate the form factor (1 + k) and its changes under different states, the correspondingly

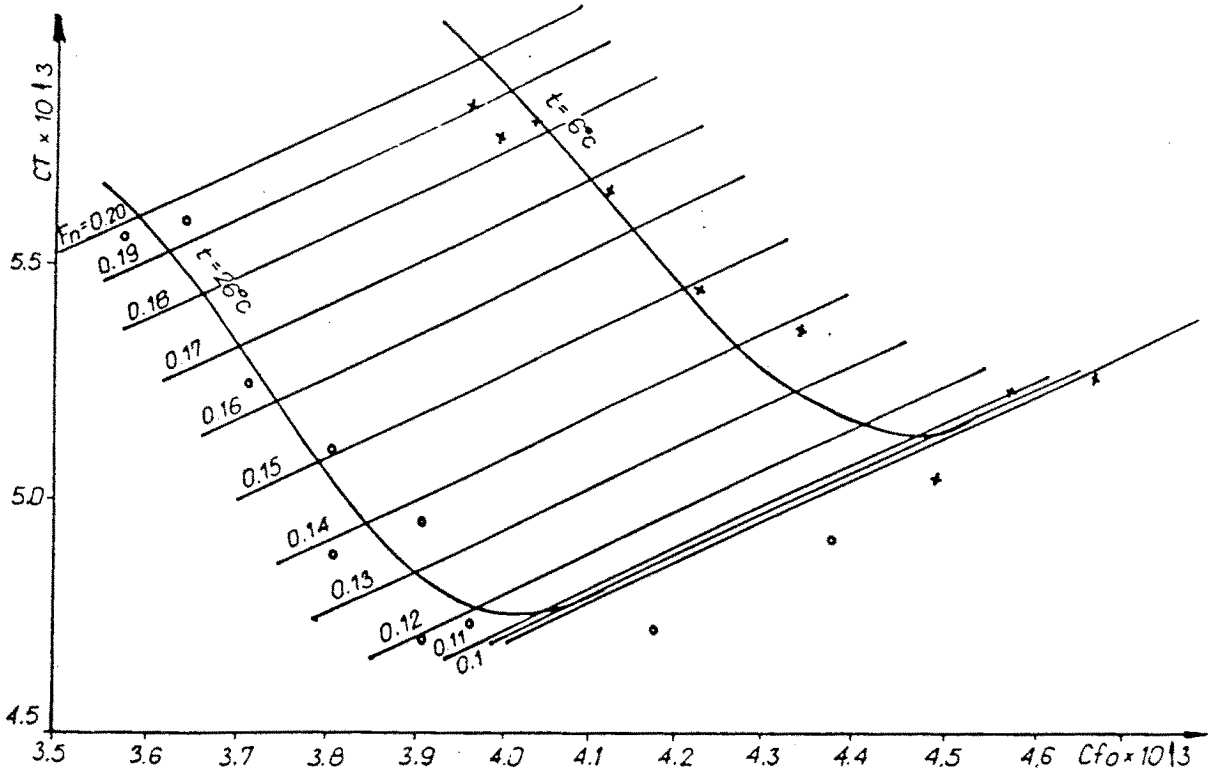

Fig. 9

obtained experimental results are compared in Figs. Nº 7–9, where C_T is total resistance coefficient and C_{fo} is friction coefficient after ITTC–1957 correlation line.

Based on the $(C_T - C_{fo})$ curves, the form factor (1+k) at different temperatures were determined by the curve slope at low isofroude numbers. The $[C_T - \log(Rn)]$ curves are shown in Figs. Nº 10–12.

The results thus obtained do not follow strictly the three–dimentional extrapolation method, as a constant term obviously occurs in the expressions of the total resistance coefficient. That is the form resistance coefficient can't simply be taken as just proportional to the friction resistance coefficient. On this ground we propose an expression for the total resistance coefficient as follows:

$$C_T = (1+k)C_{fo} + C_o + C_w$$

or let

$$C_F = kC_{fo} + C_o$$

then

$$C_T = C_F + C_{fo} + C_w$$

where C_F is introduced as a form resistance coefficient.

The constant allowance, C_o, might be positive or negative. For single barges its value is small and can be easily missed by the experimentator, but for barges configurated in a train it must not be neglected.

5. CONCLUSIONS

The practical importance of reported elaboration is predetermined by the fact that river fleets of the two cooperating countries are composed primarily by push–trains.

The careful study of the hydrodynamical interaction between constituent vessels in the push–train could

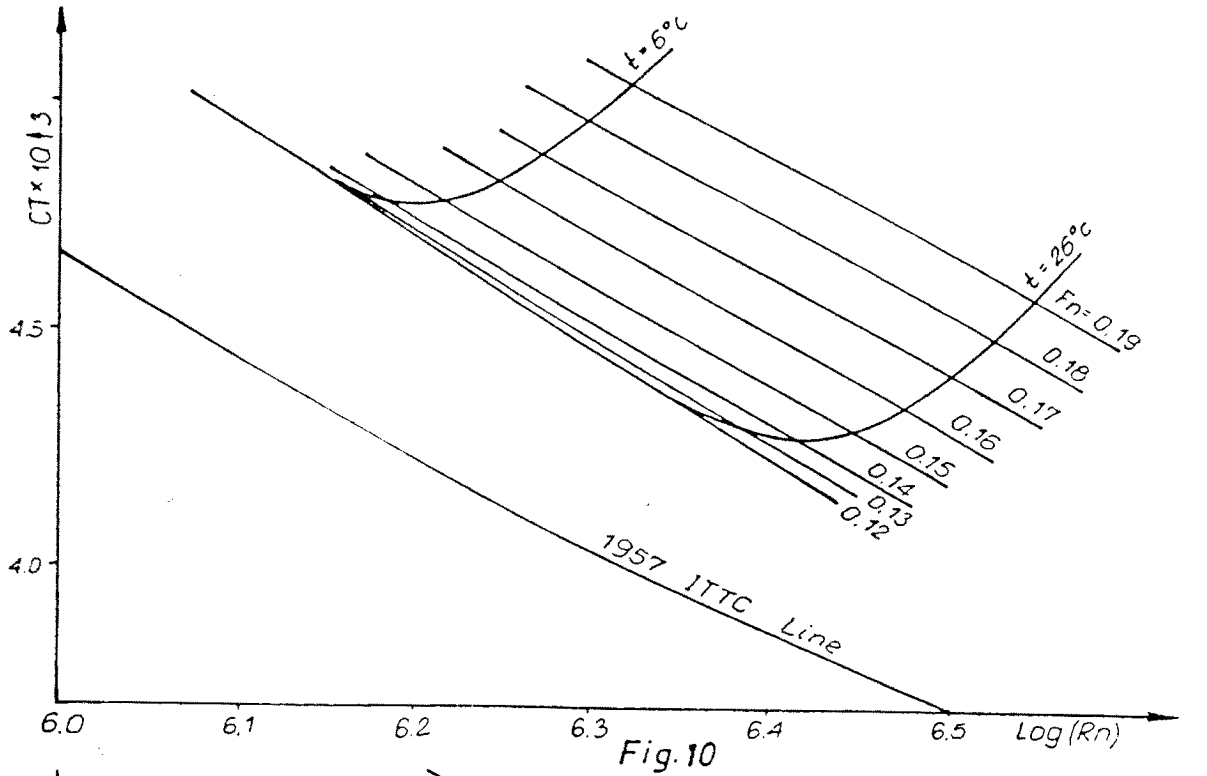

Fig. 10

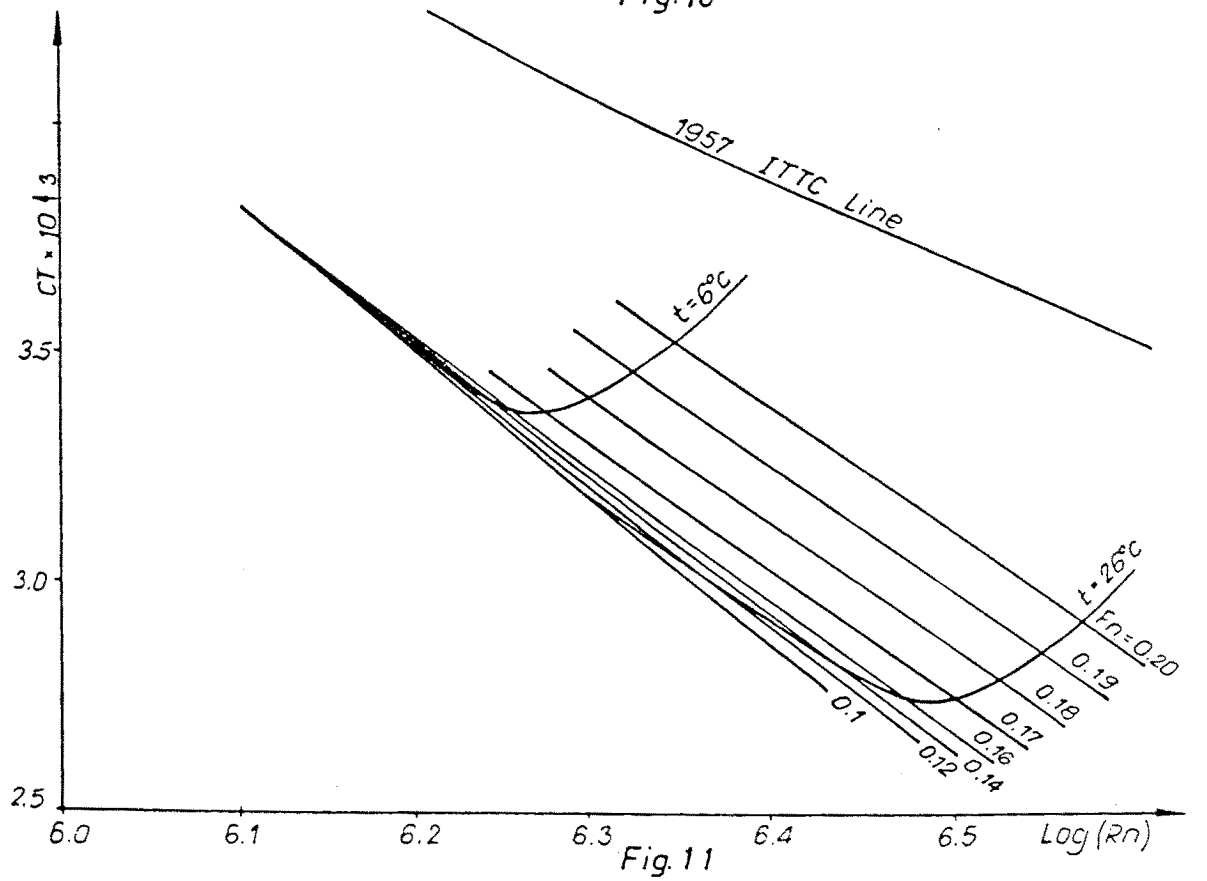

Fig. 11

serve in solving numerous practical design and optimization problems aiming at reducing the total train resistance and hence at improving its operational effectiveness.

Further elaboration of the reported approach for barge train resistance correlation to full scale is suggested on the basis of recalculation of already existing experimental data as well as in the process of new

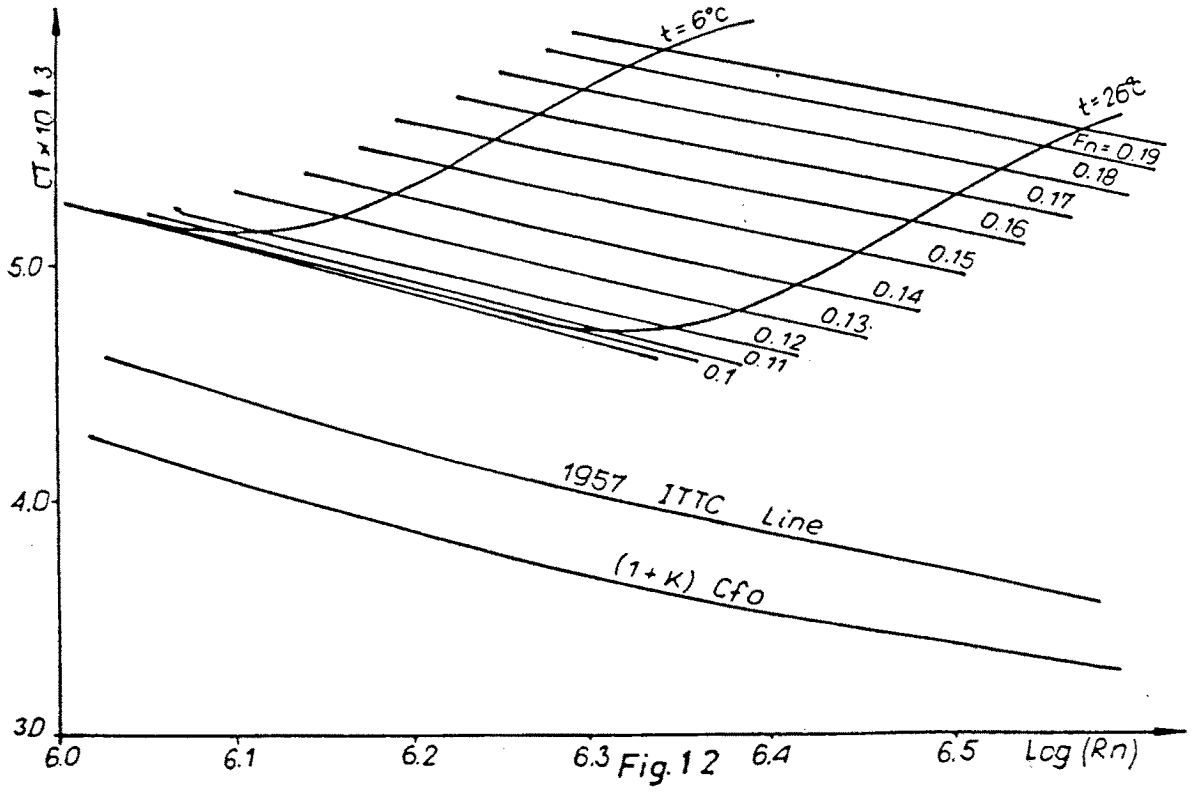

Fig. 12

model tests of the kind, in order to check the correctness and scope of its application and to get deeply in the nature of the newly introduced allowance.

References

[1] Li Shimo, Chen Keqiang, Luo Wei., "The Experimental Results for Resistance with Barge Train". WUWTE, Sept. 1990, China.

[2] Kisheva D., "Systematic Investigations of Resistance and Propulsion of Push-trains". BSHC.

[3] Velednitzkii I.O., "The Resistance of Push-trains 'TRANSPORT'". Publ. House, Moskow 1965

PS-1.9

H. JARZYNA

Ship Propeller Department, Institute of Fluid-Flow Machinery, Gdansk, Poland

GLOBAL AND LOCAL RESISTANCE AND THRUST CHANGE FACTORS

In the report of the Powering Performance Committee great attention was paid to the ITTC 78 performance prediction method.

I would like to make some comments connected with this method.

The question is to determine the global and local changes of ship resistance caused by the ship propeller and to determine the global and local changes of the

propeller thrust related with the propeller hull interaction.

The resistance changes are determined in reference to the hull drag R_o without propeller (or R_c with the propeller at zero thrust). The global and local resistance changes can be given as

$$\Delta R_o = R_B - R_o \quad (1)$$

$$d(\Delta R_o) = dR_B - dR_o \quad (2)$$

where dR_B, dR_o are the resistance of the same ΔF area of the hull.

For simplicity only the R_0 -resistance will be taken into consideration. There is no difficulty when going from R_o to R_c.

Nondimensional form of these changes can be built when dividing the rate of change by the resistance $R_B(R_o)$ or dR_B (dR_o). The resistance change factor t_R (global) or t_R $(\vec{r})$ (local) is received.

$$t_{R2}=\frac{R_B-R_o}{R_B} \quad (3)$$

$$t_{R3}=\frac{R_B-R_o}{R_o} \quad (4)$$

$$t_{R2}(\vec{r})=\frac{dR_B-dR_o}{dR_B} \quad (5)$$

$$t_{R3}(\vec{r})=\frac{dR_B-dR_o}{dR_o} \quad (6)$$

By way of analogy one can characterize the global and local changes of the propeller thrust caused by the hull action. The reference level for the thrust changes is to be fixed first of all. This reference level could be the thrust of the hypothetical open propeller (H.O.P.). The H.O.P. is the screw propeller being in every respect beyond the hull action. It is working in the uniform stream $v = -v_s$. The H.O.P. thrust T_H is equal to the hull resistance R_o. The H.O.P. diameter D_H is equal to the behind propeller diameter D_B. The H.O.P. revolution n_H is determined optimum according to the given diameter $D_H = D_B$. The H.O.P. is optimum propeller. The radial distribution of the blade circulation is in agreement with the Betz optimum criterion.

The local thrust changes of the behind propeller are

$$dT_H=\frac{dT_H}{dx}dx$$

related to the reference level

The global and local thrust changes can be determined in dimensional form

$$\Delta T=T_B-T_H \quad (7)$$

$$d(\Delta T)=dT_B-dT_H \quad (8)$$

and in nondimensional form.

$$t_{T2}=\frac{T_B-T_H}{T_B} \quad (9)$$

$$t_{T_3}=\frac{T_B-T_H}{T_H} \quad (10)$$

$$t_{T2}(X)=\frac{dT_B-dT_H}{dT_B} \quad (11)$$

$$t_{T3}(X)=\frac{dT_B-dT_H}{dT_H} \quad (12)$$

The new proposed definitions are justified and proved as follows:

1. There is an increasing need to operate parallel with the global and local resistance changes especially when numerical methods of investigations of propeller hull interaction are introduced. A common structure of definition of resistance changes factors for global and local changes should be without discussion.

Extrapolation of the definition of the resistance change factor, used up today and named the thrust deduction factor,

$$t_{RI}=\frac{T_B-R_o}{T_B} \qquad (13)$$

to the local circumstances can be formally done to the form

$$t_{RI}(\vec{r})=\frac{dT_B-dR_o}{dT_B} \qquad (14)$$

This formal expression (14) is very seldom to be physically interpreted. The force dR_o is acting on the hull area ΔF. The force dT_B is acting on the propeller area ΔA. There is no one to one correlation between the areas ΔF and ΔA. It is the matter of special investigations to find the relation between the local forces distributions on the hull and on the propeller. The definition of resistance change factor should be built using the resistance forces only. The formula (14) is at no value for propeller hull interaction investigation.

2. The calculation formula of the global resistance change factor for different special circumstances should be built based on a general definition. Analyzing the existing formulas for resistance change factors one can state that there is one formula

$$t_{RIS}=\frac{T_{BS}-R_{oS}}{T_{BS}} \qquad (15)$$

in ship scale calculations, and another formula

$$t_{RIm}=\frac{T_{Bm}+F_D-R_{om}}{T_{Bm}} \qquad (16)$$

when the model calculations are performed based upon the self propulsion tests' results. A general definition which will give in special cases both the formulaes could be found in the form

$$t_{RI}=\frac{\Delta R}{T_B}=\frac{R_B-R_o}{T_B} \qquad (17)$$

The generality of this definition is limited to the global values only. The local suction factor cannot be deduced from this definition.

The proposed definitions Nº 2 and Nº 3 fulfill the demand to be the base in forming the suction factor for all special cases, for the local suction factor too. This is shown in Table Nº 1.

In Fig. 1 four curves are presented

$$\frac{R_{Bm}}{R_{cm}}=f\langle\frac{T_{Bm}}{R_{cm}}\rangle$$

(a convex curve – 1, a straight line – 2, two concave curves – 3 and 4) in the coordinate plane

$$\langle\frac{T_{Bm}}{R_{cm}},\frac{R_{Bm}}{R_{cm}}\rangle.$$

These four curves in the coordinate plane

$$\langle\frac{T_{Bm}}{R_{cm}},\frac{R_{Bm}}{R_{cm}}-1\rangle$$

are identical with the four suction force lines

$$\frac{\Delta R}{R_{cm}}=\frac{R_{Bm}}{R_{cm}}-1=f\left[\frac{T_{Bm}}{R_{cm}}\right]$$

and with the suction factors t_{R3} according to the definition Nº 3.

			present day state	proposal No 1	proposal No 2
general definition		global	$t_{R1} = \frac{R_B - R_o}{T_B}$	$t_{R2} = \frac{R_B - R_o}{R_B}$	$t_{R3} = \frac{R_B - R_o}{R_o}$
		local	———	$t_{R2}(\vec{r}) = \frac{dR_B - dR_o}{dR_B}$	$t_{R3}(\vec{r}) = \frac{dR_B - dR_o}{dR_o}$
special cases	self propulsion tests	determination of t_R random values for $\Delta R_m \to 0$, $T_{Bm} \to 0$, $F_D \to R_{om}$	$t_{R1m} = \frac{T_{Bm} + F_D - R_{om}}{T_{Bm}}$ $t_{R1m} \to tg\gamma_m$ $0 < tg\gamma_m < (tg\gamma_m)_{max}$	$t_{R2m} = \frac{T_{Bm} + F_D - R_{om}}{T_{Bm} + F_D}$ $t_{R2m} \to 0$	$t_{R3m} = \frac{T_{Bm} + F_D - R_{om}}{R_{om}}$ $t_{R3m} \to 0$
	determination of ship propeller thrust	calculation of T_{Bs} and ΔR_s for $t_{Rm} = t_{Rs}$ random values of T_{Bs}, ΔR_s	$t_{R1s} = \frac{T_{BS1} - R_{os}}{T_{BS1}}$ $T_{BS1} = \frac{R_{os}}{1 - t_{R1m}}$ $T_{BS1} \to \frac{R_{os}}{(1 - tg\gamma_m)} \neq R_{os}$ $(\Delta R_s)_1 \to [T_{BS1} - R_{os}] \neq 0$	$t_{R2s} = \frac{T_{BS2} - R_{os}}{T_{BS2}}$ $T_{BS2} = \frac{R_{os}}{1 - t_{R2m}}$ $T_{BS2} \to R_{os}$ $(\Delta R_s)_2 \to 0$	$t_{R3s} = \frac{T_{BS3} - R_{os}}{R_{os}}$ $T_{BS3} = R_{os}(1 + t_{RS3})$ $T_{BS3} \to R_{os}$ $(\Delta R_s)_3 \to 0$
	screw and wind propeller ship	determination of t_R random values $T_{Ws} \to R_{os}$, $T_{Bs} \to 0$	$t_{RS1} = \frac{T_{Bs} + T_{Ws} - R_{os}}{T_{Bs}}$ $t_{RS1} \to t_{gs}$	$t_{RS2} = \frac{T_{Bs} + T_{Ws} - R_{os}}{T_{Bs} + T_{Ws}}$ $t_{RS2} \to 0$	$t_{RS3} = \frac{T_{Bs} + T_{Ws} - R_{os}}{R_{os}}$ $t_{RS3} \to 0$

Table 1. The comparison of t_{R1}, t_{R2} and t_{R3}.

The suction factors t_{R1} and t_{R2} are shown in the same Fig 1 related to the same four suction force lines.

There are some characteristic consequences of the suction factor definition being in use (definition Nº 1)

1. When the R_{Bm} – line is convex the increase of the suction factor t_{R1i} is related to the decrease of the suction force.

2. The random values of t_{R1i} when $T_{Bm} \to 0$ are equal to $t_{gi} \neq 0$. The suction factor t_{R1} is of non zero value when the suction force is equal zero.

3. When the ship propeller thrust is determined on the assumption t_{Rim} t_{Ris} one receives the non zero suction force on ship related to the zero suction force on model

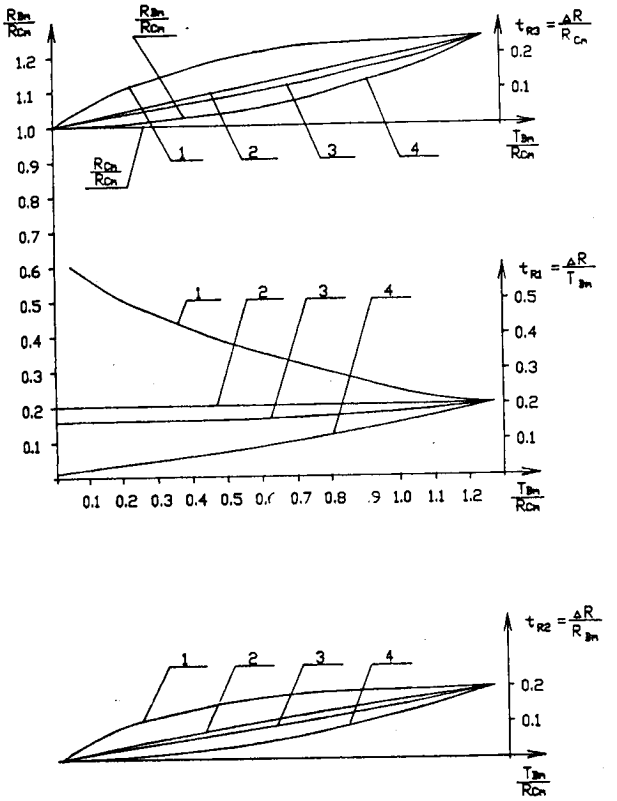

Fig. 1. Suction factors t_{R1}, t_{R2} and t_{R3} from self propulsion tests.

$$(T_{BS})_{1i}=\frac{R_{os}}{1-t_{gi}}\neq R_{os}$$

$$\Delta R_s=(T_{BS})_{1i}-R_{oS}\neq 0$$

and the decreasing suction force on ship related to the increasing suction force on model.

4. There is no possibility to build a local resistance change factor on the basis of the definition Nº 1 structure.

These characteristic features are quite different in the case of suction factor definition Nº 2 or Nº 3.

1. The smaller the suction force, the smaller the suction factor t_{R2}, t_{R3}.

2. When the suction force is zero, the suction factors t_{R2} and t_{R3} are zero too.

3. The smaller the suction force on model, the smaller the suction force on ship. The zero suction force on model is related with zero suction force on ship.

4. The local resistance change factors can be built making use of the definition structure Nº 2 and Nº 3.

Therefore the existing definition Nº 1 of the resistance change factor should be replaced by the definition Nº 3 or Nº 2.

In the case of definition Nº 3 the suction force is divided by the constant force R_o, and in the case of definition Nº 2 by the variable force R_B. From this point of view the definition Nº 3 should be preferred.

Definition Nº 2 leads to the traditional form of relation between T_B and R_o

$$T_B=\frac{R_o}{1-t_{R2}},$$

while definition Nº 3 gives a different relation

$$T_B=R_o(1+t_{R3}).$$

From this point of view one could be of the opinion that the definition Nº 2 should be accepted to satisfy the demands of tradition.

3. By analogy to the conception of propulsion efficiency

$$\eta_D=\frac{R_o\bullet V_s}{Q_B\bullet\omega_s} \qquad (18)$$

the local propulsion efficiency is sometimes built, especially when the optimum behind propeller is analyzed.

$$\eta_{DX}=\frac{dR_o\bullet V_s}{dQ_B\bullet\omega_s} \qquad (19)$$

The hull resistance element dR_o will be replaced by the behind propeller thrust element dT_B accordingly to (14)

$$dR_o=dT_B[1-t_{RI}(r)] \qquad (20)$$

or when the notation from literature will be used

$$dR_o=dT_B(1-t_x) \qquad (21)$$

One can have the often used form

$$\eta_{DX}=\frac{dT_B\bullet V_s}{dQ_B\bullet\omega_s}(1-t_x) \qquad (22)$$

Nobody can explain what is the physical meaning of the factor $(1-t_x)$., though it is in use in literature since about fifty years.

The new definition of the local thrust change factor and of the hypothetical open propeller seem to be the best way to introduce corrections to the optimizing process.

The propulsion efficiency and the local propulsion efficiency can be written in terms of the H.O.P. parameters T_H or dT_H

$$\eta_D=\frac{T_H \bullet V_s}{Q_B \bullet \omega_s} \tag{23}$$

$$\eta_{DX}=\frac{dT_H \bullet V_s}{dQ_B \bullet \omega_s}=\frac{dT_B \bullet V_s}{dQ_B \bullet \omega_s}[1-T_t(x)]= \tag{24}$$
$$=\eta_B[1-t_T(x)]$$

The factor $[1-t_T(x)]$ is no suction factor; it is the thrust change factor. In the case when the optimum radial distribution of the blade circulation G(x) the behind propeller is to be determined, the thrust change factor is a functional depending on x and on the unknown function dG(x)/dx

$$(1-t_{TX})= f\left[x,\frac{dG(x)}{dx}\right] \tag{25}$$

The local thrust change factor is in this form of importance in the optimizing process.

The results of its use in the optimizing procedure are the optimizing criteria.

One of them can be built on the assumptions made by Lerbs and its end form is

$$\frac{\tan\beta}{\tan\beta_i}=K_{1J}\frac{\sqrt{1-W_x}}{\sqrt{1-t_{TX}}} \tag{26}$$

The second one can be built on the assumptions made by van Manen with the end result

$$\frac{\tan\beta}{\tan\beta}=K_{2J}\frac{1-W_x}{1-t_{TX}} \tag{27}$$

In both cases

$$\tan\beta=f_\beta(x)$$

$$W_x=f_W(x)$$

$$\tan\beta_1=f_\beta\left[x,\frac{dG(x)}{dx}\right] \tag{28}$$

$$t_{TX}=f\left[x,\frac{dG(x)}{dx}\right]$$

These criteria used in the design procedure of the behind propeller give nonlinear integro-differential equations which can be solved by the usual methods. The only difference is that a double iterative procedure must be applied.

The result of the optimizing procedure is the optimum radial distribution of the blade circulation $G_{opt}(x)$. Then the functional

$$(1-t_{TX}) = f_t\left[x,\frac{dG(x)}{dx}\right] \tag{29}$$

with $G(x) = G_{opt}(x)$ will be a function of x only

$$(1-t_{TX})=f_t(x) \tag{30}$$

In the course of calculations for different ships we can compile data for $(1-t_{TX}) = f_t(x)$ and $(1-W_X) = f_w(x)$.

This data bank can be needful when investigations will be undertaken to receive a relation between $(1-t_{TX})$ and $(1-W_x)$

$$(1-t_{TX})=f(1-W_X) \qquad (31)$$

It is proposed

1. to introduce a definition of hypothetical open
2. to introduce the global and local thrust change factors definition.

My comments and proposals are addressed to the Powering Performance Committee, but I am sure that the Propulsor Committee will be interested too. I would be glad to receive from both Committees an information about their standpoint to the questions under discussion.

REFERENCES

[1] Lerbs H., "Bemerkungen zur Theorie und zum Entwurf von Nachstromschrauben". HSVA – Bericht Nr. 254 – 1945.

[2] Lerbs H.W., "Moderately Loaded Propellers with a Finite Number of Blades and an Arbitrary Distribution of Circulation". TSNAME Vol. 60 – 1952.

[3] Lerbs H., "Ergebnisse der angewandten Theorie des Schiffspropellers". JSTG 49. Band – 1955.

[4] Lerbs H., "Über die Entwicklung der Propulsionstheorie". Schiff und Hafen. Heft 6, 1956.

[5] van Manen J.D., "The Design of Ship Screw of Optimum Diameter for an Unequal Velocity Field". TSNAME Vol 66 – 1952.

[6] Burrill, L.G., "The Optimum Diameter of Marine Propellers. A New Design Approach". Trans. NECJ, Vol. 72, 1955–1956.

[7] Jarzyna H., "Some Defects of the Criteria of Determination of the Optimum Radial Distribution of Propeller Thrust". Proposals to Eliminate Them. ISP, Vol 33, Nº 380, April 1986.

[8] Jarzyna, H., "Die lokale Schubanderungszahl und deren Einfluss auf die optimale radiale Verteilung der Zirkulation auf der Propellerfläche". Schiffbauforschung 24–3–1985.

[9] Jarzyna H., "Some Consequences of the Analytical design Method of Ship Propeller". Proceedings of the Conference "Advance in Propeller Research and Design". Gdansk, 1981.

PS–1.10

M. FERRANDO and C. PODENZANA–BONVINO
Istituto di Ingegneria Navale, Universitá di Genova, (Italy)

A SHORT REVIEW OF FULL SCALE TESTS

This discussion has the aim of presenting a brief review of full scale tests performed during the last

years on an oceanographic vessel of the C.N.R. (Italian National Research Council). The matter is relevant not only for the Resistance and Flow Committee, but also for the Performance and Seakeeping Committees.

1. Resistance

Two series of trials have been completed, during which the vessel was towed by a tug; a load cell inserted in the tow rope measured the towing force and its signal was recorded both in analogical and in digital form for immediate visualisation and for future elaboration. (See a sample of time history of the towing force in Figure 1).

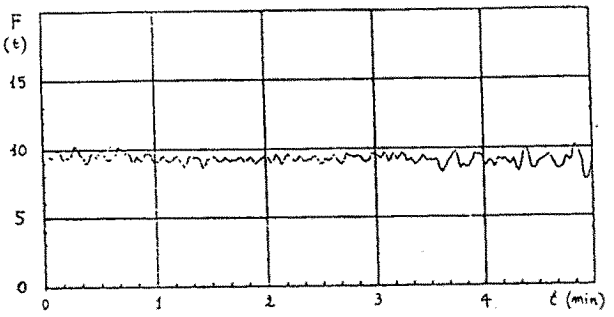

Fig. 1. Time history of full scale t owing force

The analysis of recorded data has been made following the rules of R.I.Na. (Italian Institute of Classification) for bollard pull testing [1,2], that our Institute checked during official trials on a Italian Navy tug towing the cruiser "Andrea Doria". Figure 2 shows the resistance-speed curve of the ship [3] derived from full scale data.

A complete set of resistance tests on a model of the oceanographic ship is now being carried out both in the towing tank of the University of Genoa and in the

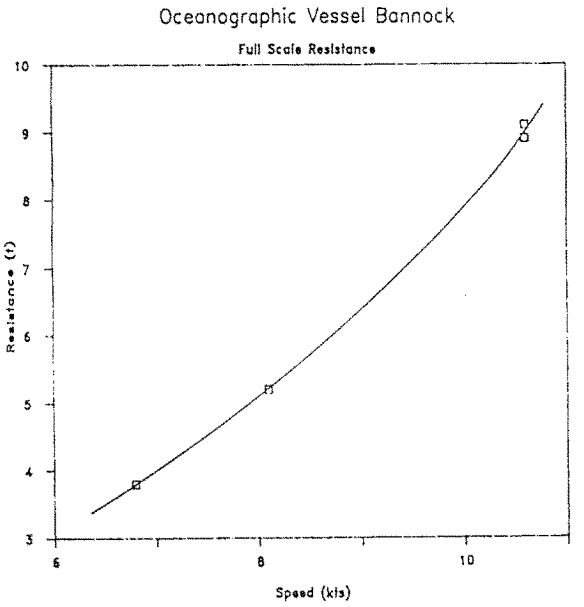

Fig. 2. Full scale resistance versus speed

tank of the University of Trieste, working within a joint research program with has the aim of investigating model-ship correlation, with particular reference to small tanks and to body appendages.

2. Flow around the hull

Within a research program in cooperation with CE.TE.NA. (Italian Ship Research Centre, Fincantieri Group), the mentioned oceanographic vessel has been equipped with a pitometer installed on the ship bottom, in a watertight opening through shell plates. During both the towing tests we just described and during self-propulsion courses, the water-hull relative velocity was measured and recorded, at various distances from the body [4,5]. Figure 3 shows the intensity of tangential velocity in the boundary layer, at different distance from the hull surface and during various ship courses.

3. Pressures around the hull

In the fore part of the same vessel six watertight pressure transducers have been installed, by means of

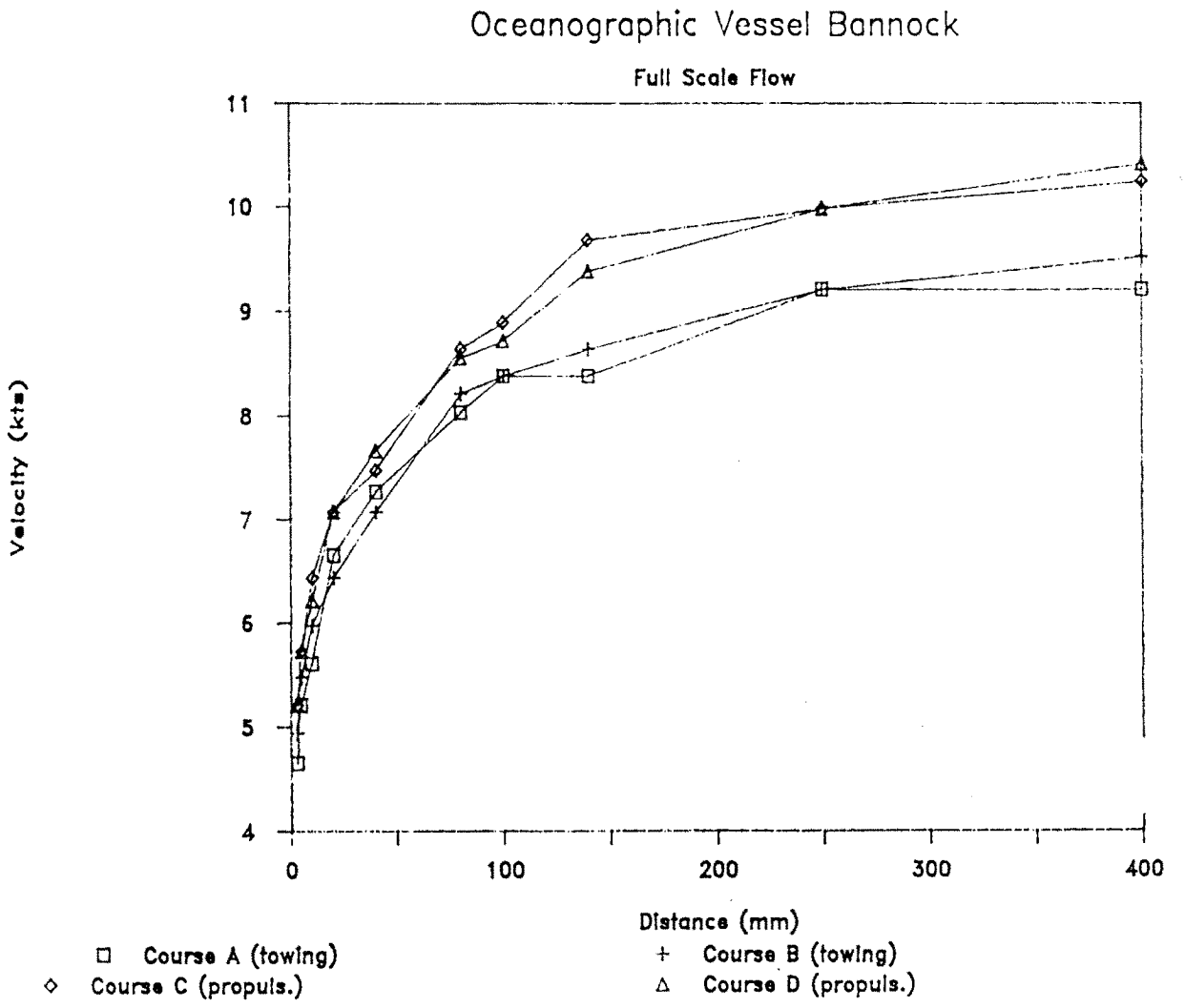

Fig. 3. Full scale velocity distribution in the boundary layer

steel bushes welded to the bow shell, where holes had been obtained. Pressures have been so recorded at different positions, during courses under tow and self-propulsion navigation, with calm water and with moderate waves. The prime aim of this research is the comparison between theoretical calculations of hydrodynamic pressures, according to strip theory based methodologies, and the experimental, full scale data [6,7]; the second one is the full scale verification of viscous flow calculations allowed by numerical hydrodynamic procedures. Only the first study has been at present accomplished.

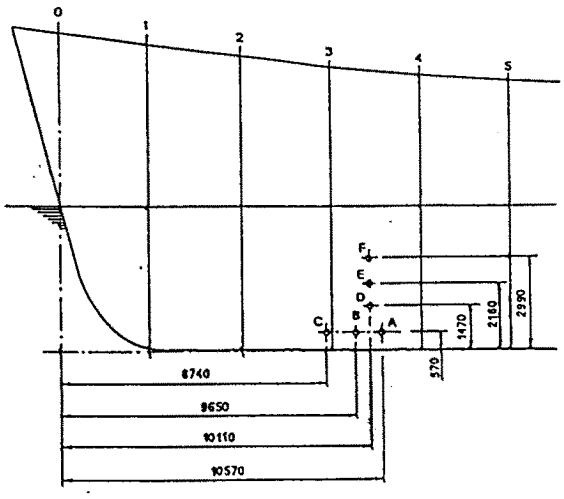

Fig. 4. Position of pressure transducers

Figure 4 shows the position of pressure transducers in the fore part of the oceanographic ship; in Figure 5 a sample power spectrum of the measured pressure is compared with the theoretical prediction.

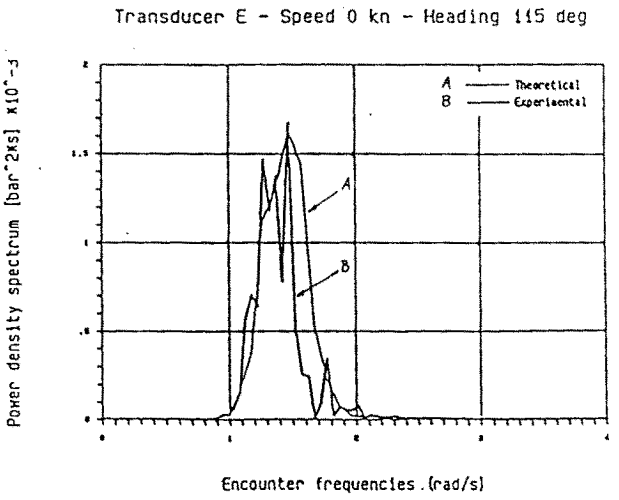

Fig. 5. Experimental and theoretical power spectra of hull hydrodynamic pressure

References

[1] Boote D., Carrera G., Ferrando M., Tedeschi R., "Criteri di valutazione delle prove di bollard pull per remorchiatori e supply vessel", MED'85 Symposium, Milano, June 1985.

[2] Registro Italiano Navale, "Guida sperimentale per l'effettuazione delle prove a punto fisso per rimorchiatori", March 1985.

[3] Ferrando M., Podenzana-Bonvino C., Tedeschi R., "Rimorchio di una nave al vero", NAV86 Symposium, Palermo, October 1986.

[4] Caprino G., Succio D., "Note sulla misura della scia viscosa in vera grandezza a mezzo di tubo de Pilot", CE.TE.NA. Report nº 3149, Genova, March 1988.

[5] Morandi Bergamini D., Irrera N., "Elaborazione dei rilievi di velocitá effettuati per mezzo Raydist durante la campagna di misura della scia viscosa in vera grandezza sulla M/n Bannock", CE.TE.NA, Report Nº 3184, Genova, May 1988.

[6] Boote D., Bruzzone D., Carrera G., "Pressioni idrodinamiche sulla carena di una nave", NAV86 Symposium, Palermo, October 1986.

[7] Boote D., Bruzzone D., Carrera G., "Some experiences in the utilisation of an oceanographic vessel on ship motion analysis", I.M.A.E.M., Athinai, June 1990.

PS-1.11

M. SCHMIECHEN

Berlin Model Basin, Berlin, Germany

PROPULSIVE PERFORMANCE OF METEOR AND HER MODEL IDENTIFIED FROM TESTS UNDER SERVICE CONDITIONS

The usual evaluation of the propulsive performance of ships has been proposed by R.A. Froude more than one hundred years ago. This traditional method is based on well understood pragmatic, but physically and practically rather shaky conventions and can in practice only be applied on model scale. Consequently most of the knowledge on scale effects

necessary for the prediction of full scale performance had to be derived from more or less vague theories.

In order to overcome the problems indicated the author has, over the last decade, systematically developed a rigorous systems identification technique in theory and practice. The final step in this well documented development was the full scale application on board the German research vessel METEOR under service conditions during a routine voyage into the Greenland Sea in November 1988. The full scale tests as well as corresponding model tests at the Hamburg and Berlin model basins sponsored by the German Ministry for Research and Technology have now been finally analysed.

The method for the identification of systems in noisy feed-back loops described by the author earlier in an MIT report proved to be completely adequate. Even at severe sea states, small quasi-steady deviations from the steady average service conditions provide sufficient information for the identification of the five parameters coherently defined by the axiomatic model introduced ten years ago and further developed to a state of maturity now.

Using a hollow shaft fitted with strain gauges and calibrated at the Berlin Model Basin averages of thrust and torque have been measured "continuously" over six or nine complete shaft revolutions. During the tests over a period of about half an hour the rate of revolution was linearly lowered by about ten percent and raised again without disturbing the ship operation itself and the other research activities on board.

Thus at any condition not only the mean values of thrust and torque but also their derivatives with respect to the rate of revolution and the ship speed over ground could be determined. The external forces causing the propeller load variation were the inertial forces due to the very small accelerations of the ship.

Due to the excellent technology, zero stability of less than 1 %, the results were perfect and totally consistent even in severe sea conditions at least in the statistical sense. The range of service conditions covered may best be described by the fourfold increase of resistance encountered due to waves and wind as compared to more moderate weather conditions.

The corresponding model tests confirmed that most of the results are obscured by the well known scale effects at the propeller model. Consequently only propulsion tests at sufficiently high propeller Reynolds numbers have been evaluated and compared with the full scale conditions.

In order to explain and demonstrate the power and potential of the method the evaluation has been based on the results of only two steady model states. To successfully use this very efficient model test technique with only two widely different external forces applied the establishment of truely steady conditions in model speed and bearing friction are the only requirements.

Comparison of the full scale and model results show for example that the scale effect in the thrust deduction fraction is nearly exactly as predicted from earlier tests utilizing boundary layer suction to simulate the full scale energy wake. The final report and forthcoming publications will provide complete

discussions of boundary layer effects in all efficiencies and factors of merit.

Additional tests with a model shortened according to Rader proved that the energy wake can in fact be influenced in the right direction. But the heavy forward trim at the necessary Froude numbers introduces additional effects in hull propeller interaction. So the extra costs for shorter models do appear not to be worthwhile for the type of testing proposed.

In conclusion, the advantages of the proposed procedure as compared to similar proposals, e.g. by Abkowitz, may be summarized as follows:

- coherent axiomatic model with a minimum of parameters identified from only one consistent set of data obtained at service conditions full scale or two steady states on model scale.

In future the method may be applied for the evaluation of model tests and trials and for monitoring of ship performance in service, eventually increasing and improving the data base on scale effects. Validation of CFD codes to be introduced into future ship design can of course only be successfully achieved along this route.

As a new paradigma on hull propeller interaction the method proposed may take some time to make its way into practice. But in view of modern optimum ship design including a symetric afterbody etc., it is more than timely that the present, very unsatisfactory practice is supplemented and, maybe some day, replaced by the new, more rational and more physical, still conventional procedure.

The Second International Workshop on the Rational Theory of Hull Propeller Interaction and its applications will be held at the Berlin Model Basin in due course, if possible in close cooperation with the Powering Performance Committee.

PS-1.12

A.J. MUSKER

Admiralty Research Establishment, Haslar, United Kingdom

DISCUSSION ON PAPER PRESENTED BY CONG AND HSIUNG

Can the authors confirm that the transom is assumed to be always dry? If this is so, can the authors comment on the surprisingly good agreement at low Froude numbers, where the transom would normally be partially wet, or was the experiment arranged to suit the above-named assumption? There is nothing wrong with the latter strategy of course, but it does need to be clarified.

PS-1.13

A.J. MUSKER

Admiralty Research Establishment, Haslar, United Kingdom

DISCUSSION ON PAPER PRESENTED BY DR XUEWEN

Can Dr. Xuewen confirm that the finite difference scheme of Dawson to advect disturbances downstream has been totally replaced in the interior region by the process of matching the flow fields across the two regions?

The trends shown in Figure 3 are very interesting since some of the non-linear results are lower than the linear calculations - an observation made also by Larson and myself last year at the ICNH5 meeting in Hiroshima. Have these results been obtained after a process of code and geometry verification and what is the source of the experimental data?

PS-1.14

LI SHIMO, CHEN KEQIANG and LUO WEI

Wuhan University of Water Transportation Engineering, Wuhan, China.

THE EXPERIMENTAL RESULTS OF RESISTANCE WITH BARGE TRAIN

In order to investigate the hydrodynamic influence between barges in barge train, a group of barge train tests have been done in WUWTE. In order to avoid the changing of ship scales, the tests were carried out under different temperatures.

1. Models and model tests.

The models used are common inland-river barges, which are made of wood, the scales are as follows:

Table 1

Basic Characteristics

Length between perpendiculars Lbp (m)	3.0
Breadth B (m)	0.692
Draught T (m)	0.0635
Displacement Δ (Kg)	112.0
Wetted surface S (m^2)	2.200
Block coefficient Cb	0.852

The surface of the models was lacquered and polished, and the water line and the station mark drawn. A wire of diameter ϕ = 1.6 mm was fitted as a turbulization wire at the theoretical station 19. The model tests were carried out in calm water. The dimensions of the tank are shown as follows:

Table 2

Length (m)	132.0
Breadth (m)	10.8
Depth of water (m)	2.0

First of all, the tests were measured under two different temperatures (6 deg. and 26 deg.) for the 1 + 1 in 1989.

Tests are as follows:

a. the total resistance.
b. the front barge resistance while the after barge fixed.
c. the after barge resistance while the front barge fixed.
d. the single barge resistance.

Secondly, the draught of models was changed to T=0.08 m, the tests have been done as above in 1990.

At last, the draught of models was changed to T=0.08 m, the tests have been done for 1+1+1 in 1990.

Tests are as follows:

a. the total resistance.
b. the front barge resistance while the after barge and the middle barge fixed.
c. the after barge resistance while the front barge and the middle barge fixed.
d. the middle barge resistance while the front barge and the after barge fixed.
e. the single barge resistance.

At a depth of approximately 2/3 T, the water temperature is measured twice (i.e. during the middle of the test and after test). In calculations, the average temperature is taken.

The model speed accepted is equal to the speed of the towing carriage and the resistance is measured by mechanical dynamometer.

2. Results and Conclusions.

The test results of resistance have been sent to Resistance Committee ITTC (through Dr. Müller).

In order to investigate form factor (1+k) and the changes of it under the different states, test results are plotted in Figure 1–Figure 3, where Ct is total resistance coefficient, Cfo is friction coefficient and Cfo is obtained from 1957 ITTC correlation line.

Based on the curves of Ct ~ Cfo, the form factors (1+k) in different states are determined by the slop at low isofroude numbers.

The results of test show that:

1. It is different from Huse's method of three dimensional correlation that there is a constant term which occurred in the expression of the total resistance coefficient. That is, form resistance coefficient cannot be simply taken as only a term which is in proportion to friction resistance coefficient.

Total resistance coefficient may be expressed as follows:

$$Ct=(1+k)Cfo + Co + Cw.$$

or let: $CF=KCfo + Co$

than: $Ct=Cfo + CF + Cw$

Where CF is form resistance coefficient and Co can be positive or negative.

The curves of total resistance coefficient of the single barge can be seen in Figure 1.

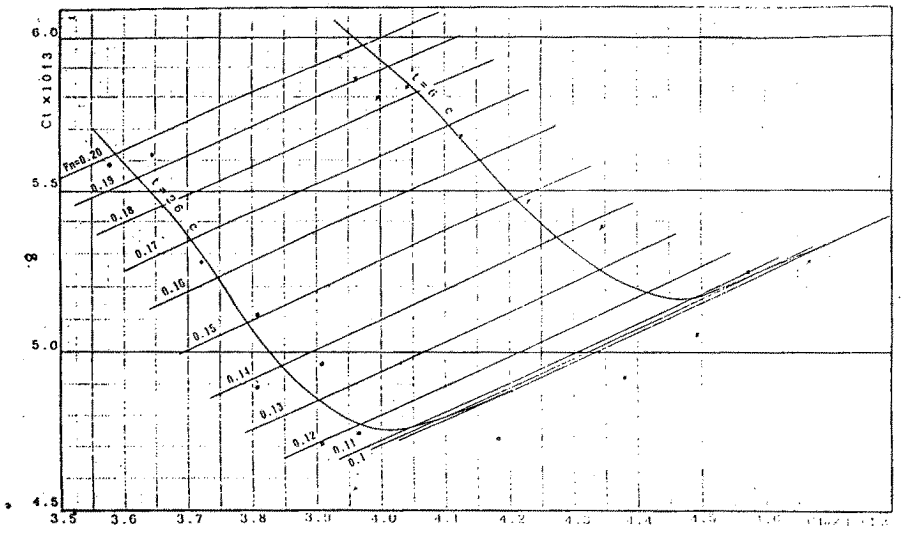

Fig. 1. The plot of Ct versus Cfo for single barge

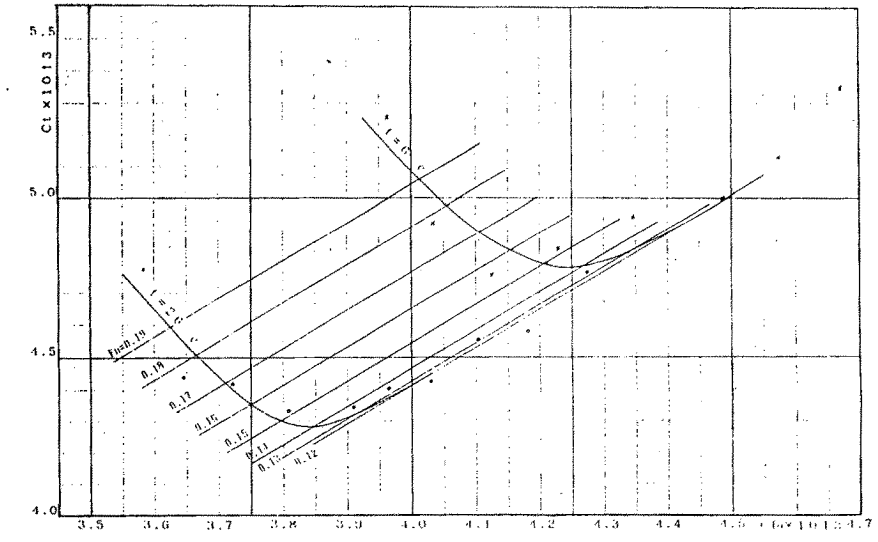

Fig. 2. The plot of Ct versus Cfo for front barge

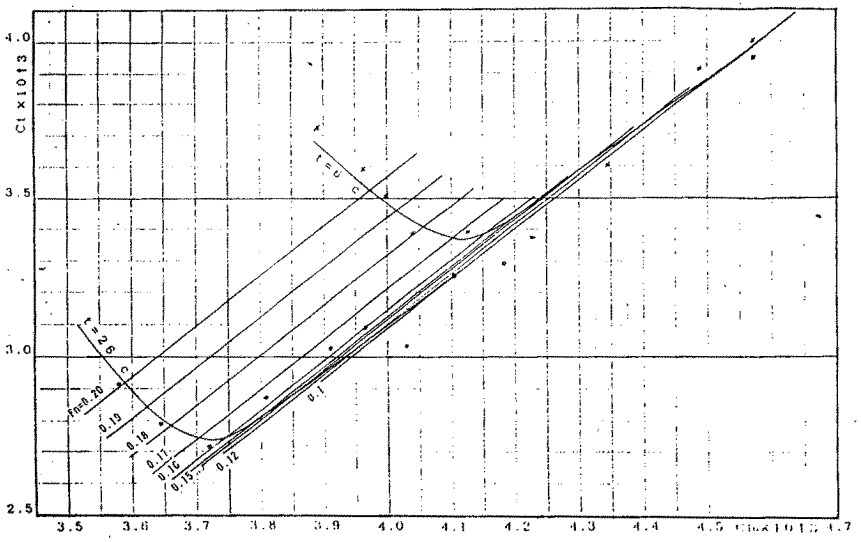

Fig. 3. The plot of Ct versus Cfo for after barge

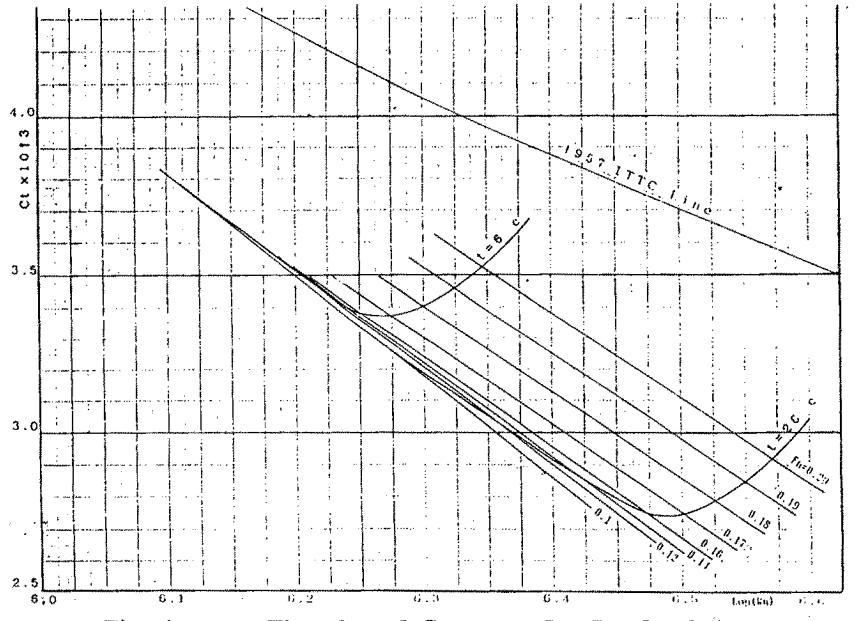

Fig. 4. The plot of Ct versus LogRn for front barge

Form factors and Co of the single barge, as well as that of the front barge and the after barge are as follows:

	1+k	Co
single barge	1.197	-0.377
front barge	1.57	-3.194
after barge	0.917	1.022

2. Front barge resistance

A. The resistance of the front barge is less than the after barge and the single barge (see Figure 5) and the total resistance coefficient is even less than Cfo calculated from 1957 ITTC line (see Figure 4).

This is unexpected but rather surprising.

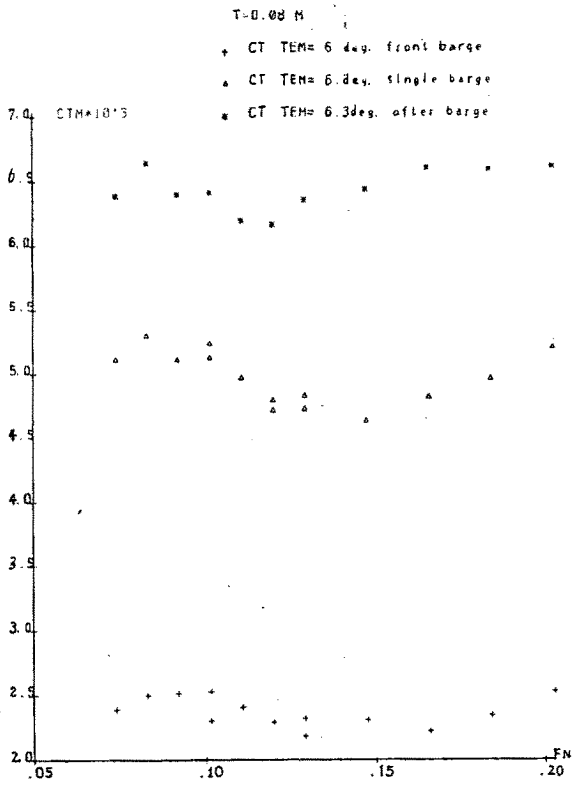

Fig. 5. Plot of Ct versus Fn for barge train (i+i)

B. It may be explained that:

Firstly, due to the existence of the after barge, high pressure area in front part of the after barge is mixed with low pressure area in the rear part of the front barge. It makes form resistance of the front barge decrease.

Secondly, due to the existence of the after barge, it makes the velocity of flow in the part of the front barge stern decrease. Or there is a part of surface which has not evolved, so the friction resistance decreases. Thus, friction resistance calculated by 1957 ITTC is greater than that of the test. So, when friction resistance is calculated by ITTC line, there is a problem of wetted surface deduction.

From the phenomenon we have observed, the bilge cortex moves to downsteam area along the two sides of the after barge. It is obviously different from the single barge; perhaps, the low pressure in the rear part of the front barge is less than that of the single barge.

3. After barge resistance.

The resistance of after barge is greater than that of the front barge and the single barge (see Figure 5~Figure 6). This is also an unexpected phenomenon and in contradiction with the general idea. Generally, when the after barge is existed in the wake and in the low pressure area of the front barge, the resistance of the after barge should be less than that of the single barge. But the results of test is contrary to the general idea, this is worth further investigation.

4. Comparing 1+1 with 1+1+1, the resistance coefficient of the front barge in 1+1 and 1+1+1 are almost the same, and so is that of the after barge (see Figure 7). That means influence among barges is mainly related to adjacent barge.

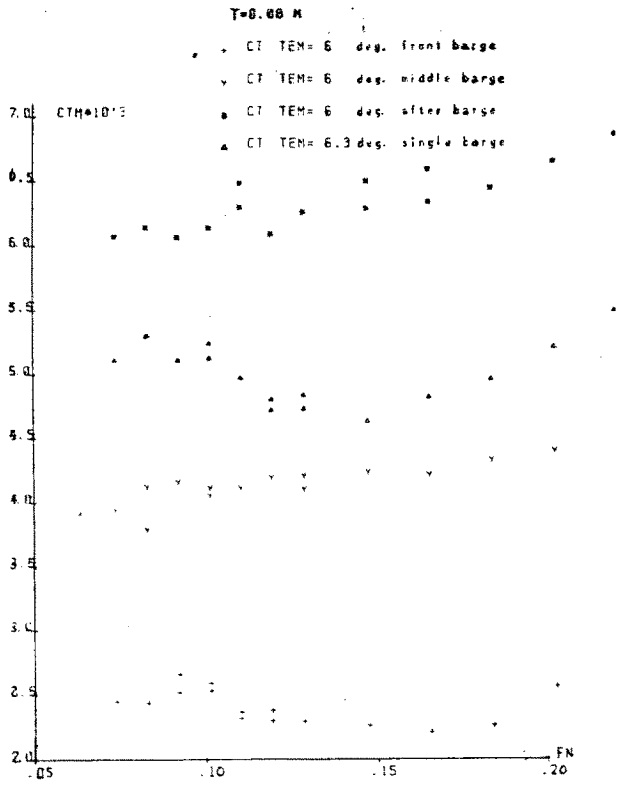

Fig. 6. Plot of Ct versus Fn for barge train (1+1+1)

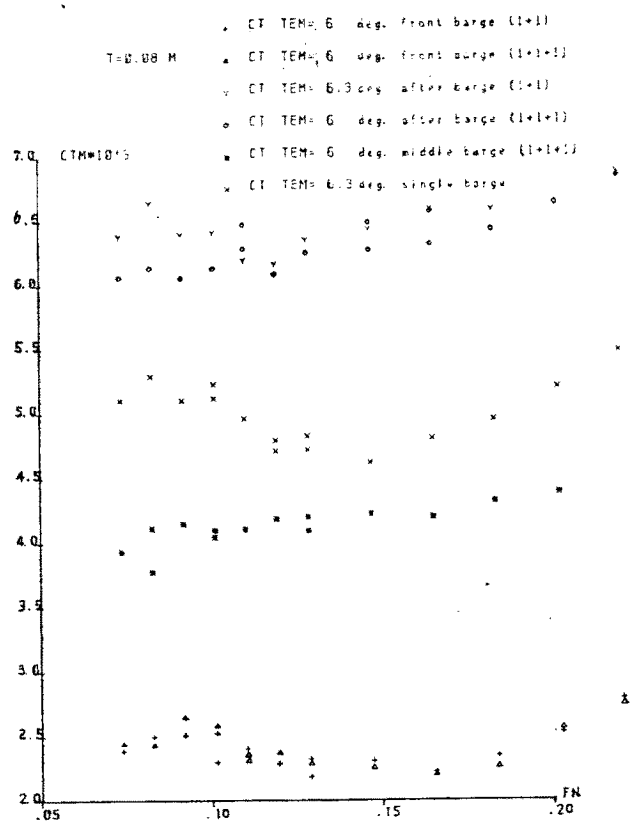

Fig. 7. Plot of Ct versus Fn for barge train

5. The resistance of middle barge is less than that of the single barge (see Figure 6–Figure 7). Middle barge is the front barge of the after barge and the after barge of the front barge, and it is affected by both barges. The results of test show that the profitable effect of the after barge is greater than that of the front barge.

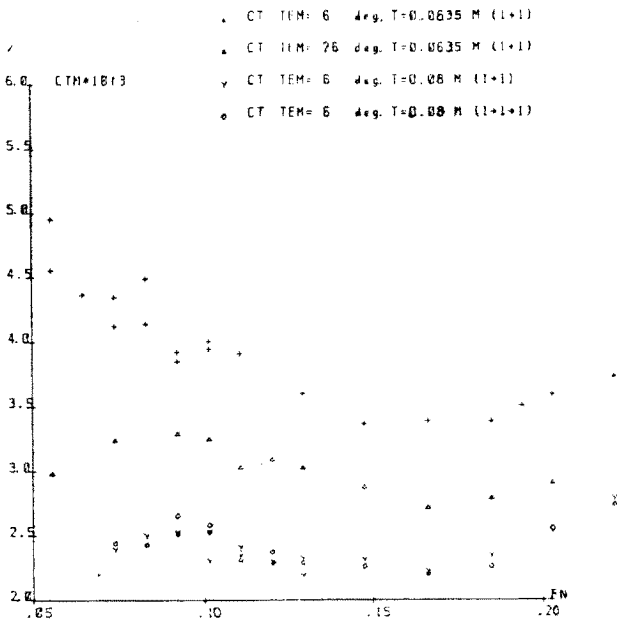

Fig. 8. Plot of Ct versus Fn for front barge

6. The greater the draught, the greater influence between barges (see Figure 8).

PS-1.15

LI SHIMO, WANG XINGQUAN and CHEN KEQINNG

Wuhan University of Water Transportation Engineering, Wuhan, China

EXPERIMENTAL RESULTS FOR RESISTANCE WITH SERIES-60 MODELS IN SHALLOW WATER

According to the ITTC cooperative experimental progam in shallow water, tests for Series-60 models have been caried out at WUWTE. The aim of the investigations was to obtain comprehensive information for the water depth influence on resistance, trim, and sinkage of ships in shallow water.

1. Models and model tests

Two wood models were manufactured following the offsets given by ITTC, namely MO172 and MO173. The characteristics of the models are tabulated in Table 1.

No.	Basic Characteristics		MO172	MO173
1.	Length between perpendiculars Lbp (m)		3.586	4.689
2.	Breadth	B [m]	0.478	0.625
3.	Draught	T [m]	0.191	0.250
4.	Displacement	Δ [m^3]	0.135	0.436
5.	Wetted surface	S [m^2]	2.169	3.709
6.	Block coefficient	Cb	0.595	0.595
7.	Scale	λ	34	26

TABLE 1

During the process of model manufacturing, special attention was paid to the accuracy of the models. A turbulization wire (ϕ=1.62 mm) was installed at 0.05 Lbp after fore perpendicular. No appendages are fitted to the hull. The model tests were carried out in the WUWTE shallow water tank and the dimensions of the tank are shown in Table 2.

Length of the tank	L[m]	132.0
Breadth	B[m]	10.8
Depth of water	H[m]	2.0

TABLE 2

The repeat tests were carried out in one year with same models, same test conditions but different temperature of water.

The model was fixed to the towing carriage in a way that the model was allowed to sink and trim freely. The water depth in the shallow water was achieved by varying the water level. The test conditions are presented in Table 3. The model speed range depends on the size of the model and varies 0.04 <Fn < 0.35. During the tests, runs are carried out compulsory with model speeds corresponding to Froude numbers for each model Fn. 0.10, 0.125, 0.15, 0.175 and 0.2. For relative depth H/T=1.2, model speeds are determined by the condition to avoid "grounding" of the model to the tank bottom.

H/T	Depth of water H[m]	
	MO172	MO173
H/T > 8	2.0	2.0
H/T = 2.0	0.382	0.5
H/T = 1.5	0.287	0.375
H/T = 1.2	0.229	0.30

TABLE 3

The time interval between the runs is selected normally between 10 minutes to 20 minutes depending on the water depth, model size and speed.

The water temperature is measured at a depth of approximately 2/3 'T (model draught from the water level), twice a test (i.e. half-way through the tests and after tests). The average temperature is taken into account.

The model speed is accepted equal to the speed of the towing carriage and the resistance is measured by mechanical dynamometer.

2. The Test Results and Conclusions

The test results of resistance are presented in Table 4~Table 5. They are the experimental points directly taken from the towing carriage. No processes or fairing has been done. The data shown in Table 4 were obtained in 1989 and the data shown in Table 5 were obtained in 1990 (repeat tests). The total resistance coefficients Ct(Fn) and the residuary resistance coefficient Cr(Fn) are shown in Figure 1~Figure 2. For the convenience of analysis and discussion, both test data (obtained in 1989, temperature about 25 degrees and obtained in 1990, temperature about 10 degrese) are plotted in the same Figure. I would like to show some examples here, but it should be noticed that the residuary resistance coefficients shown in Tables and Figures are calculated using the two-dimensional method which is recommended by ITTC.

That is,

CT=f(Fn)

CR=CT-Cfo=f(Fn)

Cfo is obtained from 1957 ITTC correlation line.

EXPEREMENTIAL RESULT

SHIP NAME : M0172
LENGTH OF WATERLINE--------LWL(M) 3.5860
DEPTH OF WATER---------- H(M) .2868
RELATIVE DEPTH----------H/T 1.5000
WETTED SURFACE----------S(M**2) 2.1692
TEMPERATURE----------TEM(deg) 24.0000

Table 4

No	Vm M/S	Rm G	Ctm 10**3	Crm 10**3	Cfo 10**3	LgRn	FN	FH
1	.400	100.0	5.667	1.407	4.260	6.196	.067	.238
2	.450	126.0	5.642	1.404	4.238	6.247	.076	.268
3	.550	176.0	5.215	1.223	3.992	6.334	.093	.328
4	.600	206.0	5.180	1.265	3.914	6.372	.101	.358
5	.650	234.0	5.022	1.160	3.862	6.407	.110	.388
6	.700	270.0	4.996	1.190	3.806	6.439	.118	.417
7	.750	306.0	4.932	1.177	3.755	6.469	.126	.447
8	.800	360.0	5.100	1.391	3.709	6.497	.135	.477
9	.838	388.0	5.010	1.334	3.676	6.517	.141	.499
10	.838	392.0	5.061	1.386	3.676	6.517	.141	.500
11	.800	366.0	5.185	1.476	3.709	6.497	.135	.477
12	.800	478.0	5.351	1.725	3.626	6.548	.152	.537
13	.838	404.0	5.216	1.541	3.676	6.517	.141	.500
14	.600	96.4	5.463	1.203	4.260	6.196	.067	.238
15	.500	149.2	5.611	1.341	4.070	6.293	.084	.298
16	.600	202.0	5.087	1.164	3.924	6.372	.101	.358
17	.700	260.0	4.811	1.005	3.806	6.439	.118	.417
18	.800	369.0	5.228	1.519	3.709	6.497	.135	.477
19	1.100	748.0	5.605	2.114	3.491	6.635	.185	.656
20	1.200	919.0	5.786	2.352	3.434	6.673	.202	.715
21	.900	498.0	5.574	1.949	3.626	6.548	.152	.537
22	1.000	608.0	5.513	1.959	3.554	6.594	.169	.596

EXPEREMENTIAL RESULT

SHIP NAME : M0172
LENGTH OF WATERLINE--------LWL(M) 3.5860
DEPTH OF WATER---------- H(M) .2868
RELATIVE DEPTH----------H/T 1.5000
WETTED SURFACE----------S(M**2) 2.1692
TEMPERATURE----------TEM(deg) 14.0000

Table 5

No	Vm M/S	Rm G	Ctm 10**3	Crm 10**3	Cfo 10**3	LgRn	FN	FH
1	.400	115.6	6.539	2.052	4.487	6.080	.067	.238
2	.443	144.4	6.659	2.268	4.391	6.133	.075	.264
3	.498	163.6	5.970	1.685	4.285	6.184	.084	.297
4	.552	187.6	5.572	1.377	4.195	6.228	.093	.329
5	.600	221.0	5.556	1.432	4.124	6.265	.101	.358
6	.652	265.0	5.641	1.587	4.055	6.301	.110	.389
7	.671	271.0	5.447	1.416	4.031	6.313	.113	.400
8	.700	298.0	5.504	1.507	3.997	6.332	.118	.417
9	.750	326.8	5.258	1.315	3.942	6.362	.126	.447
10	.801	396.0	5.586	1.694	3.891	6.390	.135	.473
11	.837	434.0	5.606	1.749	3.858	6.409	.141	.499
12	.851	430.8	5.383	1.938	3.845	6.416	.143	.507
13	.899	469.2	5.256	1.450	3.804	6.440	.152	.536
14	.920	507.6	5.427	1.641	3.787	6.450	.155	.548
15	.952	528.7	5.279	1.516	3.762	6.465	.161	.568
16	1.001	615.0	5.555	1.829	3.725	6.487	.169	.597
17	1.013	596.0	5.256	1.540	3.717	6.492	.171	.604
18	1.050	669.2	5.493	1.802	3.691	6.508	.177	.626
19	1.090	746.0	5.602	2.018	3.665	6.524	.184	.650
20	1.100	764.0	5.714	2.056	3.658	6.528	.185	.656
21	1.150	876.8	6.000	2.373	3.627	6.547	.194	.686
22	1.170	922.0	6.095	2.480	3.615	6.555	.197	.698
23	1.201	1001.8	6.205	2.608	3.597	6.566	.202	.716
24	1.251	1206.4	6.976	3.407	3.569	6.584	.211	.746
25	.800	378.0	5.356	1.464	3.892	6.390	.135	.477
26	.650	250.0	5.355	1.298	4.057	6.299	.110	.388
27	.500	154.0	5.575	1.294	4.281	6.186	.084	.298
28	.700	288.4	5.326	1.329	3.997	6.332	.118	.417

They are the experimental points directly from the tank. No processes or fairing has been done.

In order to investigate the form factor (1+k) and its dependence on water depth, the results obtained in different temperature are plotted in the form of Ct versus Cfo, shown in Figure 3~Figure 6. The slope at low Froude number is the form factor (1+k). For high Froude number, the isofroude lines do not parallel

each other. This can be considered as the influence of wall effect. In diagram, full lines are obtained by tests, the dash lines are determined by isofroude line parallel to the line of low Froude number.

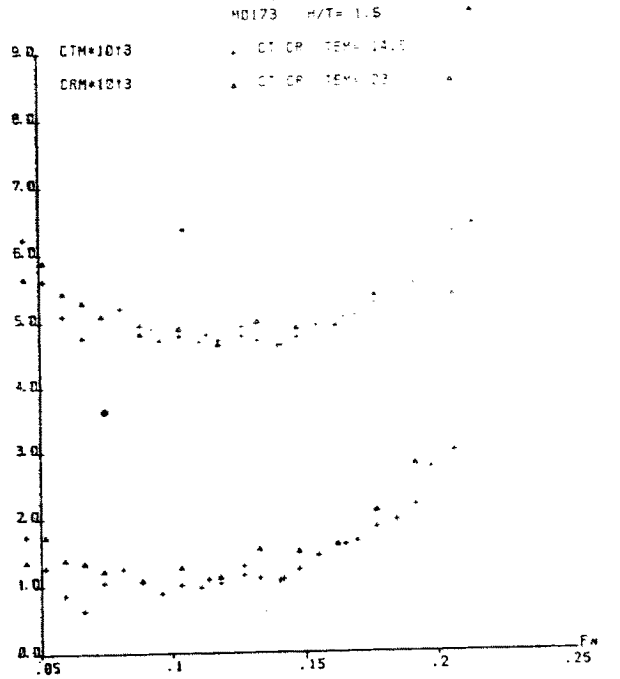

Fig. 1. Plot of Ct Cr on basis of Fn in shallow water

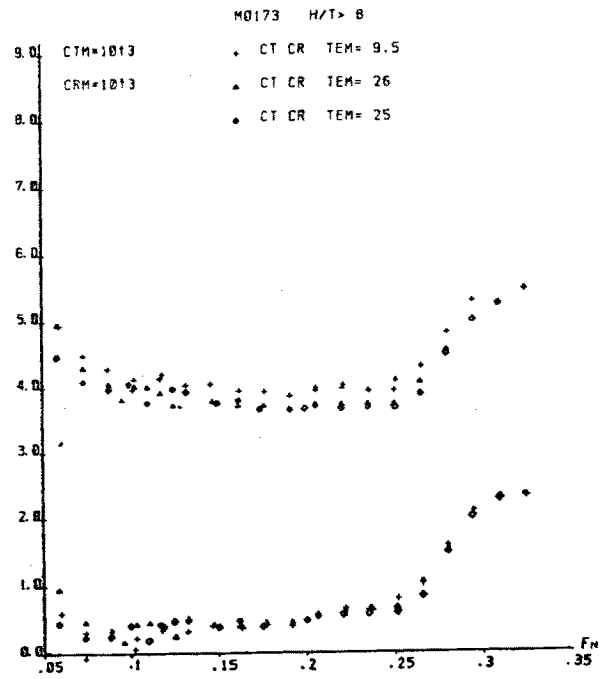

Fig. 2. Plot of Ct Cr on basis of Fn in deep water

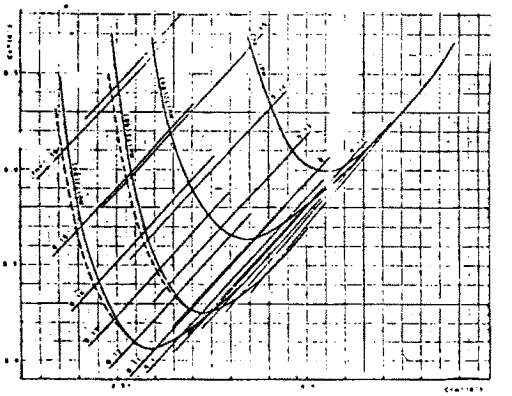

Fig. 3. Plot of Cf on basis of Cfo in shallow water H/T=1.2

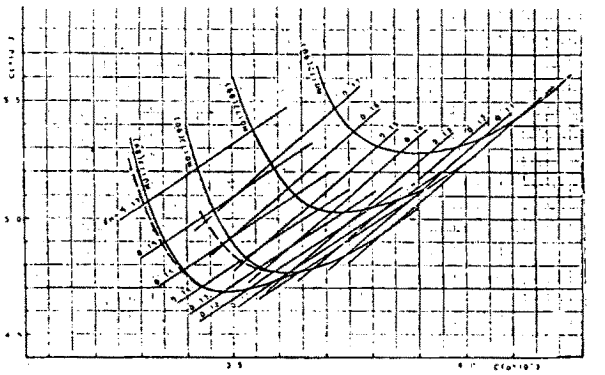

Fig. 4. Plot of Ct on basis of Cfo in shallow

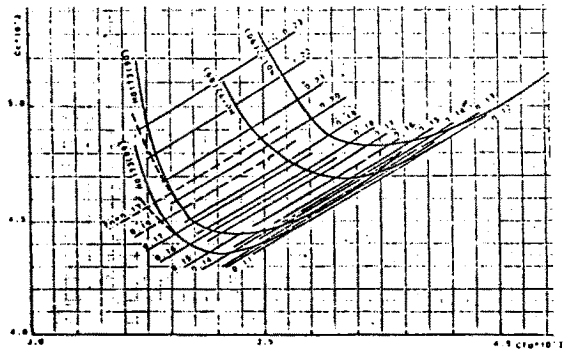

Fig. 5. Plot of Ct on basis of Cfo in shallow water H/T=2.0

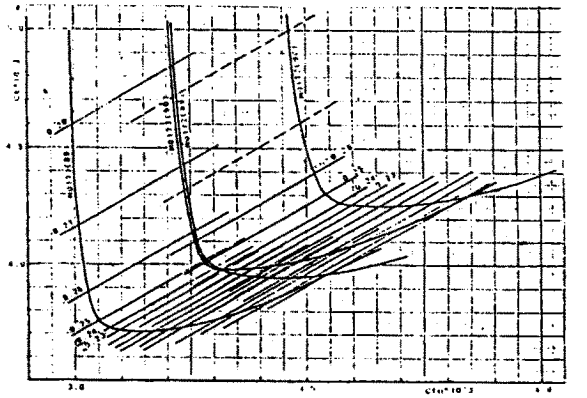

Fig. 6. Plot of Ct on basis of Cfo in deep water

As a result of model tests and investigations carried out with Series-60 geosim models, the following conclusions can be made:

1. For deep water, as we can see in Figure 6 of CT versus Cfo in deep water, the isofroude lines almost have same slope not only at low Froude numbers but also at high Froude numbers, the form factor does not practically depend on model scale.

2. For shallow water, the depth of water has an obvious influence on the form factor, with the decrease in water depth the form factor increases. (1+k)=f(h/t) is shown in Figure 7.

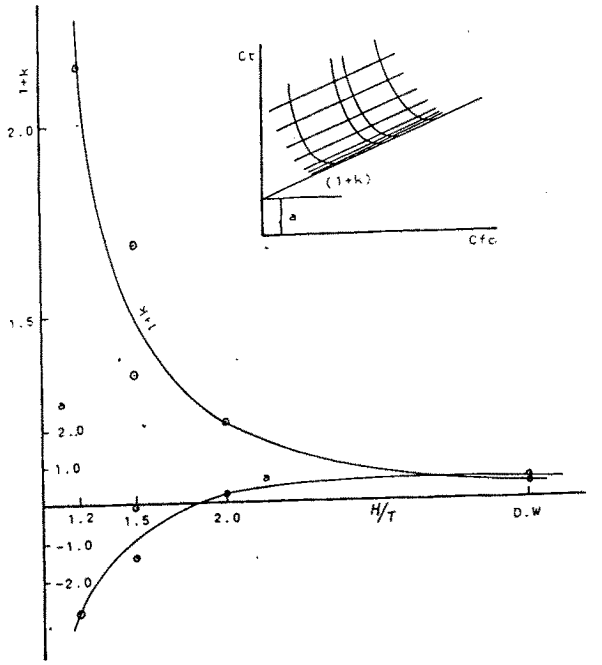

Fig. 7. Form factor (1+k)

3. For shallow water, the isofroude line, (at low speed, say Cw=0) in the Figure 3 of CT versus Cfo seems not to pass through the origin of coordinates. The intercepting "a" on coordinate, "a"=f(h/t), is shown in Figure 7. This does not influence the ship-model correlation, but influences the split of different resistance components, i.e. the total resistance coefficient may be written as:

$$CT=a+(1+k)Cfo+Cw$$

4. Especially we can see that a<0 while h/t<1.8, what is the physical meaning of a<0 is worth further consideration.